NASA CONTRACTOR REPORT

NASA CR-625

NASA CR-625

N67 12757

(ACCESSION NUMBER)

(THRU)

146

(PAGES)

1

(CODE)

CR-625

(NASA CR OR TMX OR AD NUMBER)

03

(CATEGORY)

FACILITY FORM 602

STEADY-STATE AND DYNAMIC OPERATING CHARACTERISTICS OF A SIMULATED THREE-LOOP SPACE RANKINE-CYCLE POWERPLANT

by J. R. Hooper

Prepared by
UNITED AIRCRAFT CORPORATION
East Hartford, Conn.
for Lewis Research Center

GPO PRICE $ ______

CFSTI PRICE(S) $ 3.00

Hard copy (HC) ______

Microfiche (MF) 1.00

ff 653 July 65

NATIONAL AERONAUTICS AND SPACE ADMINISTRATION • WASHINGTON, D. C. • NOVEMBER 1966

NASA CR-625

STEADY-STATE AND DYNAMIC OPERATING CHARACTERISTICS OF A SIMULATED THREE-LOOP SPACE RANKINE-CYCLE POWERPLANT

By J. R. Hooper

Prepared under Contract No. NAS 3-2335 by
UNITED AIRCRAFT CORPORATION
East Hartford, Conn.

for Lewis Research Center

NATIONAL AERONAUTICS AND SPACE ADMINISTRATION

For sale by the Clearinghouse for Federal Scientific and Technical Information
Springfield, Virginia 22151 – Price $3.00

ABSTRACT

Experimental investigations were conducted with a facility which simulated heat transfer and fluid flow in a Rankine-cycle space power-conversion system of the SNAP 8 type. Water was used as the working fluid. Steady-state condenser and boiler data are presented in a form suitable to a linearized analysis of the interactions of these components with the rest of the system. Frequency response data was obtained by varying the power-loop flow rate at the boiler inlet. Experimental stability maps are presented as a function of the pressure-flow slope imposed at the boiler inlet.

FOREWORD

This report was prepared by Pratt & Whitney Aircraft Division of United Aircraft Corporation, East Hartford, Connecticut to describe work conducted during the period May 15, 1964 to May 1, 1965 in fulfillment of Task II of Contract NAS3-2335, Experimental Investigation of Transients in a Space Rankine-Cycle Powerplant. This task consisted of an investigation of the steady-state operating characteristics and transient response characteristics of a three-loop Rankine-cycle powerplant similar in type to the SNAP 8 powerplant. Experimental investigations were conducted with a facility designed and built by Pratt & Whitney Aircraft, which used water as the working fluid and was designed to simulate many fluid-flow and heat-transfer aspects of a space power-conversion system.

Two previous summary reports, PWA-2227 and NASA CR-54179 (PWA-2342) were issued under this phase of the contract. These reports described investigations of starting procedures in two-loop powerplants.

The experimental work described in this report was performed by D. P. Olsson, J. L. Plourd, and the author. Technical assistance was provided by M. U. Gutstein, G. Hurrell, and D. R. Packe of the Lewis Research Center, National Aeronautics and Space Administration.

TABLE OF CONTENTS

	Page
I. Summary	1
II. Introduction	3
III. Description of Experimental Facilities	5
A. Electrical Heater	6
B. Boiler	6
C. Condenser	7
D. Radiator Simulator	7
E. Pumps	8
F. Instrumentation	8
G. Automatic Controls	10
H. Facilities for Eliminating Noncondensables and Impurities from Working Fluids	11
IV. Steady-State Operating Characteristics	12
A. Condenser Performance Maps	12
1. General Discussion	12
2. Condenser Maps with Coolant Flow an Independent Variable	13
3. Condenser Maps with Coolant Outlet Temperature Controlled	18
B. Boiler Performance Maps	19
1. General Discussion	19
2. Test Results	21
V. Dynamic Response Characteristics	24
A. System Response Data	24
B. Boiler Response Data	26
C. Boiler Stability Data	30
1. Description of Test Procedure and Observed Instabilities	30
2. Stability Maps	31
VI. Concluding Remarks	34
Appendix A - Details of Simulator Flow Passages	36
Appendix B - Auxiliary Control Circuits	41
Appendix C - Exploratory Boiler, Condenser and System Maps	52
Appendix D - Tables	55
Appendix E - Nomenclature	68
Appendix F - Linearized Condenser Variable Relationships	70

I. SUMMARY

Experimental investigations were conducted with a facility which simulated heat transfer and fluid flow in a Rankine-cycle space power-conversion system of the SNAP 8 type. These tests were designed to support the analysis of powerplant control problems being performed by NASA, and served two general purposes. The first was to obtain data showing interrelations among the variables defining the thermodynamic state at various locations in the powerplant. The second purpose was to document dynamic interactions which influence stability in a closed Rankine-cycle loop. Specifically, these tests were directed towards solution of the problems of controlling condensing pressure and of determining conditions required for stable coupling of the boiler with other system components.

Steady-state performance characteristics of the condenser were experimentally mapped while each of the variables affecting heat transfer was independently controlled. This data indicated that the performance of the powerplant condenser was reasonably predictable, and that an analysis of condensing pressure in a closed Rankine-cycle loop based on the position of the liquid-vapor interface in the condenser is possible. During these tests it was also observed that pressure fluctuations in the condenser tubes due to slugging flow, which is commonly encountered, were found to be of insufficient magnitude to affect operation of the rig. Steady-state tests were also made to investigate a method of maintaining a fixed condensing pressure by controlling coolant flow rate in order to maintain a constant coolant outlet temperature. In these tests this control effectively eliminated changes in condensing pressure due to changes in the radiator exit temperature.

Steady-state data were also obtained to investigate how the relation between flow and pressure drop in a high performance counterflow boiler depends on other powerplant variables. One of the purposes of these tests was to provide an evaluation of the boiler pinch-point temperature difference as a possible correlating parameter for the effect of several variables on boiler pressure drop. These steady-state data also provided a background for subsequent transient testing in which sine-wave perturbations in the power-loop flow were introduced at the boiler inlet, and the phase and amplitude response of boiler temperature and pressures were recorded. The frequency response of the power-loop boiler-inlet pressure to variations in boiler-inlet flow rate was used to establish a criterion for matching a power-loop pump to the boiler in order to avoid possible unstable system interactions. In order to directly investigate the limits of stable boiler operation, a control was constructed to impose various linear negative slopes of pressure/flow at the boiler inlet. Unstable boiler operation was encountered at slopes predicted reasonably well by the frequency response data. These slopes were lower than those present in normal operation of this powerplant. However, the slope at which instabilities started appeared to be a function

of other variables such as: heater-loop flow rate, heater-loop boiler-inlet temperature, and power-loop flow rate.

In addition to the tests described above, in which a working-fluid accumulator was employed in the Rankine-cycle loop to facilitate investigation of boiler and condenser characteristics, a limited amount of testing was performed with a fixed inventory in the Rankine-cycle loop. Included were steady-state performance mapping tests and tests in which step-change and sine-wave perturbations were induced in the power-loop flow rate. No system interactions of an obviously detrimental nature were encountered in the constant-inventory tests.

II. INTRODUCTION

Starting and control problems in a Rankine-cycle space power-conversion system are complicated by the fact that the mechanisms of two-phase flow in a closed boiling and condensing loop are not completely predictable. One means of obtaining information necessary for effective measures to prevent instabilities and unfavorable operating conditions in a projected powerplant is to simulate the operation of the powerplant with a flexible experimental facility in which a fluid is actually boiled and condensed. Experimental data which reflect the physical mechanisms of boiling, condensing and two-phase flow are thus provided to guide, supplement and verify analyses of the problems.

Space Rankine-cycle starting modes, control problems, and system variable interactions are being studied at the NASA Lewis Research Center in support of the SNAP 8 program. To aid in these studies, experiments were conducted at Pratt & Whitney Aircraft with a facility using water as the working fluid, and designed to simulate many fluid-flow and heat-transfer aspects of a Rankine-cycle space power-conversion system similar to SNAP 8*. The tests described in this report were planned by NASA personnel to support their analytical efforts and were directed principally towards two possible problem areas in a SNAP 8-type powerplant which are currently receiving attention.

One of these problem areas was control over condensing pressure during starting and operation of the powerplant. The condensing pressure is critical since both the turbine exit pressure and the pump inlet pressure closely follow the condensing pressure. This occurs because the condenser typically has a small pressure drop. An increase in turbine exit pressure causes the turbine power output to decrease, while a relatively small decrease in the pump inlet pressure may be detrimental if the pump is normally operated near its cavitation limit (as may be desirable to maximize system efficiency). Therefore, it is important to control the condensing pressure within narrow limits. The most direct way to control the condensing pressure would be to place a working-fluid accumulator at the exit to the condenser and regulate the pressure on the liquid in the accumulator at the desired level. Another method of controlling condensing pressure which shows promise is to regulate local heat transfer rates in the condenser with a control on the condenser-coolant flow rate. Because a liquid-metal accumulator tends to be complex and because the use of an accumulator may present problems in the ground simulation of zero gravity effects with

*The SNAP 8 is a 35-kilowatt nuclear turbo-dynamic space power system that utilizes a mercury Rankine cycle. Two additional liquid loops, one to carry energy from the nuclear heat source to the Rankine-cycle boiler, and the other to carry heat rejected from the condenser to a space radiator, are employed.

liquid metals, the condenser-coolant flow-rate control may offer an advantage. In order to design such a control, relationships among the condensing pressure, working-fluid inventory, and heat transfer rates at a given vapor flow rate must be accurately known. These relationships were experimentally investigated in this contract task.

Another problem area is the possible unstable interactions between the boiler and other components in the Rankine cycle. Two important characteristics of a forced-convection boiler which determine the nature of the interaction between the boiler and the rest of the system are:

1) The steady-state pressure drop versus flow rate characteristics of the boiler depend on the variation of liquid fraction and quality throughout the boiler, which in turn depend on variations in heat flux in the boiler.

2) A time-dependency exists between an independent change in flow rate at the boiler inlet and the adjustment of the pressure drop and exit flow rate to their new steady-state values. The nature of this time-dependency is affected by the rate of change of liquid fraction with time in the boiler, and consequently by the dynamic interrelations among flow rate, heat transfer rate and liquid fraction.

The first characteristic is important to static stability of the design and off-design points at which the Rankine cycle must operate. The second characteristic gives rise to the possibility of dynamically unstable or oscillatory-type interactions.

The steady-state pressure drop versus flow rate characteristics of the boiler were experimentally mapped in this contract task. The frequency response of boiler temperature and pressure to variations in boiler inlet flow was also experimentally obtained. Unstable system operating conditions were deliberately created by changing the pressure versus flow rate characteristic imposed at the boiler inlet, and the resulting dynamic instabilities were observed.

III. DESCRIPTION OF EXPERIMENTAL FACILITIES

Figure 1 is a schematic of the powerplant simulator showing the three-loop configuration tested during the period covered by this report. The three fluid loops, all of which employed water as the energy transfer medium, are described below.

1) Heater Loop - A liquid loop transferred energy from an electrical heat source to the shell of a Rankine-cycle boiler. This loop was pressurized to prevent vaporization at temperatures up to 435°F.

2) Rankine-Cycle Power Loop - A two-phase loop, in which the fluid was completely evaporated and recondensed as would occur in a working Rankine-cycle loop. The fluid was vaporized in the tubes of the boiler, flowed through a valve which provided a pressure drop similar to that which would occur in a turbine with choked nozzles, condensed in the tubes of the condenser, and returned to the boiler inlet through a pump. Since no energy was extracted from the fluid at the turbine-simulator valve, the energy that would be removed by a turbine in a working Rankine cycle was rejected in the condenser. However, since the amount of energy extracted by a turbine in a typical Rankine cycle is a small percentage of the energy rejected by the condenser, the effect on the simulated powerplant system of the additional heat load in the condenser was small.

All flow passages in this loop were placed in a horizontal plane to minimize the effects of gravity, and passages containing vapor were sized to give the fluid velocities expected in a typical powerplant.

3) Radiator Loop - A liquid loop transferred energy from the shell of the condenser to a unit which simulated the flow passages and heat capacity of a space radiator. Heat was ultimately rejected from the radiator simulator, by convection, to a nearly constant-temperature sink stream. A bypass around the condenser shell was provided for the radiator loop fluid.

A photograph of the facility appears in Figure 2. Figure 3 is a line drawing, with the power loop drawn to scale, showing the location of the instrumentation and valves. Line sizes, valve sizes and insulation are given in Appendix A. Figures A1, A2, and A3 show the approximate flow passage areas and typical transport times in each of the three loops. The components of this system are described in detail below.

A. Electrical Heater

The electrical heater used is shown in Figure 4. It consisted of 19 Calrods, 0.496 inch in diameter and 6 feet long, distributed in circular patterns and encased in a Schedule 40 stainless steel pipe. The Calrods were capable of delivering up to 115 kilowatts to the heater-loop fluid flowing longitudinally along them. The electrical power input was controlled to maintain the boiler-shell inlet temperature constant at various desired values.

B. Boiler

The Rankine-cycle boiler, shown in Figure 5, was a single-pass shell-tube type heat exchanger, with the heater-loop fluid flowing in the shell along the outside of the tubes in a direction counter to the flow of the vaporizing Rankine-cycle fluid inside the tubes. Nineteen stainless steel tubes, with an outside diameter of 0.25 inch, a wall thickness of 0.049 inch and eight feet in length were enclosed in a two-inch stainless-steel pipe, with manifolding arrangements to allow for thermal expansion and to permit access to the tubes.

In order to approximate the pressure drop characteristics of a SNAP 8-type boiler, the inserts shown in Figure 6 were constructed and placed inside the tubes of the previously existing boiler. These inserts consisted of two sections. The first section, which was attached to a low pressure-drop orifice at the entrance to the tubes, was a solid core with a wire wrapped around it in a spiral to provide a spiralled annular passage. The first section extended to the point at which the quality in the tubes was approximately 10 to 20 per cent in the normal operating range of the boiler. The second section consisted of a spirally-twisted tape which extended to the point at which vaporization was normally nearly completed.

The heater loop was also modified to enable the heater-loop flow rate to be reduced so that the boiler "pinch-point" temperature difference between the heater-loop fluid and the boiling fluid would undergo a significant percentage change when the heater-loop flow rate, the boiler-shell inlet temperature, or the boiler-tube inlet pressure were varied around their normal operating points. The pinch-point temperature difference in a counterflow boiler occurs at the point at which bulk boiling starts. It is the minimum temperature difference driving heat transfer in the boiling region and consequently is an important parameter in boiler performance.

Fluid temperature measurements were taken with immersion thermocouples at the inlet and outlet to the boiler on the shell and tube sides. Thermocouples were also attached to the outside skin of the boiler shell at four-inch intervals to obtain an indication of the shell fluid temperature variation. These thermocouples only provided a rough approximation of shell fluid temperatures, as explained in Section F. Instrumentation. A computed bulk-temperature profile believed to be typical of this boiler is shown in Figure 7a. Pressure measurements were taken at the inlet and exit to the boiler in the power loop.

C. Condenser

The condenser, shown in Figure 8, consisted of three Ross BCF-7M300-8C8 heat exchangers connected together in series to provide straight-through flow for 56 brass tubes with an inside diameter of approximately 0.20 inch. The internally-baffled shells of the three heat exchangers were externally connected. The Rankine-cycle fluid was condensed in the tubes of the condenser by the radiator-loop liquid coolant which flowed in the shell in a direction counter to the condensing fluid. A bypass around the condenser shell for a portion of the radiator-loop fluid, seen schematically in Figure 1, provided a means for controlling the coolant flow rate in the condenser shell while maintaining a nearly constant radiator-loop flow.

The condenser was designed to have a low pressure drop (typically 2 to 3 psi) on the power-loop side. Orifices at the exit to each tube, with a (liquid) pressure drop approximately 10 per cent of the total condenser pressure drop, aided distribution in the tubes and provided a large restriction to vapor should vapor be present at the exit of one or more of the tubes. Pressure measurements were taken at the inlet and exit to the condenser on the power-loop side.

Fluid stream temperature measurements were obtained with immersion thermocouples at the inlet and exit to the condenser on the shell and the tube sides and in the intermediate external connections of the shell. Temperature measurements in the condensing stream inside the condenser tubes were provided by sheathed thermocouples inserted into twelve of the tubes through holes drilled in the orifice plugs at the tube exits. These thermocouples were located at different lengths up to twelve inches from the condenser exit. A computed bulk-temperature profile believed to be typical of this unit appears in Figure 7b.

D. Radiator Simulator

The unit designed to approximate the flow passages and heat capacity of a space radiator is shown in Figure 9. The radiator simulator consisted of three identical segments which could be operated independently. Sixty-one stainless steel tubes of 0.25 inch outside diameter in each segment were imbedded in a copper slab 34 x 22 x 1.5 inches which provided the heat capacity.

Heat was rejected from the radiator simulator by convection to a liquid sink stream flowing beneath the copper slabs. The sink stream had a sufficiently high flow rate that a negligible temperature rise (3° to 5°F) occurred as the stream passed from one end of the radiator simulator to the other. The temperature level of the sink stream was controlled by regulating the injection of CO_2 into a mixing tank, shown in Figure 3, and by regulating flow from the mixing tank to the sink loop. This control operated automatically from a thermocouple signal in the sink loop. The heat transfer coefficient from the radiator simulator to the sink was independently controlled by regulating the flow rate in the sink loop.

E. Pumps

The heater-loop pump was a Dean Brothers RIL centrifugal pump, and the radiator-loop pumps, one located at the exit to each of the three segments, were Pacific Pump Company N5-AB turbine pumps. Since the pressures in the heater loop and radiator loop do not affect heat transfer in the boiler and condenser (so long as they are high enough to keep the fluid in a liquid state), the pressure-flow characteristics of these pumps do not affect the operating characteristics of the power loop. The pressure-flow characteristics of the power-loop pump, on the contrary, have an important influence on the operating characteristics of the power loop, because heat transfer and pressure drop of the power-loop fluid in the boiler depend both on flow rate and pressure level. The cavitation characteristics of the power-loop pump also fix the minimum allowable condenser exit pressure.

The power-loop pump system consisted of two 2-stage Aurora Model B-4-T turbine or drag pumps in series. This pump is shown in Figure 10. The pumps were belt-coupled to fixed-speed motors by means of variable-diameter pulleys, so that the pump speed could be changed over a limited range. The head-flow curve of the pump system operating at various speeds is plotted in Figure 11, together with the cavitation limit at one speed, obtained from the manufacturer's data.

F. Instrumentation

The powerplant simulator was instrumented to obtain continuous recordings of temperature at the inlet and exit of each component in the system, flow rate in each separate flow path, and pressure at the inlet and exit of each component in the power loop. In addition, a duplicate set of manual readout instrumentation was provided to monitor the operation of the simulator at many points, and for use during steady-state testing. Instrument stations are located on the line diagram in Figure 3. Additional thermocouples were placed along the outside skin of the boiler shell, and inserted into twelve of the condenser tubes.

1. Temperatures

All stream temperature measurements were made with 1/32-inch sheathed chromel-alumel immersion thermocouples with an accuracy of ±1.5°F. Time constants of thermocouples in liquid streams were less than 75 milliseconds at the nominal design flow rate, while those in vapor streams were approximately 300 milliseconds. It is estimated that thermocouples attached to the shell of the boiler only indicated the average shell fluid temperature at a given location to within ±4°F due to radial temperature gradients in the fluid and axial temperature gradients in the shell metal. Monitoring temperatures were read on a Brown potentiometer through a Lewis switch.

2. Pressures

Continuous pressure signals were obtained from DC-activated strain-gage transducers. These transducers had accuracies better than 1 per cent of full range and frequency responses flat to greater than 500 cps. The transducer at the boiler exit in the power loop was offset from the flow passage by approximately one foot of 1/4 inch copper tubing for cooling purposes. Part of this tubing was filled with condensed liquid, but the compressibility of the vapor in the tube reduced the frequency response of this pressure readout. However, it was still considered adequate for the purpose of these tests. Bourdon tube gages, with an accuracy of 1 per cent of full scale, were used for steady-state readout. Due to the length of the lines from the pressure taps to the Bourdon gages in the control room, provisions were made to shut off these lines at the pressure taps during transient operation.

3. Flow Rates

Flow rates were measured with turbine flowmeters having magnetic pickups which provided a variable frequency output signal, with an accuracy of ±1 per cent of full scale. Orifice meters were used to check the turbine flowmeters during steady-state testing. The output signal from the turbine flowmeters was translated into a DC voltage level for continuous recording and for use with the electrohydraulic control valves. The time constant of the turbine element was approximately 5 milliseconds, and an additional time constant of 32 milliseconds was introduced by the translating unit.

4. Recording Oscillograph

System temperatures, pressures and flow rates were continuously recorded during transient operation on a recording oscillograph. The galvonometers used with the oscillograph had a frequency response flat to approximately 60 cps. The absolute accuracy of the oscillograph readout has been estimated at ±2 per cent of the maximum reading, while variations were obtained to an accuracy of approximately ± 1 per cent.

G. Automatic Controls

1. Electrohydraulic Control Valves

Two electrohydraulic feedback control valves were employed in the simulator. These control units each consisted of an Annin valve, an electrohydraulic actuator with a Moog servovalve, and an Annin electronic controller which provided operational and servo-amplifiers and additional control functions.

One control unit was located at the boiler inlet in the Rankine-cycle power loop to control the power-loop flow at that point, or to control the boiler-inlet pressure-flow rate characteristics. In the flow control mode a signal voltage from a turbine flowmeter located upstream of the valve was fed back to the control unit, where it was compared to a reference voltage, and the valve was actuated to maintain the flow rate at a level designated by the reference voltage. Time-varying functions, such as ramps, step changes or sine waves could be externally generated for the reference voltage. When the valve was used to control the pressure flow slope which would occur in response to a perturbation in either of these variables, the signal from a DC strain gage pressure transducer at the boiler inlet was used as the reference voltage. The valve itself was a 1/2-inch valve with a percentage plug (flow proportional to valve stroke at constant pressure drop).

The second electrohydraulic valve was located in the radiator loop at the branch between the inlet to the condenser shell and the condenser-shell bypass, to control the flow split between the condenser shell and the bypass. A signal from a thermocouple at the condenser-shell exit was fed back to the control unit, and the valve acted to maintain the temperature at this point at a designated level by controlling flow through the condenser shell. A 1 1/2-inch two-way valve at the flow branch, and a 3/4-inch valve with a percentage plug in the condenser-shell line, were used at different times.

The response of the measuring devices associated with these controls was discussed in the preceding section. A block diagram of the controllers and a manufacturer's frequency response curve for the electrohydraulic actuators are given in Figures B1 and B2 of Appendix B. In Appendix B the calibration of auxiliary electric circuits used in conjunction with these controls to create two-variable "slopes" is described. The operation of the controller, together with these auxiliary circuits is discussed in Appendix B.

2. Electrical Power Input Regulator

The temperature at the inlet to the boiler shell was maintained at a desired level by regulating the electrical power input to the heater. This control, which was roughly proportional over a limited range of variation, consisted of a photocell circuit connected to a meter reading the output of a thermocouple at the boiler-shell inlet, magnetic amplifiers amplifying the output of the photoelectric circuit, and a large saturable-core reactor directly controlling the power input to the Calrods.

H. Facilities for Eliminating Noncondensables and Impurities from Working Fluids

Water for the three fluid loops was obtained by condensing steam and storing it under pressure at 150°F to minimize mineral content and air entrainment. The power loop was evacuated at the end of each test and refilled. The power loop was also periodically flushed with a weak acid solution and detergents to clean the heat transfer surfaces. The heater and radiator loops were periodically evacuated and refilled, and bled from high points in the loop.

IV. STEADY-STATE OPERATING CHARACTERISTICS

Steady-state operating characteristics of the powerplant simulator were experimentally mapped in order to explore steady-state interrelations among variables in a powerplant of the SNAP 8 type. In general, these tests were designed by NASA personnel to provide data in order to interrelate powerplant variables for a linearized analysis. For this purpose, variables which would be interdependent in a space powerplant were made independent in these tests, by use of a working fluid accumulator in the power loop and other controls which would not be available in a space system.

Preliminary exploratory tests were made to provide data for the selection of a nominal design operating point which yielded operating characteristics in the boiler and condenser as similar as possible to those in a projected SNAP 8 type powerplant. A few tests were also made in which the power loop was operated with a fixed inventory of working fluid and a fixed flow control valve for two different pump speeds. Data from these exploratory tests are presented in Appendix C. The nominal design operating point selected on the basis of these tests is given in Table 1, Appendix D. The criteria used by NASA for the selection of the nominal design operating point are discussed in Appendix C.

After the design operating point had been selected, experimental performance maps of the condenser and boiler were obtained by changing controllable variables in the condenser and boiler, one at a time, about the nominal design operating point.

A. Condenser Performance Maps

1. General Discussion

The condensing pressure in a Rankine-cycle loop must be maintained within limits to prevent cavitation in the power-loop pump due to too low a condenser exit (pump inlet) pressure and power loss in the turbine due to too high a condenser inlet (turbine exit) pressure. The pressure drop in a condenser is typically small, so condenser inlet and exit pressures are nearly equal. The relationship between condensing pressure and other system variables is discussed below.

A closed Rankine-cycle loop, when operating in steady state, must satisfy two basic requirements, 1) the total fluid inventory must remain constant, and 2) the heat added in the boiler and the energy added by other components, such as the pump, must equal the heat removed in the condenser plus the energy removed by other components, such as the turbine. The energy added by the pump and removed by the turbine are typically a small fraction of that transferred in the boiler and condenser (actually, in the simulator no energy was removed by the valve that corresponded to the turbine). Consequently, since the primary changes in system inventory take place in the boiler and condenser, these two units must have a total inventory that is approximately constant while transferring about the same amount of heat. Application of these necessary conditions to an analysis of condensing pressure in a constant-inventory loop requires a knowledge of how condensing pressure is related to condenser inventory and heat transfer rates in the condenser.

If the condenser is considered to be filled with only vapor up to the point at which complete condensation has occurred, the condenser inventory may be simply related to the position of this liquid-vapor interface. Actually, liquid is present upstream of the point at which condensation is completed. Also, the point at which condensation is completed may be fluctuating even at steady-state conditions. However, the error introduced by visualizing a simplified interface at a discrete location is probably not excessive, and experimental condenser operating characteristics obtained with the condenser separated from the system may be used to predict the steady-state interaction of the condenser with the system if data on the interface location is included.

First consider a condenser with a given geometry which is separate from the powerplant. The following variables are independently controllable:

1) Condenser exit (or inlet) pressure
2) Condensing-fluid flow rate
3) Coolant inlet temperature
4) Coolant flow rate
5) Condensing-fluid inlet enthalpy, which will be considered fixed near its saturated vapor value in this discussion.

The position of the interface in the condenser will depend on the average heat transfer rate in the condensing region and the condensing fluid flow rate. This dependency is approximately represented in the equation below, in which any entering superheat has been neglected[1].

$$(wH_{fg})_{\text{condensing fluid}} = U_{\text{mean}} \left(T_{\substack{\text{saturation,}\\ \text{condensing}\\ \text{fluid}}} - T_{\text{coolant}}\right)_{\text{mean}} \phi I \qquad (1)$$

[1] See Appendix E for nomenclature

where ϕ is the heat transfer perimeter and I is the distance of the interface from the entrance to the condensing tubes, i.e. the condensing length.

The heat transfer rate $U_{mean} (T_{sat,\ cf} - T_{coolant})_{mean}$, depends on the independent variables as follows:

1) Condensing pressure, as it determines $T_{sat,\ cf}$ (the vapor-pressure curve of the condensing fluid gives this relationship)
2) Condensing-fluid flow rate, as it affects U_{mean}
3) Coolant inlet temperature, as it affects $T_{coolant\ mean}$
4) Coolant flow rate, as it affects $T_{coolant\ mean}$ and U_{mean}

When the condenser is replaced in a constant-inventory Rankine-cycle loop the condensing pressure is no longer an independent variable, but depends on conditions in other parts of the loop, since the available fluid must fill the loop at the local equilibrium temperatures and pressures. Although the calculations involved are too cumbersome for this necessary condition to be applied precisely to analysis of interactions in the loop, the situation may be simplified by making approximations. If all of the loop fluid is considered as residing in the liquid portions of the loop (which is a fair approximation because the vapor density is small compared to the liquid density), then the fixed inventory condition may be applied as a requirement on the relative movements of the liquid-vapor interfaces in the condenser and boiler. For instance, if an increase in inventory is imposed on parts of the loop other than the condenser (e.g., by changing the heat transfer rate in the boiler), then a corresponding inventory decrease must take place in the condenser. This inventory decrease may be roughly related to a change in interface location by the expression

$$\Delta I = \frac{\Delta \text{ inventory}}{\rho \text{ liquid} A} \tag{2}$$

From the heat transfer equation, a change in interface location at a constant condensing flow rate requires a change in the heat transfer rate in the condensing section of the condenser. If the coolant flow rate and inlet temperature are held constant, then this change in heat transfer rate must occur through a change in condensing pressure. So a change in condensing pressure is related to an independent change in inventory in other parts of the Rankine-cycle power loop through the values of the terms in the heat transfer equation and the vapor pressure curve of the fluid. The heat transfer equation, and the relationships between the independent variables and the heat transfer rate, also indicate the magnitude of change required in the coolant flow rate to maintain the condensing pressure constant when the interface location or one of the other variables is changed by a given amount.

The steady-state performance of the condenser was experimentally mapped to explore the relationship between condensing pressure and condensing length, with the power-loop flow rate and the condenser-coolant flow rate and inlet temperature as parameters. A second series of tests was made at approximately the same operating conditions in which the condenser coolant flow rate was automatically controlled to maintain a near-constant coolant outlet temperature.

2. Condenser Maps with Coolant Flow an Independent Variable

a) Tests and Analysis

Tests were run to obtain condenser operating maps. The variables independently controlled in these tests were the condenser-coolant flow rate, condenser-shell inlet temperature, power-loop flow rate, and condensing pressure. The condenser-shell inlet temperature was controlled independently of the radiator-loop flow rate by regulating the heat rejection rate from the radiator simulator. The condensing pressure was regulated with a liquid accumulator located near the condenser exit. Gas pressure on a bladder in the accumulator was set to give the desired condenser inlet pressure (condenser inlet pressure was taken as an indication of condensing pressure in these tests). The data from the condenser tests are listed in Table 2, Appendix D. Figures 12, 13 and 14 show the variation of condensing pressure with interface location as a function of each of the independent variables.

The interface position in the condenser tubes was determined by means of temperature measurements in the condensing stream and coolant stream. Temperatures in the condensing stream were obtained from twelve sheathed thermocouples inserted into the tubes from the condenser exit and shaped to keep the tip away from the wall. Each thermocouple was put in a separate tube but at a different distance from the condenser exit.

Frequent failures occurred in the condenser tube thermocouples, and anomalous temperature readings were obtained. The thermocouples were replaced twice with no appreciable improvement. The anomalous readings apparently were due to maldistribution of flow between the condenser tubes and flow fluctuations (slugging) in the tubes. Slugging in the condensing stream, which has often been noted in the literature[1], appeared in oscillograph recordings as a high-frequency, low-magnitude pressure fluctuation at the condenser exit, and as irregular temperature excursions in readings from the condenser tube thermocouples.

Consequently, although temperature measurements in the condensing stream indicated the general area in which the liquid-vapor interface was located, they could not be used to pinpoint this location. Thus, the temperature gradient of the coolant was used to determine the average interface location. Coolant fluid temperature measurements were made with immersion thermocouples at the inlet and exit to the condenser shell and in the two external connectors of the condenser shell, one-third and two-thirds of the distance along the condenser.

The interface at each operating condition was located by:

1) Calculating the heat balance between the coolant and the condensing fluid in the subcooled region of the condenser in order to obtain the coolant temperature at the liquid vapor interface, and

2) Graphically extrapolating the measured coolant temperatures to the calculated coolant temperature at the interface. Typical plots of condenser temperature versus length in which this extrapolation has been made are shown in Figure 15. The four operating conditions in Figure 15 were chosen to show the interface progressively farther upstream from the condenser exit.

Checks on the accuracy and consistency of the data were provided by:

1) Oscillograph recordings taken before and after data were manually read. The recordings were compared to make sure a steady state existed during the period in which data was taken.

2) Calculated heat balances between the power loop and radiator loop. Data points which showed differences between the calculated enthalpy changes in the two loops in excess of 5 per cent were discarded. An average difference of 2 per cent was obtained.

3) A plot of NTU (condensate) = $U A_s / wC_p$ (condensate) in the subcooled region of the condenser versus the determined subcooled length. The NTU - subcooled length plot is shown in Figure 16, with a best-fit

---

[1] Wyde, S. S. and H. R. Kunz, Experimental Condensing-Flow Stability Studies, NASA CR-54178, PWA-2315

straight line drawn through the data. An approximate straight-line relationship is theoretically predicted, because from the heat transfer equation $wC_p \; \Delta T_{sc} = U \phi l_{sc} \Delta T_m$:

$$l_{sc} = \frac{wCp}{U\phi} \left(\frac{\Delta T_{sc}}{\Delta T_m} \right) = \frac{wCp}{U\phi} \left(\frac{UA_s}{wCp} \right) \qquad (3)$$

and w $Cp/U\phi$ is nearly constant since U changes with w to a power near one. Since the ratio $\Delta T_{sc}/\Delta T_m$ may be calculated from measured temperatures, the scatter of the data is a measure of the inaccuracies in taking the data and determining the subcooled length. The scatter in subcooled length is seen to be about 4 per cent, except at large subcooled length. At large subcooled lengths the difference between the measured temperatures used to calculate $UA_s/w\,Cp$ becomes small compared to the accuracy of the measurements, so more scatter is to be expected. Data points differing more than ±2 per cent from the best-fit line at small subcooled lengths were discarded.

b) Discussion of Results

The approximate expression for heat transfer in the condenser given in Equation (1) was used to derive equations for the linearized change of interface position produced by separately changing each of the independent variables around the nominal design operating point. These derivations are presented in Appendix F, together with estimated values of constants in the simulator which are required to evaluate the equations. Calculated values of various slopes at the nominal design point are compared below to slopes obtained from the data plots.

	Calculated	Data
$\partial I / \partial P_{sat} \left(\frac{\%\ \text{cond. length}}{\text{psi}} \right)$	-0.071	-0.062
$\partial I / \partial w_{cool} \left(\frac{\%\ \text{cond. length}}{\text{lb/hr}} \right)$	-0.00015	-0.00015
$\partial I / \partial w_{\substack{power\\loop}} \left(\frac{\%\ \text{cond. length}}{\text{lb/hr}} \right)$	0.0053	0.0056
$\partial I / \partial T_{\substack{cool\\in}} \left(\frac{\%\ \text{cond. length}}{°\text{F}} \right)$	0.022	0.019

The calculated values agree with the experimental values reasonably well. This suggests that by using basic heat transfer equations in which secondary effects are neglected, the relation between interface position and other condenser variables may be adequately expressed in a simple analytic form.

3. Condenser Maps with Coolant Outlet Temperature Controlled

Control of the condensing pressure must be maintained over a wide range of operating conditions when the powerplant is started in space. Since the radiator metal may be considerably colder prior to starting than during steady-state operation, the radiator-loop fluid temperature at the condenser-shell inlet would initially be lower than its steady-state value, and remain so until the relatively great heat capacity of the radiator metal and radiator-loop fluid have been overcome by heat rejected from the condenser. By use of a condenser-shell bypass and a valve, the condenser-shell flow rate can be regulated between zero flow and its design value to compensate for the low shell-inlet temperature and other starting conditions. In this way the local heat transfer rates in the condenser may be adjusted to provide a suitable condensing pressure as conditions change.

Tests were made to investigate the effect of changing the power-loop flow rate and condenser-shell inlet temperature when the condenser-shell flow rate was controlled so as to maintain the condenser-shell exit temperature constant at its nominal design value. The electrohydraulic control valve in the radiator loop maintained the desired temperature to within ±1.5°F by regulating the condenser-shell flow rate. The purpose of these tests was to determine if maintaining the condenser-shell exit temperature constant keeps the variation of condensing pressure within acceptable limits as conditions change within the normal operating range of the powerplant. Should this prove to be true, then the condenser-shell flow control could be operated automatically by a signal from a thermocouple at the condenser-shell exit, as was done on the simulator, or could be preprogrammed from calculations or experimental data to maintain a constant exit temperature during starting and changes in operating conditions, and in this way maintain adequate control over the condensing pressure.

The methods described in the previous section for determining interface position were used in these tests, and the same checks for accuracy and consistency were applied. The data is listed in Table 3, Appendix D, and plotted in Figures 17 and 18. Values of (UA/wC_p) are plotted versus subcooled length for this data in Figure 19.

The data show that the change produced in the steady-state condensing pressure by changing the power-loop flow rate or shell inlet temperature is lessened appreciably by maintaining the shell exit temperature constant. This can be seen by comparing Figure 13 with 17 and 14 with 18. The reduction results mainly because the temperature difference driving heat transfer in the condenser changes less as the two independent variables are changed. A change in the overall heat transfer coefficient due to changing the shell flow is a secondary effect. The characteristics of the condenser in the powerplant simulator were such that when the condenser-shell exit temperature was held constant, change in the pressure-interface relationship due to change in the condenser-shell inlet temperature was almost eliminated, as seen in Figure 18. This indicates that the condenser-shell exit temperature could be a very effective control variable during the starting period, when the condenser-shell flow control must compensate for the initially-low shell-inlet temperature, in order to maintain a condensing pressure high enough to prevent pump cavitation. In order to further investigate this effect, the range of variation of shell inlet temperature was extended at one condensing pressure. The shell temperature data from these tests are plotted in Figure 20, and the interface position at different inlet temperatures is indicated.

B. Boiler Performance Maps

1. General Discussion

The pressure drop in a forced-convection boiler depends on the variation of quality and liquid fraction in the boiler. This dependency results in a pressure drop versus flow rate characteristic in the boiler which differs significantly from the characteristic in a single-phase element. This pressure versus flow characteristic is affected by system variables which affect the heat flux in the boiler. A typical curve of pressure drop versus flow rate for a boiler with a fixed heat input is shown below.

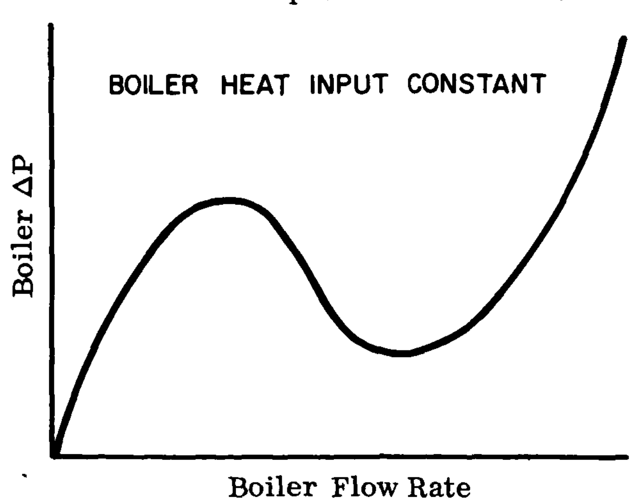

The incremental pressure drop in the boiler increases as the vapor-to-liquid flow ratio increases in an increment. If the heat-transfer rate in the boiler and the entering fluid temperature are fixed, an increase in the flow rate entering the boiler decreases the vapor-liquid ratio in a given increment and may decrease the incremental pressure drop. Consequently the negative slope shown in the curve may occur in one flow-rate region because the integrated effect of decreasing local quality by increasing the flow rate overrides the normal increase of pressure drop with an increase in flow rate.

In the SNAP 8-type boiler investigated in this task the heat input was not constant, but varied with the power-loop flow rate. Additional complications were introduced into the pressure drop characteristics of the boiler because:

1) The location at which a certain quality exists shifted from one degree of restriction to another as flow rate or heat input rate changed since variable-area inserts were used,

2) The temperature difference between the two fluids was so small that the local heat transfer rates in the boiler strongly depended on the saturation temperature of the boiling fluid, and consequently on the local pressure levels of the boiling fluid, and

3) The counterflow heating fluid in the shell of the boiler underwent a temperature drop which was sizable compared to the temperature difference between the heating and boiling fluids, so that the heat transfer rate at any locality strongly depended on the amount of heat extracted from the shell fluid before reaching that locality. The pressure drop characteristics of the boiler also depended on values of the heater-loop flow rate and inlet temperature, since these affected heat input to the boiler.

The pressure drop in the Rankine-cycle boiler (as opposed to the condenser) is typically an appreciable portion of the total Rankine-cycle pressure drop. Consequently the complicated pressure drop versus flow rate characteristic plays a significant role in interactions among system components, influencing both steady-state performance of the powerplant, and its dynamic characteristics. The steady-state tests described in this section were made to explore the effect of changes in system variables on pressure drop in a SNAP 8-type boiler, and to provide data indicating matching characteristics required between the boiler and other system components, particularly the power-loop pumps. These tests were also intended to provide data in a form suitable for use in a linearized analysis of boiler dynamic characteristics.

2. Test Results

The boiler variables considered independent for the purpose of these tests and varied, one at a time, about the nominal design point, were: boiler-shell flow rate, boiler-shell inlet temperature, power-loop flow rate, and boiler-tube inlet temperature. The turbine-simulator valve was set at its nominal design setting so that a fixed relationship among boiler exit pressure, boiler exit temperature (or quality), and flow rate was imposed at each of these data points. The boiler inlet pressure was adjusted by means of the pump throttling valve to give the desired power-loop flow rate.

In Figures 21 through 24 the boiler pressure drop is plotted against each of the independent variables. Variation of boiler exit pressure and superheat is shown in Figures 24 and 25. Three additional data points were obtained to indicate the change in boiler pressure drop produced by changing the setting of the turbine-simulator valve, and these are plotted in Figure 26. Values of $w\sqrt{T}/P$ noted beside each data point in this figure are roughly proportional to the choked area of the valve, since from isentropic relationships

$$A_{choked} = \left[\frac{w\sqrt{To}}{Po} \right] \left[\sqrt{\frac{K}{R}\left(\frac{2}{K+1} \right)^{\frac{K+1}{K-1}}} \right] \tag{4}$$

and the second term on the right is nearly constant for a limited range of temperature variation.

Figure 27 shows the variation of boiler pressure drop with pinch-point temperature difference as each of the independent variables is changed.

In order to check the accuracy and consistency of the data the following tests were applied and data points which fell outside a prescribed tolerance were discarded.

1) Oscillograph recordings of the system variables were taken before and after data was manually read, and were compared to make sure that a steady state had been attained.

2) Heat balances among the heater loop, power loop, and radiator loop were calculated. Data points which showed differences in the calculated enthalpy changes in the three loops in excess of 5 per cent were discarded. An average difference of 3.2 per cent was obtained.

3) The value of $w\sqrt{T}/P$ at the inlet to the choked turbine-simulator valve setting was calculated. The average value of this parameter at the design setting of the turbine-simulator valve was 59.5 $in^2/hr\sqrt{°F}$ lb_m/lb_f.

Data points with a design setting of the turbine-simulator valve which deviated more than 1 per cent from the average value were discarded.

The data appears in Table 4, Appendix D, together with the check values. Approximate values of the boiler pinch-point temperature difference were calculated as follows. A constant 4 psi pressure drop in the power-loop fluid between the boiler inlet and pinch point was assumed in order to calculate the power-loop fluid saturation temperature at the pinch point from the measured inlet pressure. The 4 psi pressure drop was estimated for design conditions in the absence of internal pressure measurements. Although this pressure drop changed with operating conditions, an error of one psi in the assumed value only produced an error of 0.5°F in ΔT_{pp}, or approximately 2 per cent. The shell fluid temperature at the pinch point was calculated by adding the heat transferred to the power-loop stream in the subcooled region of the boiler to the exit enthalpy of the shell fluid. Consequently the equation used to calculate the pinch-point temperature difference was:

$$\Delta T_{pp} = T_{\substack{\text{boiler}\\\text{shell}\\\text{exit}}} + \left[\left(T_{\substack{\text{sat at boiler-}\\\text{tube inlet pres-}\\\text{sure minus 4 psi}}} - T_{\substack{\text{boiler}\\\text{tube}\\\text{inlet}}} \right) \times \frac{w_{\text{power loop}}\, C_p}{w_{\text{heater loop}}\, C_p} \right] - T_{\substack{\text{sat at boiler}\\\text{tube inlet pressure}\\\text{minus 4 psi}}} \tag{5}$$

The pinch-point temperature difference ΔT_{pp} is a possible correlating parameter for the effect of certain variables on boiler pressure drop. The pinch point in a counterflow boiler occurs where bulk boiling begins, as seen in Figure 7. The minimum temperature difference driving heat transfer in the boiling region occurs at the pinch point, so that the temperature difference at this point carries the most weight in determining the average heat transfer rate and consequently the local qualities in the boiler. If a reasonable correlation exists between ΔT_{pp} and the boiler pressure drop, then the effect of system variables on boiler pressure drop may be expressed in a much simpler form when data on a given boiler is available, because the relationship between shell-fluid flow rate and inlet temperature and the ΔT_{pp} is fairly straightforward. A plot of boiler pressure drop versus ΔT_{pp} with variation in heater-loop flow rate, power-loop flow rate, heater-loop boiler-inlet temperature and power-loop boiler-inlet temperature is shown in Figure 27.

These data plots show a similar, though not identical, trend as heater-fluid inlet temperature, heater-loop flow rate and power-loop flow rate are changed. The relation is quite different when the boiling-fluid inlet temperature is changed. Consequently, this data indicates that boiler ΔP cannot be correlated to ΔT_{pp} alone, and that the relationship is affected by other parameters.

It was necessary to calculate the boiler exit superheat also, expecially at low values of superheat, because imperfect distribution in the boiler tubes caused droplets of water to hit the immersion thermocouple at the boiler exit even when the bulk of the stream was superheated. Consequently, the boiler exit thermocouple often fluctuated or read the saturation temperature when other measurements indicated superheat. Boiler exit superheat was calculated from the measured temperature and pressure downstream of the turbine-simulator valve by assuming constant enthalpy between that point and the boiler exit.

The tabulated data includes readings from thermocouples attached at four-inch intervals along the outside skin of the boiler shell. This technique of measuring the shell fluid temperature does not yield the local variation of shell fluid temperature with distance with great accuracy because of imperfect mixing of the shell fluid, conduction along the shell, and heat losses. However, the overall temperature profile of the shell fluid is indicated.

Occasionally, unstable conditions which were characterized by excursions or drifting between two operating points were encountered during steady-state testing. The causes of these unstable conditions were traced to fluctuating line voltages, faulty controls, or to one or more of the boiler inlet orifices being plugged with slivers of the Teflon used to seal pipe connections in the power loop. Each of the operating points originally found unstable was rerun and found to be stable when these faults were corrected. It is worthy of note that the plugging of the inlet orifice of just one of the nineteen boiler tubes sometimes caused an unstable condition.

V. DYNAMIC RESPONSE CHARACTERISTICS

In order to investigate possible causes of unstable operation due to the dynamic response characteristics of the powerplant, tests were made in which step changes and sine-wave variations were induced in the power-loop flow rate, and the subsequent response of certain system variables was recorded. After limited testing involving the entire system, investigations were concentrated on the boiler, and the frequency response to sine-wave flow variations at the boiler inlet was obtained for different values of the controllable variables which affect the heat transfer rate in the boiler.

Data from the sine-wave input tests were reduced to show the normalized amplitude of variation and the phase lag with respect to the induced sine-wave flow-rate variation at the boiler inlet. Further reduction of this data is contingent on the possibility of being able to express the mechanisms involved in boiling heat transfer and pressure drop in a sufficiently general and simple analytic form. Uncertainties concerning such things as the boiling heat transfer coefficient and the amount of slip between the vapor and liquid phase in the boiler make the construction of a general and simple model for the dynamic characteristics of a boiler difficult. However the experimental frequency response of the power-loop boiler inlet pressure to variations in the boiler-inlet flow rate indicates pump characteristics which are required to avoid possible unstable interactions between pump and boiler.

The effect of the pressure-flow relationship imposed by a pump at the boiler inlet was directly investigated with an experimental arrangement (described in Appendix B) which allowed different negative linear pressure-flow slopes to be generated with an electrohydraulic control valve at the boiler inlet. Stability limits as a function of the pressure-flow slope were determined at different values of variables which affect heat transfer in the boiler.

A. System Response Data

Tests were made in which a step change was imposed on the power-loop flow rate by making a step change in the reference voltage of the electrohydraulic flow control at the boiler inlet. The power-loop inventory was fixed and the condenser-shell flow rate and heater-loop flow rate were constant in these tests. The temperature of the sink stream cooling the radiator simulator and the boiler-shell inlet temperature were regulated at their design values. The system variables were continuously recorded on a recording oscillograph. Before the step change was imposed, the independent system variables were near their nominal design values, listed in Table 1. Tests were made with two power-loop inventories, and with two different magnitudes of the flow-rate step, but no significant change in the form of the response resulted. Data from two of the tests is plotted in Figures 28 through 33, from which the form and the approximate time constant of the response of the system variables may be obtained.

Sine-wave variations in the power-loop flow rate were imposed with the boiler-inlet flow control at the nominal design point over the frequency range 0.01 to 1.0 cycle per second. Power-loop inventory, condenser-shell flow, and heater-loop flow were constant, and the sink temperature and boiler-shell inlet temperature were regulated as in the step-change tests. Figure 34 is a reproduction of an oscillograph recording at one input frequency, with the more active variables labeled. The data was reduced to show the phase lag and the normalized amplitude of the variation of each dependent system variable as a function of the frequency of the sine-wave input. The normalized amplitude is the ratio of the recorded amplitude of variation to the change that occurs in the variable when the power-loop flow rate is changed by the same amount at zero frequency (steady-state conditions). Figures 35 and 36 are plots of steady-state data taken in order to normalize the frequency response data, which is shown in Figures 37 through 40.

An interesting feature of this data, which will also be seen in the boiler response data presented in the next section, is that the amplitude of the variation of the boiler inlet and exit pressure rise above their steady-state values at a certain frequency, and apparently approach the zero frequency point from a normalized amplitude greater than one. The frequency response of the boiler, and its significance for system stability, will be discussed in the next section where more extensive frequency response testing on the boiler is described.

The form of the boiler exit pressure response may partially explain the condenser pressure data, which appear somewhat anomolous in that the normalized amplitude decreased at the lowest frequency in Figure 39. Since the turbine-simulator valve was choked, the flow rate through the valve was proportional to the boiler exit pressure, if changes in the boiler exit temperature are neglected. Consequently, the power-loop flow-rate variation in the condenser was not the constant amplitude variation imposed at the boiler inlet, but one which was decreasing in amplitude as frequency decreased toward 0.01 cps, as is indicated by the boiler exit pressure curve in Figure 37. Changes in boiler exit temperature (or quality) also influence the pressure-flow characteristics of the choked valve, thereby complicating the pressure-flow relationship at the boiler exit.

The radiator-loop condenser-inlet temperature also affected the condenser pressure response. However, a sizable variation in condenser-shell inlet temperature could only occur at low frequencies, since high-frequency temperature variations were damped out by the very large heat storage capacity of the radiator simulator. At frequencies low enough for the variation in condenser-shell inlet temperature to be appreciable, an influence on the amplitude and phase shift of the condenser pressure response which was not present at higher frequencies would be expected. The nature of this influence would depend on the phase relationship between variations in condenser-shell inlet temperature and variations in power-loop flow rate. This phase relationship, in turn, depended on transport time and heat capacity in the radiator loop. The effect of the condenser-shell inlet temperature may explain the anomalous behavior of the condenser pressure frequency response curves in Figure 40, where there is an apparent discontinuity below a frequency of 0.05 cps.

B. Boiler Response Data

The frequency response of the dependent boiler variables to sine-wave variations in the power-loop flow rate at the boiler inlet was obtained at five operating conditions. These operating conditions were chosen to represent pinch-point temperature differences between 20 and 36°F with different combinations of the independent boiler variables. The operating points are listed below.

Point No.	Boiler-Shell Inlet Temp.	Boiler-Shell Flow Rate	Mean Power-Loop Flow Rate	ΔT_{pp} at Mean Flow Rate
1	422°F	6400 lb/hr	233 lb/hr	35.8°F
2	414	5600	255	20.6
3	418	7900	244	33.9
4	418	4600	244	25.4
5	424	6000	244	32.0

The mean power-loop boiler inlet temperature was kept near its design value of 173°F, and the nominal design setting of the turbine-simulator valve was maintained in all of these tests. The control on the electrical power input was used to keep the boiler-shell inlet temperature at its designated value during variations in the power-loop flow rate. Time delays in the system allowed a variation of ±1°F to occur.

The data is plotted in Figures 41 through 55. Preceding the frequency response data at each operating point is a plot of experimental data showing the steady-state change in the dependent variables with power-loop flow rate. This data was used to normalize the amplitude of variation of each dependent variable to its steady-state value. The normalized amplitude is the ratio of the recorded amplitude of variation to the change that occurs in the variable when the power-loop flow rate is changed by the same amount at zero frequency (steady-state conditions).

Because of minor irregularities in the traces of the dependent variables on the oscillograph recordings (see Figure 34), some interpretation is required in reducing the data to obtain the amplitude and phase shift. In order to check the repeatability of the raw data and its subsequent interpretation, four frequencies of power-loop flow variation were rerun at operating point No. 2. This data is superimposed on the original data in Figures 55 and 56. The average deviation of the normalized amplitude from the original data is 8 per cent.

The frequency response of the boiler inlet pressure indicates the dynamic head-flow characteristics which are required in the power-loop pump in order to avoid unstable system interactions. A stability criterion for matching the pump and boiler will now be discussed. The coupling between boiler inlet pressure and pump exit pressure, and between boiler-inlet flow rate and pump-exit flow rate is represented schematically below, using control notation. It will be assumed in the following discussion that the pump exit pressure versus flow rate characteristics are linear, and there are no time delays between changes in flow rate in the pump and pump exit pressure. This assumed condition is approximated in a powerplant when the pump inlet pressure is held constant.

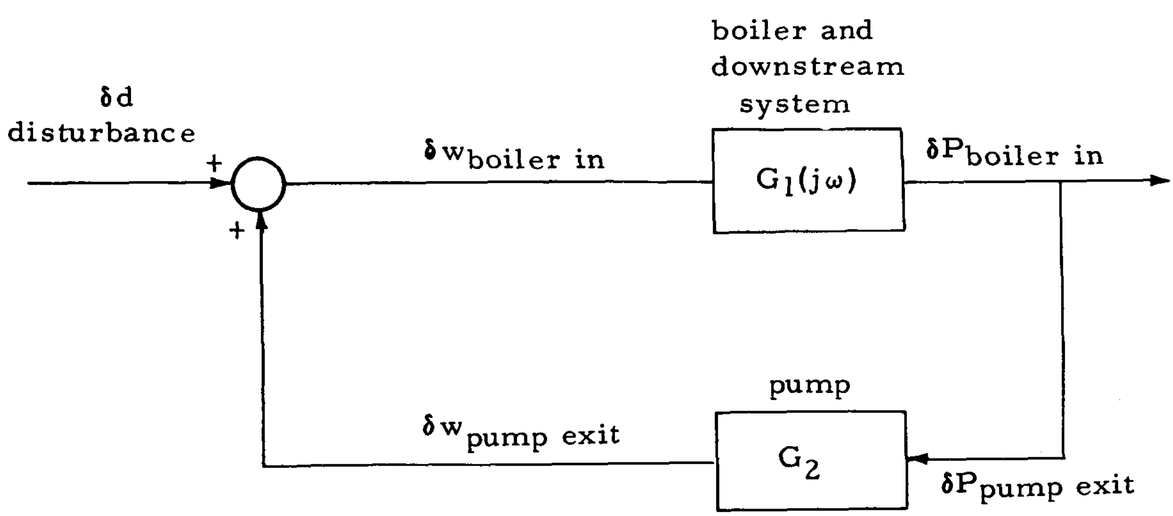

Since the fluid between the pump exit and boiler inlet is liquid and lengths involved are small, the effects of fluid compressibility and momentum are small, and the pressure and flow rates are approximately equal at the pump exit and boiler inlet. A disturbance has been assumed to be introduced into this coupled system, and the response of the boiler inlet pressure to the disturbance δd may be written

$$\delta P_{\text{boiler in}} = \frac{G_1\,(j\omega)}{1-G_1\,(j\omega)\,G_2}\;\delta d$$

If it is assumed that the boiler is stable when operated in an open loop, then the closed-loop system diagrammed would be unstable when the denominator $1 - G_1 (j\omega) G_2$ is zero, that is when

$$G_1 (j\omega) G_2 = 1$$

From the assumed linear pump characteristics

$$P_{\text{pump exit}} = A - B \; w_{\text{pump exit}}$$

It follows that

$$G_2 = \frac{\delta w_{\text{pump exit}}}{\delta P_{\text{pump exit}}} = - \frac{1}{B}$$

Consequently this simplified analysis indicates that the system is unstable when

$$G_1 (j\omega) = \frac{\delta P_{\text{boiler in}}}{\delta w_{\text{boiler in}}} (j\omega) = -B$$

The system investigated had special characteristics because of the choked restriction at the boiler exit, since the pressure downstream of this restriction was independent of the flow rate through the restriction. Consequently, the transfer function $G_1 (j\omega)$ depended only on the dynamic pressure drop versus flow rate characteristics of the boiler and the inlet pressure versus flow rate characteristics of the choked restriction.

A pump-boiler combination in a Rankine-cycle power loop is typically statically stable, in spite of a possible negative slope of the boiler pressure loss versus flow curve. That is, the steady-state value of $\delta P_{\text{boiler in}} / \delta w_{\text{boiler in}}$ is generally positive. This positive pressure-flow slope occurs because the steady-state increase in pressure at the turbine inlet is typically greater than the possible steady-state decrease in pressure drop in the boiler with an increase in flow rate. However, the above analysis indicates that a dynamic instability is possible, and that oscillations will occur at the frequency at which $\delta P_{\text{boiler in}} / \delta w_{\text{boiler in}}$ has a phase angle of 180 degree (thereby changing its sign from plus to minus) if the amplitude of $\delta P_{\text{boiler in}} / \delta w_{\text{boiler in}}$ at this frequency is equal to B.

A 180-degree phase shift in $G_1(j\omega) = \delta P_{boiler\ in} / \delta w_{boiler\ in}$ is possible because the average fluid density in the boiler does not immediately adjust to its new steady-state value after the boiler inlet flow rate is changed. This lag in the adjustment of the density of the fluid in the boiler occurs because heat flux in a two-fluid heat exchanger cannot immediately adjust to a change in inlet flow rate. The lag affects the boiler inlet pressure response in two ways:

1) The vapor flow rate at the boiler exit lags the boiler inlet flow rate. The instantaneous difference between the two flow rates is proportional to the rate of change with time of the average fluid density in the boiler. Since the pressure at the inlet to the choked restriction is proportional to the flow rate through the restriction, the consequence of a lag in boiler exit flow rate is a lag in boiler exit pressure.

2) The local pressure drop per unit length in the boiler depends on the local density (together with the flow pattern in the two-phase region). Consequently, the lag in the adjustment of the local densities in the boiler produces a lag in total boiler pressure drop.

Using the approach outlined above, the significance of boiler operating parameters for system stability may be investigated by writing an analytic expression for the transfer function $G_1(j\omega)$. Such an expression may be obtained from equations of continuity, motion, energy and thermodynamic state for the boiler and choked valve written in operational form. Analytic dynamic boiler models have been constructed with some success for boilers with simpler physical boundary conditions[1]. The fact that the boiler in this investigation was a two-fluid counterflow heat exchanger complicates the energy equation, while variable-area inserts and uncertainties concerning two-phase flow patterns in swirl flow complicate pressure drop predictions. Consequently, rather extreme simplifications are required to put an analytic dynamic model into manageable form. However, data on the frequency response of the boiler exit pressure and temperature, and the heater-loop boiler-exit temperature are available to verify certain analytic components of an expression for $G_1(j\omega)$.

A first attempt at constructing an analytical solution for $G_1(j\omega)$ was made which gave fair agreement with experimental data. It is beyond the scope of the present report to discuss this analysis in detail. However, one result of interest will be mentioned. A variation in boiler exit temperature, which modifies the pressure versus flow rate characteristics of the choked restriction, appears to be the factor which produces normalized amplitudes greater than one

[1]Quandt, E.R., Analysis and Measurement of Flow Oscillations, Chem. Eng. Prog. Symp. Series, No. 32, Vol. 57. Quandt was dealing with a boiler in which uniform heat flux, and constant inlet and exit pressures could be assumed.

in the boiler exit and inlet pressures at low frequencies. Variations in exit temperature, or especially quality, also appear to have the effect of decreasing the amplitude of the boiler-inlet pressure variation at the frequency at which its phase angle is 180 degrees. Consequently, one important way in which boiler operating conditions appear to affect boiler inlet-pressure frequency-response, and therefore system stability, is by determining the slope of temperature (or quality) versus flow rate at the inlet to the choked restriction at the boiler exit.

Table 5 shows values of the frequency and the amplitude ratio $\delta P_{boiler\ in} / \delta w_{boiler\ in}$ at which a 180-degree phase shift occurs between boiler inlet pressure and flow in the data from Figures 41 through 55. These are the frequency of oscillations and the unstable pump slope that would be predicted for the operating conditions of these tests by the preceding analysis. Extrapolation of the data was made to obtain these values since, in general, absolute variations experimentally recorded were too small to obtain accurate data at these frequencies. Values of $\delta P_{boiler\ in} / \delta w_{boiler\ in}$ were obtained by multiplying the normalized amplitude of the boiler inlet pressure variation by the experimental steady-state values of $\Delta P_{boiler\ in} / \Delta w_{boiler\ in}$.

C. Boiler Stability Data

Experiments were made to directly investigate the effect on boiler stability of changing the pressure-flow relationship imposed at the boiler inlet. Power-loop flow rate, boiler-shell flow rate, and boiler-shell inlet temperature were parameters in these tests.

In an actual powerplant a pressure-flow relationship would be imposed at the boiler inlet by the head-flow slope of the power-loop pump, or by the pump together with a flow control restriction between the pump exit and the boiler inlet. For the purpose of these tests on the simulator, the electrohydraulic flow control at the boiler inlet was used to impose a linear negative pressure-flow slope that could be independently varied between zero and infinity. The electric circuit constructed to enable the control unit to perform this function is described in Appendix B.

The test procedure and the observed instabilities are described qualitatively below, and then plots of data showing the effect of different operating conditions on stability limits are discussed.

1. Description of Test Procedure and Observed Instabilities

At a given set of steady-state operating conditions, a pressure-flow slope at the boiler inlet was first established which gave stable operation. By means of the control system described in Appendix B, the imposed slope, which governed the relationship between boiler inlet flow rate and pressure during perturbations in either flow rate or pressure, could be changed independently of the steady-state operating point. This slope was gradually increased towards zero at the same steady-state operating conditions until unstable conditions were encountered.

As the pressure-flow slope was increased, a condition of incipient instability was first encountered. This condition was characterized by small perturbations in inlet flow rate above and below the steady-state operating flow rate. The timing and magnitude of these perturbations were irregular. As the slope was further increased, the maximum amplitude of the flow-rate perturbations became greater. Finally (in most of the tests), a pressure-flow slope was reached at which regular flow oscillations began. After the oscillations began, the imposed slope was kept at the same value, but the amplitude of the flow oscillations continuously increased until the control valve at the boiler inlet was cycling between full open and full closed, and it was necessary to return to a stable operating point to prevent damage to the rig. In order to return to a stable operating point by means of the slope control, it was necessary to decrease the slope to a value considerably lower than that at which oscillations began, i.e., the inception and withdrawal from oscillations appeared not to be reversible. It was not possible to obtain neutral or constant-amplitude flow-rate oscillations. Figure 56 is an oscillograph recording of the divergent oscillations.

2. Stability Maps

The test described above was performed at 13 steady-state operating conditions. Power-loop flow rate, boiler-shell inlet temperature and boiler-shell flow rate were changed one at a time to two steady-state values above and two values below the design operating point.

An attempt was made to map the region of incipient instability by arbitrarily defining the limit of the region by the minimum pressure-flow slope at which flow perturbations of 5 lb/hr or greater were encountered. The minimum pressure-flow slopes at which such perturbations were encountered at different steady-state operating points are plotted in Figure 57. Since these flow perturbations were extremely irregular, it is reasonable to expect that the probability of encountering a perturbation of a given magnitude would increase with the time period over which observation was made at a given slope setting. Since the time available for observation at each slope setting was limited, the scatter exhibited by the incipient instability points in Figure 57 might be expected.

The onset of divergent oscillations was immediately evident since the change from irregular flow perturbations to regular flow oscillations was a marked one. The minimum pressure-flow slope at which oscillations began at the different steady-state operating conditions are also plotted in Figure 57. The apparent trend is towards a zero slope as the operating conditions approach those which produce saturated vapor at the boiler exit at steady state. The approximate value of each of the three steady-state variables at which the boiler exit temperature reaches the saturation temperature has been noted in Figure 57. A possible explanation of this trend is the fact that the steady-state change of boiler exit temperature with flow rate increases as saturation conditions at the exit are approached. The effect of a change in boiler exit temperature on the boiler inlet pressure response was discussed in the previous section.

The 0.32 cps frequency of oscillation shown in the oscillograph recording, Figure 56, was typical of the oscillation frequency encountered in all of these tests. This agrees well with the extrapolated frequencies at which $\delta P_{boiler\ in} / \delta w_{boiler\ in}$ is at a phase angle of -180 degrees in the frequency-response data (0.27 to 0.32 cps, see page 68). The pressure-flow slope at which divergent oscillations began, plotted in Figure 57, may be compared to the extrapolated amplitude of $\delta P_{boiler\ in} / \delta w_{boiler\ in}$ ($\angle$-180 degrees) from the frequency-response data at three operating conditions. These values are tabulated below, with the value of the variable which was changed from its nominal design value listed. Frequency-response tests 1 and 2 are not directly comparable to the stability data because more than one variable was changed in those tests.

Frequency-Response Test No. (Fig. No.)	Variable Value	$\dfrac{\delta P_{boiler\ in}}{\delta w_{boiler\ in}}$ ($\angle$-180 degr.) From Frequency Response Tests	Experimental Pressure-Flow Slope for Divergent Oscillations
3 (47, 48, 49)	boiler-shell flow (7900 lb/hr)	0.048	0.011
4 (50, 51, 52)	boiler-shell flow (4600 lb/hr)	0.005	0.0018
5 (53, 54, 55)	boiler-shell inlet-temp. (224°F)	0.051	0.013

The unstable slope predicted from the frequency-response tests falls between the slopes at which incipient instabilities and divergent oscillations were encountered in the stability tests except for the first test listed above, where the incipient instability data is questionable. On the basis of this limited testing, the predicted unstable slopes apparently follow the trend of the experimental slopes at which divergent oscillations began, and are approximately four times as great.

Delays in the action of the control system used to create the dynamic pressure-flow slope at the boiler inlet represent a possible source of error in the stability testing. These delays would cause the slope actually imposed in a dynamic situation to deviate from the slopes obtained from static calibrations. However, since the delays are estimated to be two orders of magnitude less than the frequency of oscillations encountered, it is felt that the error introduced by the control delays is not great.

VI. CONCLUDING REMARKS

The data presented in this report describes steady-state and dynamic interrelationships among powerplant variables that might be expected in a SNAP 8 - type powerplant.

The following observations, based on the test results, may be made concerning the problems of controlling condensing pressure and maintaining stable boiler operation.

A. The experimentally-determined change in the condensing pressure-condenser interface-position curve produced by changing the values of the power-loop flow rate and the coolant flow rate and inlet temperature around the nominal design point was predicted with reasonable accuracy by using simplified heat transfer equations. Since the condenser interface position may be related to system operating conditions by the requirement of constant fluid inventory in the power loop, the relationships required to design a control to regulate condensing pressure in a powerplant with a fixed-inventory Rankine-cycle loop may therefore be amenable to analysis.

B. A control designed to keep the condenser-coolant outlet temperature at its design value by regulating the coolant flow rate in the condenser shell maintains the condensing pressure very near its design value as the coolant inlet temperature (or radiator outlet temperature) changes.

C. The steady-state slopes of boiler pressure drop versus pinch-point temperature difference exhibited similar trends as boiler-shell inlet temperature, shell flow rate, and boiling-fluid flow rate were independently changed around the design operating point. However, the differences in individual slopes were great enough to indicate that boiler ΔP cannot be correlated to ΔT_{pp} alone, and that the relationship is affected by other variables.

D. According to an approximate stability criterion, system instabilities occur when the dynamic pressure-flow slope at the boiler inlet is equal to or more negative than the feed system pressure-flow slope at the frequency at which a 180-degree phase shaft occurs between boiler inlet pressure and flow rate. Stability data showed that this criterion, when applied to experimental frequency-response data, indicated the correct trend for the onset of instabilities as powerplant parameters are changed.

E. A technique was demonstrated for experimentally determining pump characteristics required for stable operation with a boiler of given operating characteristics. This technique employed an electrohydraulic control valve with feedback from both boiler inlet pressure and flow rate in order to create an independently controllable pressure-flow slope at the boiler inlet. Using this technique, the simulator boiler was found to be stable with pump slopes greater than those normally encountered in a powerplant of this type. However, since the pump slope at which instabilities occurred showed a dependency on power-loop flow rate, heater-loop flow rate, and heater-loop inlet temperature, the possibility exists that changes in operating conditions or design of the boiler might cause instabilities.

APPENDIX A

Details of Simulator Flow Passages

Figures 1 and 3 are referenced for notation.

A. Loop Flow Areas vs Length

The approximate flow areas and calculated fluid transport times versus length in the heater loop, power loop and radiator loop are shown in Figures A1, A2 and A3.

B. Line Sizes (excepting small areas for special fittings)

Pipe sizes given below are nominal.

1. Heater loop - 2-inch stainless steel pipe (9.3 ft)

2. Power loop

   Boiler exit to turbine simulator valve - 3/4-inch stainless steel pipe (1.8 ft), 0.824 inch in inside diameter, 0.113 inch wall

   Turbine-simulator valve to condenser inlet - 2-inch copper tubing (4.9 ft), 1.875 inch in inside diameter, 0.0625 inch wall

   Condenser exit to boiler inlet - 1/2-inch stainless steel pipe (20 ft), 0.402 inch in inside diameter, 0.049 inch wall

3. Radiator loop

   Condenser shell bypass - 1-inch copper tubing (2.3 ft)

   Condenser shell inlet and exit - 3/4-inch copper tubing (2.2 ft)

   Radiator segment inlet and exits - 1 1/2-inch copper tubing (7.5 ft total)

   Remainder (including external radiator manifolds)-2 1/8-inch copper tubing (23.2 ft)

4. Lines from accumulator to power-loop pump inlet - 3/4-inch stainless steel tubing (12 ft)

C. Insulation

1. Heater loop - 1.0 inch thickness, Thermobestos (standard steam pipe insulation, approximate thermal conductivity 0.05 Btu/hr - ft - °F) throughout, except at pipe joints.

2. Power loop - approximately 1.0 inch thickness of Thermobestos from the boiler exit to the inlet to the condenser. A single layer of asbestos tape was wrapped on the line from the condenser exit to the boiler inlet.

D. Valve Sizes (see Section III for description of automatic control valves)

A. 1/2-inch ball valve (turbine-simulator valve)
B. 1/2-inch ball valve (normally completely open)
C. 1/2-inch gate valve (normally completely open)
D. 2-inch gate valve (heater-loop pump bypass control)
E. 1-inch gate valve (normally completely open)
F. 1-inch gate valve (condenser-shell bypass pressure drop control)
G. 2-inch gate valve (normally completely open)
H. 1-inch gate valves (radiator segment on-off, and pump throttling)
I. 1/2-inch ball valves (accumulator on-off)

E. Lines From Power-Loop Pressure Taps to Gages

1/4-inch copper tubing. These lines could be cut off at the pressure tap for transient operation. The approximate length of lines from numbered pressure taps (Figure 3) to gages is as follows:

6	12.6 ft
7	19.2
8	20.3
9	21.1
10	17.4
11	19.4
13	18.8

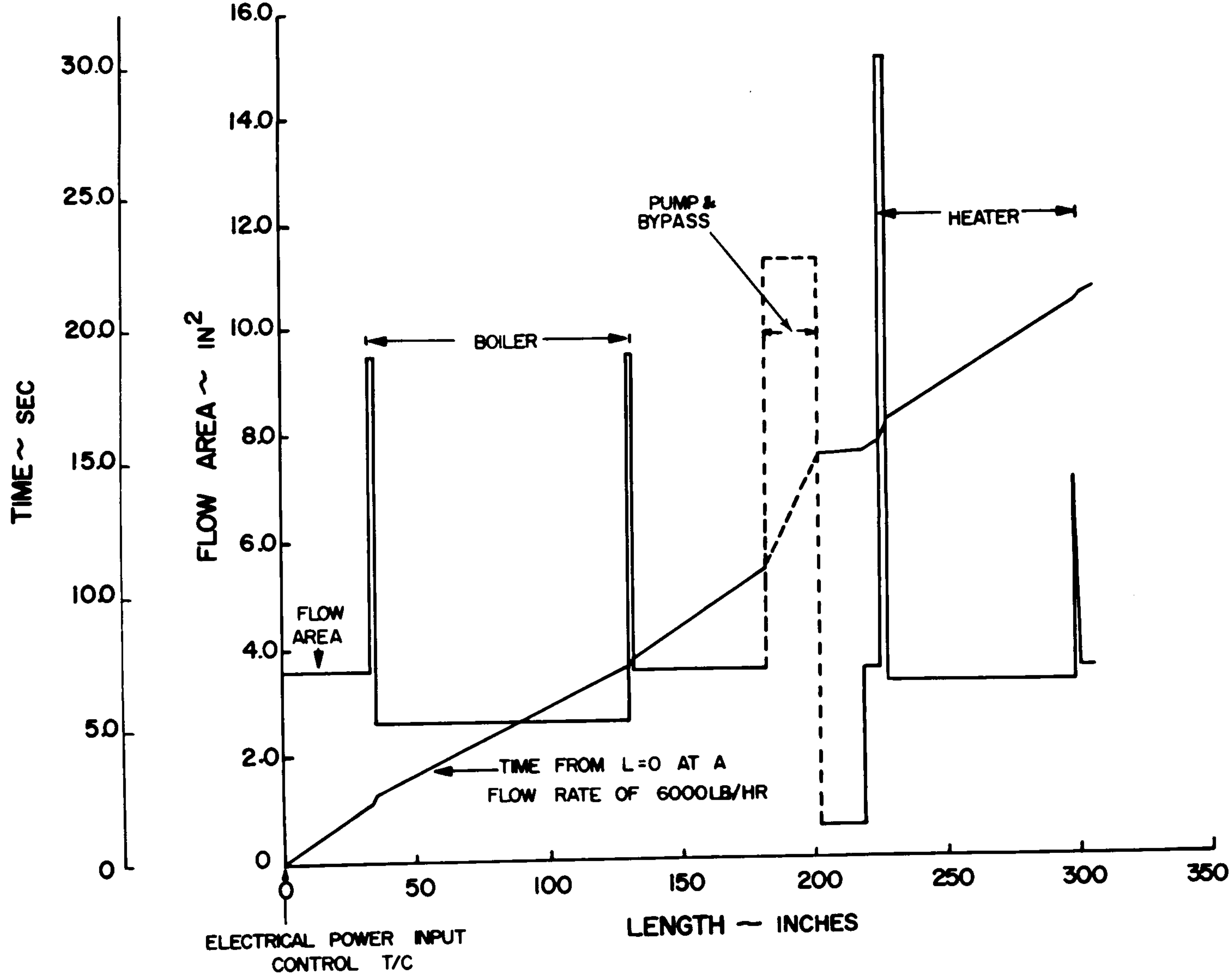

Figure A1 Heater-Loop Flow Area and Fluid Transport Time vs Length

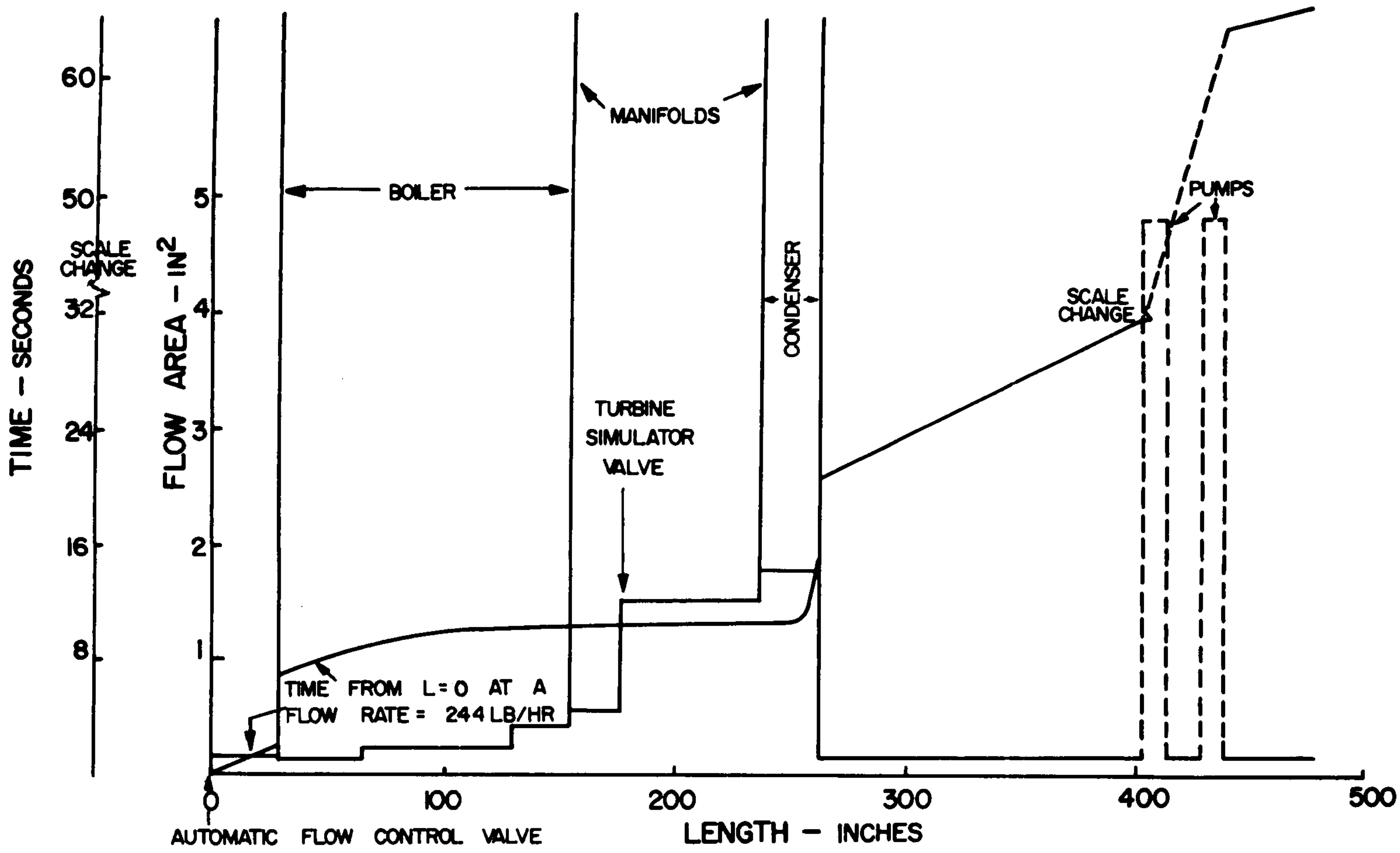

Figure A2   Power-Loop Flow Area and Fluid Transport Time vs Length

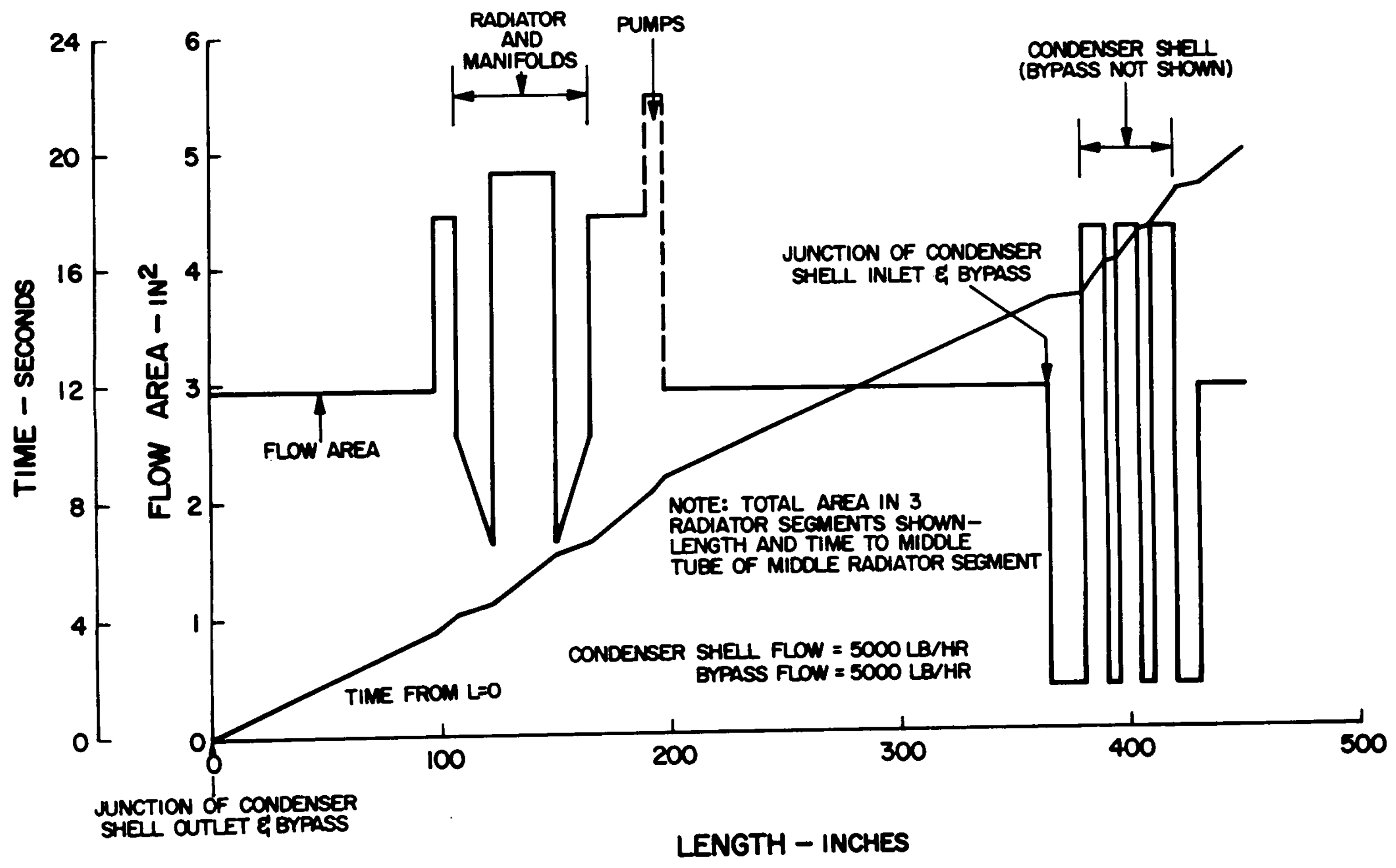

Figure A3 Radiator-Loop Flow Area and Fluid Transport Time vs Length

APPENDIX B

Auxiliary Control Circuits

1. Slope Circuits

Auxiliary electric circuits were constructed to be used with electrohydraulic control valves to provide variable "slopes" at the power-loop boiler inlet and at the condenser exit in the radiator loop. The purpose of using the boiler-inlet control to simulate different pump (pressure-flow) slopes has been described in Section V of this report. The condenser-shell control was designed to provide a variably proportional relationship between condenser-shell flow and condenser-shell exit temperature.

a. Description of Circuits

A block diagram of the electrohydraulic control unit is shown in Figure B1. In normal use, this control operates to maintain a variable such as pressure or temperature at a designated fixed level by controlling the position of a control valve. The voltage input to the "set point" designates this level. A signal is fed back from the controlled variable to the "process input", compared to the set point voltage, and the difference between the two voltages, the error signal, drives the valve in such a way as to maintain the variable at the desired value. The manufacturer's frequency-response curve for the electrohydraulic actuator is reproduced in Figure B2.

The auxiliary slope circuit, which is identical for both applications, is shown in Figure B3. This circuit provides a dual feedback to the control unit by putting a signal from a second variable into the set point. Consequently the error signal which activates the control valve now depends on two variables. The relative effect of the two variables depends on the settings of the gain potentiometers in this circuit.

At the boiler inlet, a signal from a turbine flowmeter, which has been translated into a DC voltage level, is put through the auxiliary circuit into the process input. An amplified DC signal from a strain-gage pressure transducer is put through the auxiliary circuit into the set point. Both of these sensors are immediately downstream of the control valve. Since the amplitude of the signals from the sensors is proportional to the amplitude of the sensed variables (negatively proportional in the case of pressure) the effect of the dual input is to make the valve act to produce a linear variation of pressure with flow rate at the valve exit when one of these variables is independently changed. The slope of this linear variation may be changed by changing the settings of the gain potentiometers.

The condenser-shell control circuit was designed to act in a similar manner to provide a variable linear increase in flow rate with condenser-shell exit temperature.

b. Calibration of Circuits

Consider the process input side of the auxiliary circuit which is shown below.

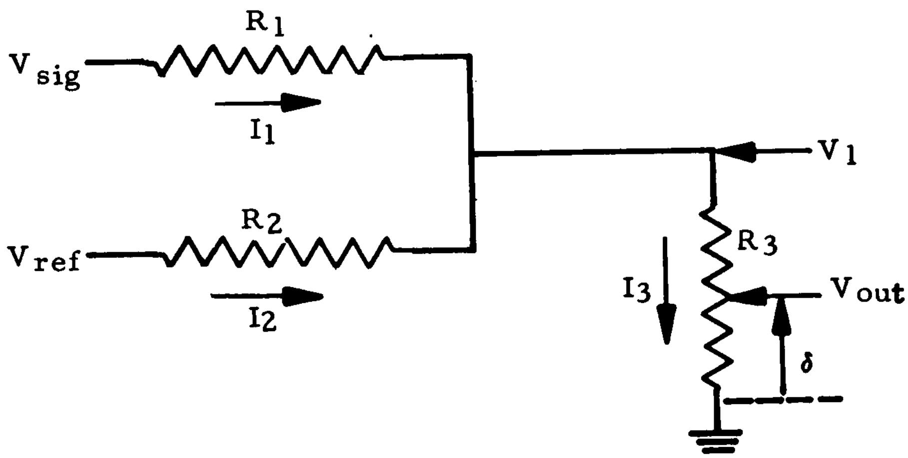

Since $I_1 + I_2 = I_3$

$$\frac{V_{sig} - V_1}{R_1} + \frac{V_{ref} - V_1}{R_2} = \frac{V_1}{R_3}$$

$$\frac{V_{sig}}{R_1} + \frac{V_{ref}}{R_2} = V_1 \left[\frac{1}{R_3} + \frac{1}{R_1} + \frac{1}{R_2} \right]$$

Or, since $R_1 = R_2$ in the circuit

$$\frac{V_{sig} + V_{ref}}{R_1} = V_1 \left[\frac{1}{R_3} + \frac{2}{R_1} \right]$$

$$V_1 = (V_{sig} + V_{ref}) \left[\frac{1}{\frac{R_1}{R_3} + 2} \right]$$

and

$$V_{out} = \delta_1 V_1 = \delta_1 (V_{sig} + V_{ref}) \left[\frac{1}{\frac{R_1}{R_3} + 2} \right]$$

The set point input side is identical except that the gain potentiometer is reversed with respect to ground, so that

$$V_{out} = (1 - \delta_2) V_1 = (1 - \delta_2)(V_{sig} + V_{ref}) \left[\frac{1}{\frac{R_1}{R_3} + 2} \right]$$

At a given operating point, as defined by values of the two variables, the input to the electrohydraulic control unit must be such that

$$V_{out\,(process)} = K_1 V_{out\,(set\ point)}$$

so

$$\delta_1 (V_{sig} + V_{ref})_p \left[\frac{1}{\frac{R_1}{R_3} + 2} \right]_p = K_1 (1 - \delta_2)(V_{sig} + V_{ref})_{sp} \left[\frac{1}{\frac{R_1}{R_3} + 2} \right]_{sp}$$

or since

$$\left[\frac{1}{\frac{R_1}{R_3} + 2} \right]_p = \left[\frac{1}{\frac{R_1}{R_3} + 2} \right]_{sp}$$

$$\delta_1 (V_{sig} + V_{ref})_p = K_1 (1 - \delta_2)(V_{sig} + V_{ref})_{sp}$$

Considering the control used at the power-loop boiler inlet

$$V_{out\,(process)} = K_2 \times \text{flow rate}$$

$$V_{out\,(set\ point)} = -K_3 \times \text{pressure}$$

With the V_{ref}'s set at a value to obtain a given operating point, the pressure-flow slope through this operating point will be

$$\frac{\partial(\text{pressure})}{\partial(\text{flow rate})} = \frac{-K_3\,\partial(V_{out\,p})}{K_2\,\partial(V_{out\,sp})} = \frac{-K_1K_3}{K_2}\left(\frac{\delta_1}{1-\delta_2}\right)$$

Using this relationship, tests were made to confirm that the slope controls could be accurately calibrated using the rig instrumentation.

The boiler inlet control was calibrated with the power loop filled with water at room temperature. A hand valve was installed downstream of the control valve and its associated sensors. The design operating flow rate and pressure were established by a simultaneous adjustment of the hand valve and the V_{ref}'s. Then, with a given setting of the gain potentiometers, flow rate and pressure were recorded at several settings of the hand valve. This process was repeated for several settings of the gain potentiometers. The condenser shell control was calibrated with the radiator loop at room temperature using a calibrated voltage in place of the thermocouple signal.

The results of these calibration tests are plotted in Figures B4 and B5.

The required linear relationship between slope and $\dfrac{\delta_1}{1 - \delta_2}$ was obtained with relatively minor scatter. The values of K_1, K_2, and K_3 depend, in part, upon sensors that have to be replaced frequently so that no attempt was made to obtain a standard calibration. When the stability mapping tests were run, a calibration was obtained in the region of interest after each series of tests.

If the voltage V_1 in both legs of the circuit is adjusted to zero at the operating point (by setting $V_{ref} = V_{sig}$), then the slope may be changed by changing the settings of the gain potentiometers without changing the operating point, as may be seen in the equations above. This is desirable when changing the slope during stability testing. In practice it was found that only an approximate null could be maintained at V_1.

2. Ramp Generator Circuit

A device was constructed to be used with the power-loop electrohydraulic control valve to provide a linear variation of power-loop flow rate with time during starting tests. A schematic of the circuit which provides a time-varying voltage input to the control unit set point is shown in Figure B6. The flow ramp consists of two sections as shown in the sketch below.

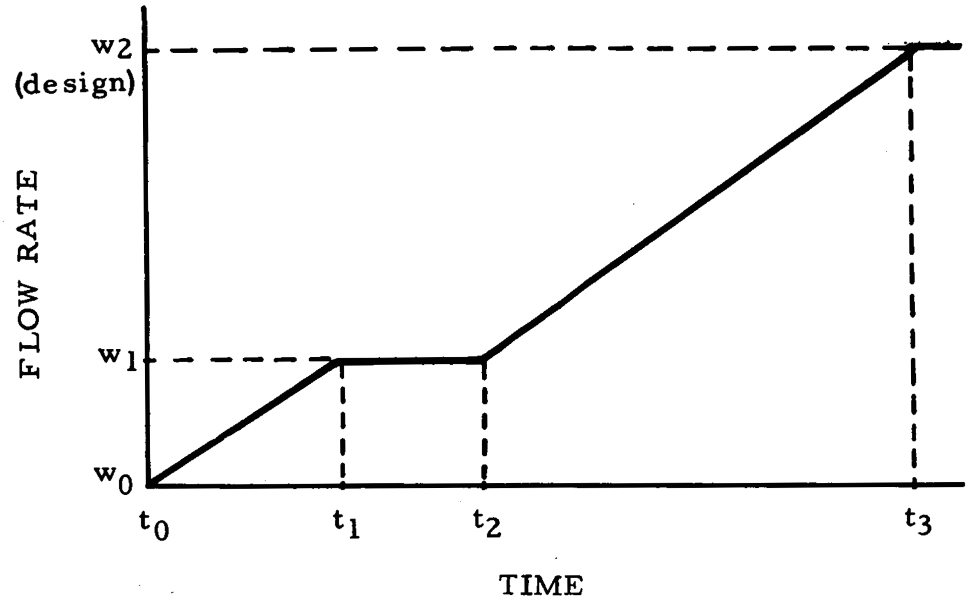

With the 100K rotating potentiometer arm fully clockwise, and the switch SW1 in the position shown in Figure B6, a voltage designating the initial flow level w_o is entered at the controller set point at time t_o. The left-hand motor is turned on and the potentiometer arm rotates counterclockwise, linearly increasing the voltage until at time t_1 the potentiometer arm is fully counterclockwise and the flow rate is w_1. A slip clutch allows the motor to continue rotating. At time t_2 switch SW1 is thrown, reversing the polarity of the clockwise terminal of the potentiometer, and the right-hand motor is turned on and rotates the potentiometer arm clockwise through a differential gear. The flow rate then increases to w_2 at time t_3. The flow levels w_1, w_2, and w_3 are set by the settings of the 50K potentiometers in the circuit.

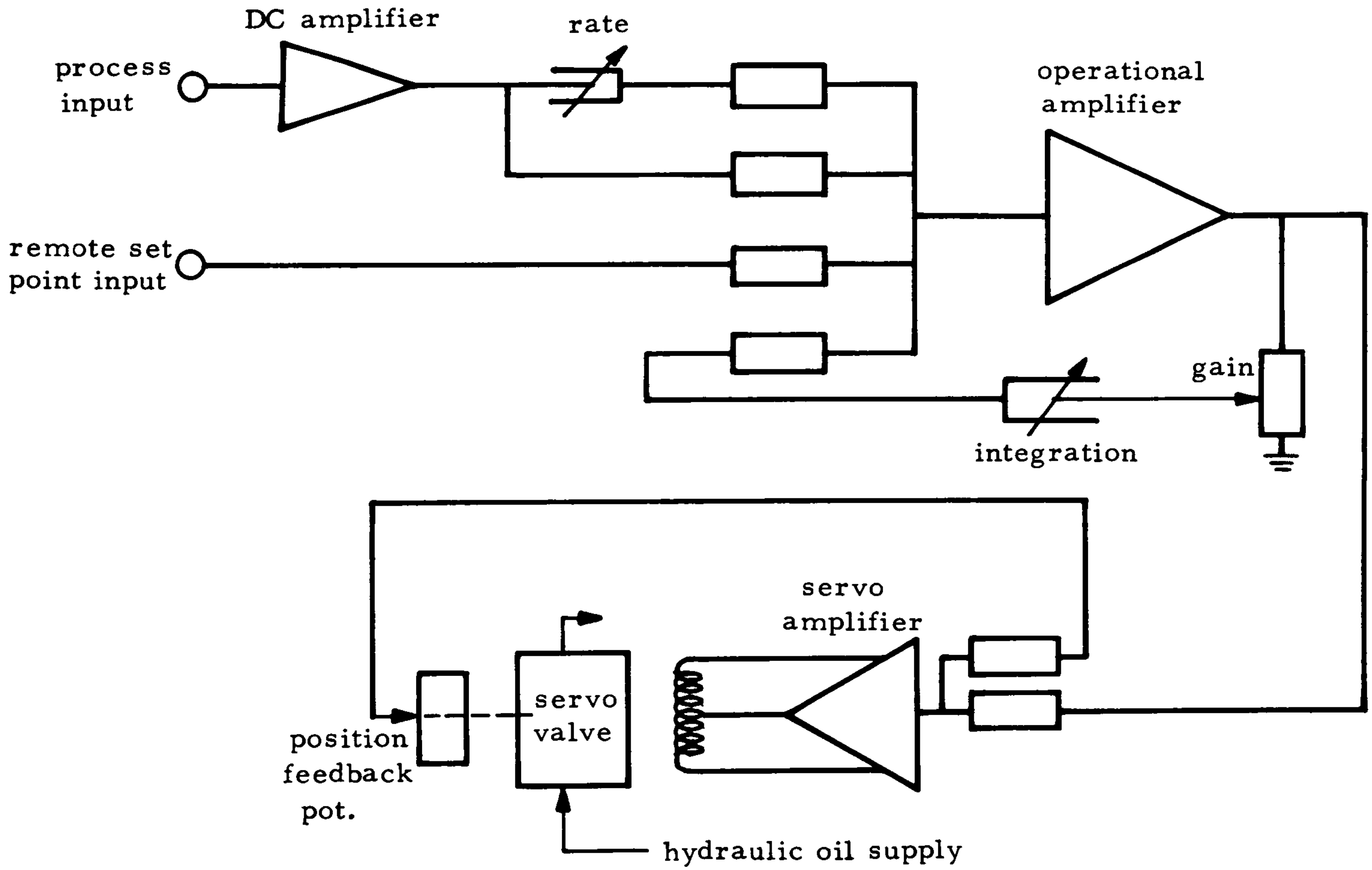

Figure B1 Block Diagram of Electrohydraulic Controls Used at Condenser Shell and Power-Loop Boiler Inlet

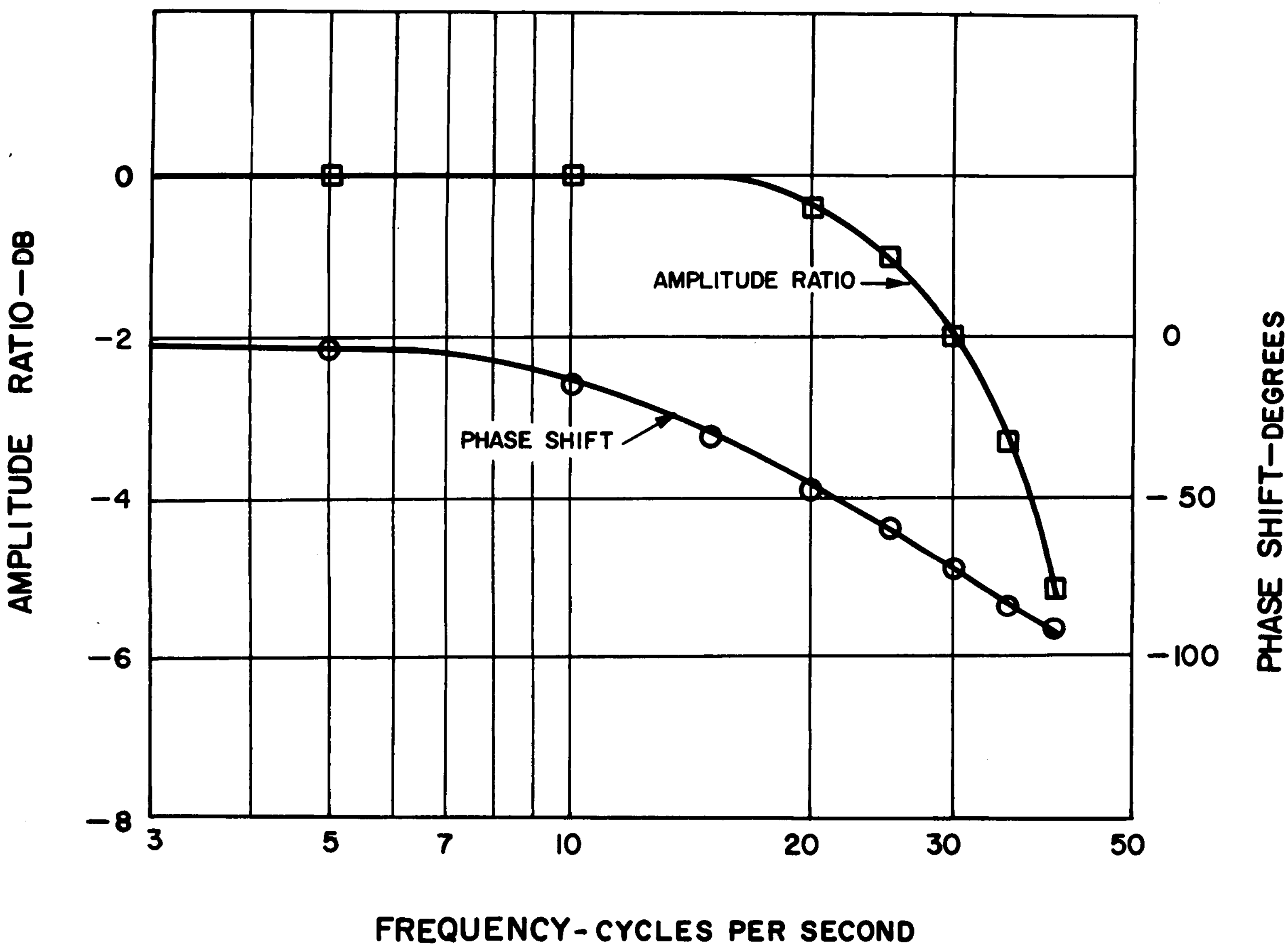

Figure B2 Frequency Response of Electrohydraulic Actuator with No External Load (Response of Valve Stroke to Electrical Signal Input). Manufacturer's Data

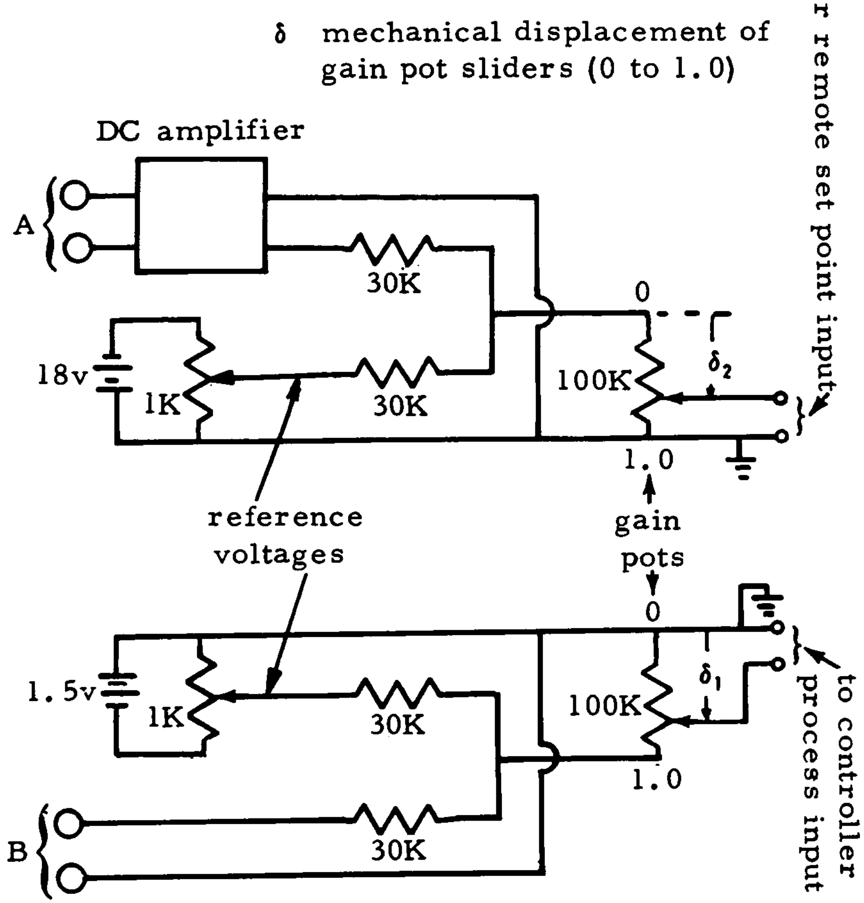

input terminal		boiler inlet flow-pressure slope control	condenser shell flow-temperature slope control
A	sensor	DC-activated strain gage pressure transducer	thermocouple
	effect of increase	close valve	open valve
B	sensor	turbine flowmeter-DC translater	turbine flowmeter-DC translater
	effect of increase	close valve	close valve

Figure B3 Circuit Diagram of Boiler-Inlet Flow-Pressure Slope and Condenser-Shell Flow-Temperature Slope Controls

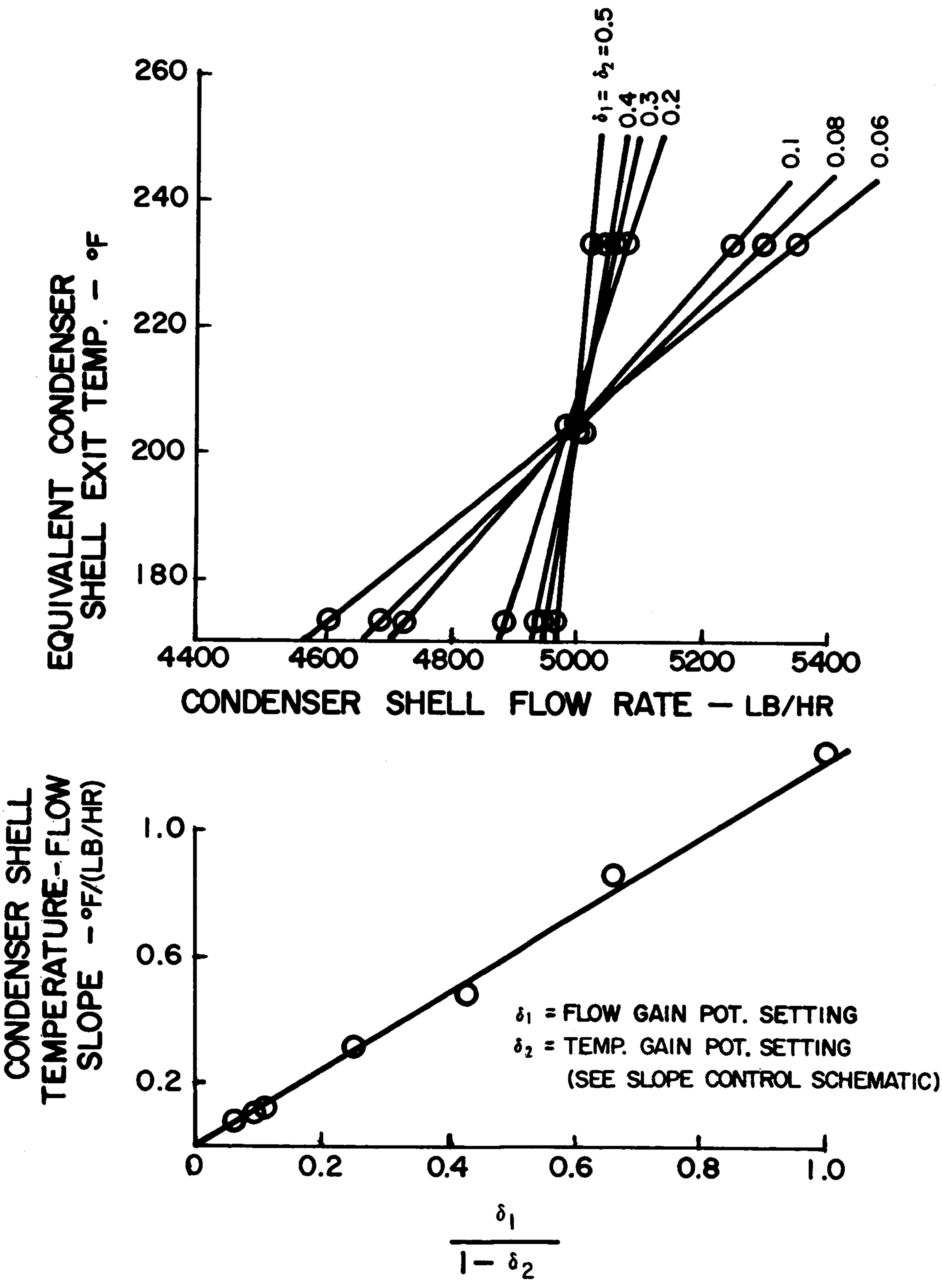

Figure B4 Condenser-Shell Temperature-Flow Slope Control Calibration Tests

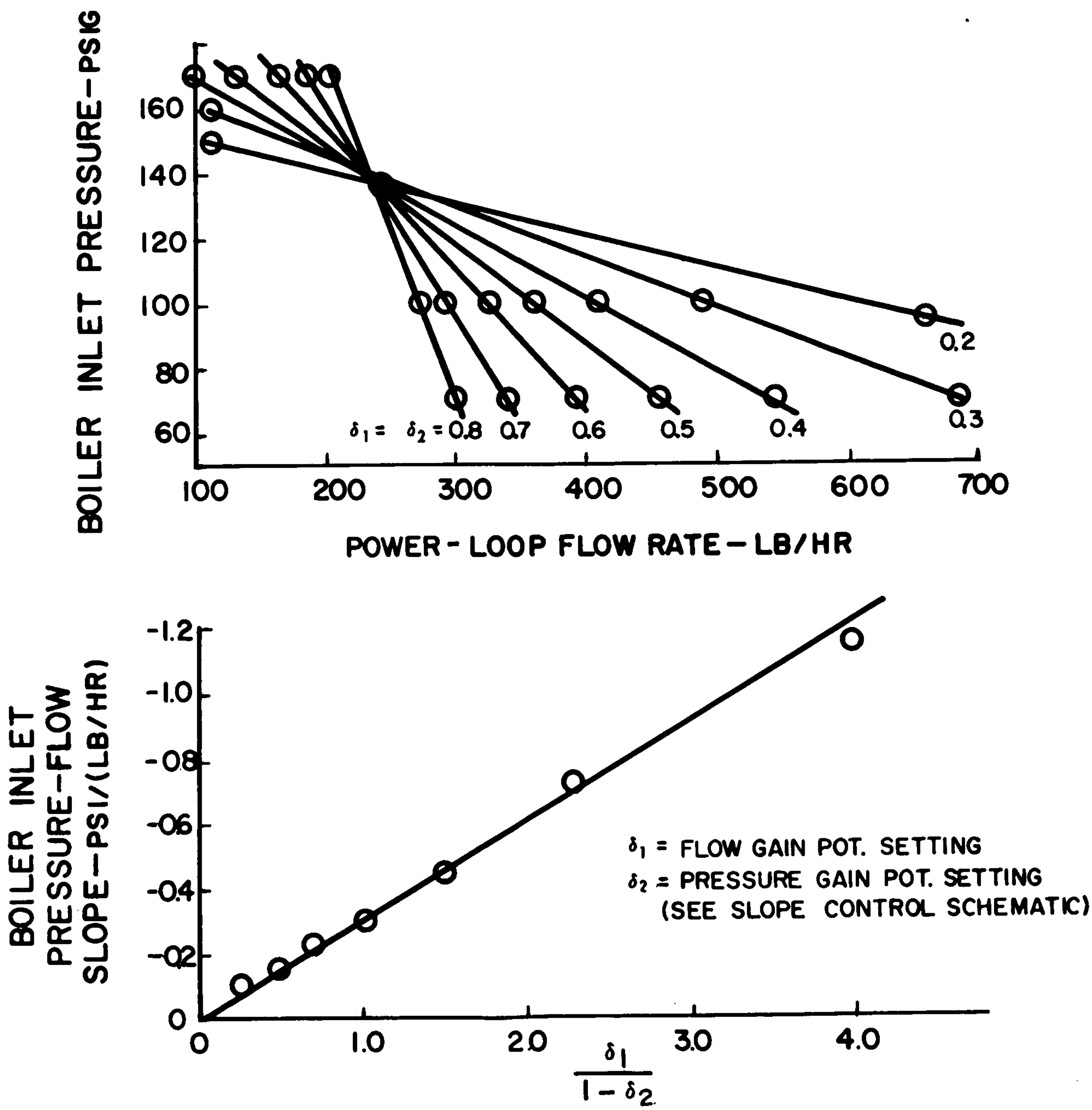

Figure B5 Boiler-Inlet Pressure-Flow Slope Control Calibration Tests

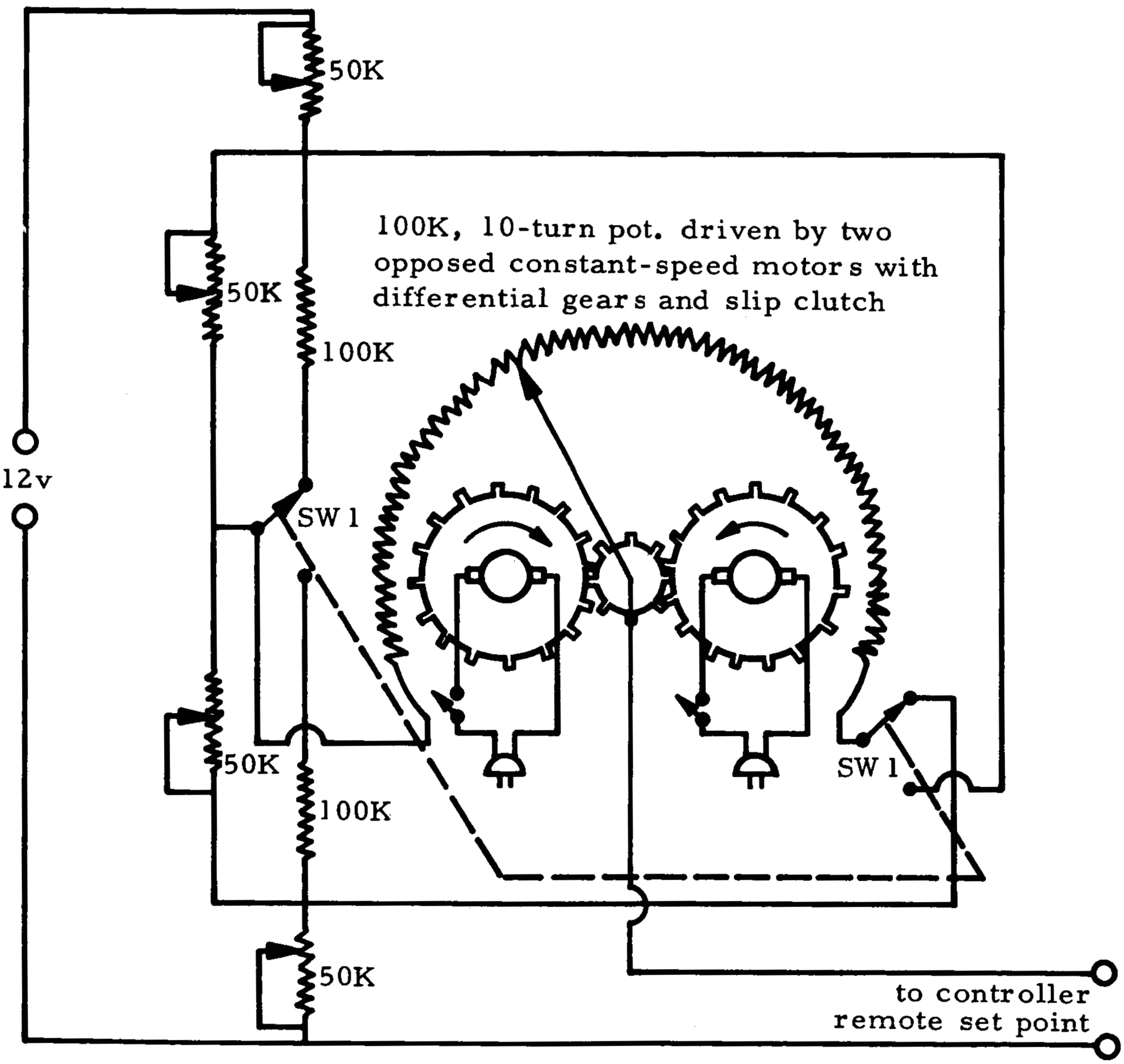

Figure B6 Circuit Diagram of Time Ramp-Flow Generator

APPENDIX C

Exploratory Boiler, Condenser and System Maps

The tests described in this appendix constituted a preliminary investigation of the operating characteristics of the powerplant simulator. One purpose of this investigation was to provide data for the selection of a nominal design operating point for the tests described in the body of the report. The design operating point (see Table 1) was selected to provide approximate correspondence to the SNAP 8 powerplant in the characteristics listed below. In the absence of analytical matching criteria, these characteristics were believed representative of the SNAP 8 powerplant for the purpose of the investigations conducted under this contract task. The characteristics used to select the nominal design operating point were:

1) The position of the liquid-vapor interface in the condenser (see Figures 12, 13, and 14 for the design interface position on curves of condensing length versus condensing pressure).

2) The following boiler operating characteristics:

   The ratio of pinch-point ΔT to heating fluid temperature drop (28°F/40°F)

   The ratio of boiler pressure drop to boiler exit pressure, (32 psi/ 119 psia)

   Moderate superheat at the boiler exit (45°F) and subcooling at the condenser exit (42°F)

1. Exploratory Boiler and Condenser Maps

Data plots showing how boiler pressure drop and condenser interface position are affected by values of independent powerplant variables are presented in Figures 58 through 61. These figures show the boiler pressure drop as a function of various combinations of the variables: power-loop flow rate, heater-loop flow rate, boiler-shell inlet temperature, and the setting of the choked turbine-simulator valve (which determines the relationship between the boiler exit pressure, boiler exit temperature, and power-loop flow rate). The boiler exit superheat and boiler exit pressure have been crossplotted on these figures. The boiler data is tabulated in Table 6, Appendix D, which includes calculated values of the pinch-point temperature difference in the boiler.

In Figure 62 condensing length is shown as a function of the variables: condensate flow rate, coolant flow rate, coolant inlet temperature, and condenser exit pressure. Coolant flow rate divided by condensate flow rate was used as a parameter in these plots. This ratio roughly determines a condenser effectiveness for a given coolant inlet temperature and condenser exit pressure.

Details of the procedures used to reduce the boiler and condenser data are given in Section IV.B.3. of this report where boiler and condenser maps around the design point are discussed.

2. Constant Inventory System Maps

After the desired design operating conditions in the boiler and condenser had been approximately determined, the operating characteristics of the power loop as a whole in the neighborhood of the design conditions were investigated.

Tests were made to determine the effect of changing the inlet temperatures and flow rates in the heater loop and radiator loop when the power loop had a fixed inventory, and when the settings of the turbine-simulator valve and the flow-control valve downstream of the power-loop pump were fixed. Under these conditions, the power-loop flow rate was a dependent variable. Tests were made at two pump speeds. At each pump speed the pump throttling valve was set as required to give the same flow rate at the same set of operating conditions. The pump speeds were chosen to give extreme values of the pressure-flow slope at the boiler inlet. One speed was such that the common flow point was obtained with the pump throttling valve wide open, so that the pressure-flow slope at the boiler inlet nearly corresponded to the pump slope. The other pump speed was the maximum obtainable, so that a large pressure drop across the pump throttling valve was required, and a much steeper pressure-flow slope at the boiler inlet resulted.

This data is tabulated in Tables 7 and 8, Appendix D. Figures 63 and 64 are plots showing the effect of varying the boiler-shell inlet temperature and condenser-shell inlet temperature on the power-loop pressure and flow rate. Varying the boiler-shell flow rate and condenser-shell flow rate produced a similar trend so this data was not plotted.

Two additional series of tests were made. In one, the power-loop inventory was changed with all other controllable variables held constant. In the second test, with a fixed inventory, the setting of the pump throttling valve was changed to give different flow rates with constant values of the other variables. The results are tabulated in Tables 7 and 8 and plotted in Figures 65 and 66.

The imposition of fixed-inventory power-loop operation did not result in any detrimental interactions between the loop components for these tests in the neighborhood of the nominal design point.

The steady-state condenser and boiler mapping tests presented in Section IV of this report were planned on the basis of the exploratory tests described in this Appendix.

APPENDIX D

Tables

TABLE 1

Nominal Design Operating Conditions as Defined by Independent Variables

Power-loop flow rate - 244 lb/hr
Heater-loop flow rate - 6000 lb/hr
Condenser-shell flow rate - 5000 lb/hr
Boiler-shell inlet temperature - 418°F
Boiler-tube inlet temperature - 173°F
Boiler exit pressure (determined by the setting of the turbine-simulator valve) - 119 psia
Condenser-shell inlet temperature - 153°F
Condenser exit pressure (determined by pressure on a fluid accumulator at the condenser exit, or by inventory when the power loop has a fixed inventory) - 16.0 psia

TABLE 2

Condenser Maps with Coolant Flow an Independent Variable

Point No.	PSIA Condenser Exit Pressure	PSIA Condenser Inlet Pressure	°F Condenser Shell Inlet Temp	Lb/Hr Power Loop Flow Rate	Lb/Hr Condenser Shell Flow Rate	°F Condenser Shell Temperatures: Inlet	1/3 Dist.	2/3 Dist.	Exit	°F Condenser Tube-Side Temperatures: Combined Exit	Combined Inlet
	P13	P9	T22	FM2	FM5	T22	T12	T11	T10	T13	T9
1	16.4	18.7	153	242	5050	153	165	186	203	173	356
2	17.4	19.7	153	242	5050	153	163	185	203	170	351
3	18.6	20.9	154	243	5060	154	162	185	205	169	350
4	19.5	21.8	154	242	5060	154	159	183	205	166	357
6	23.3	25.7	154	242	5040	154	156	178	205	163	354
7	25.5	27.6	153	242	5040	153	155	175	204	161	356
8	35.6	38.1	154	242	5040	154	154	169	206	160	356
9	15.3	17.7	153	242	5050	153	167	186	202	179	350
10	14.7	17.4	153	242	5050	153	170	190	203	187	350
11	13.2	15.9	153	242	5060	153	172	190	202	200	350
12	12.7	15.7	150	242	5070	150	170	187	200	201	355
13	13.1	15.7	150	242	5070	150	168	186	200	196	350
15	16.3	18.7	150	242	5060	150	161	182	200	170	351
16	17.9	20.5	151	243	5010	151	160	182	203	169	347
17	19.5	21.8	150	244	5060	150	157	178	202	163	347
18	21.0	23.3	150	244	5060	150	155	176	202	160	346
19	21.1	23.4	147	242	5060	147	150	170	198	156	347
20	19.5	21.8	147	243	5060	147	152	173	199	158	350
21	17.9	20.3	147	242	5070	147	153	175	199	161	349
22	16.4	18.7	147	243	5060	147	156	178	199	166	349
23	15.3	17.8	147	242	5060	147	159	179	198	169	348
24	13.6	16.3	147	243	5060	147	163	182	197	182	352
25	12.6	15.3	147	243	5060	147	163	182	196	188	351
26	21.1	23.4	156	245	5040	156	162	185	207	170	343
27	19.4	21.7	156	245	5040	156	165	188	207	173	347
28	17.9	20.1	156	245	5030	156	169	190	207	177	350
29	16.3	18.7	156	245	5030	156	172	192	207	185	350
31	16.2	18.9	159	244	5040	159	176	195	208	204	356
32	15.3	18.5	159	245	5040	159	178	195	209	211	354
33	18.0	20.4	158	244	5030	158	173	193	209	189	346
34	19.5	21.9	160	244	5020	160	172	192	209	182	346
39	30.5	32.9	154	246	4980	154	155	171	206	159	345
40	30.5	32.9	160	244	4970	160	161	180	211	165	355
41	16.4	18.9	153	245	5510	153	160	179	200	169	337
42	14.7	17.5	152	246	5510	152	161	180	199	173	337
43	13.1	16.8	153	246	5500	153	166	183	200	182	335
46	25.5	28.0	153	246	5500	153	155	170	200	163	336
47	30.5	33.2	153	246	5490	153	154	168	200	162	340
48	30.5	33.2	153	245	5230	153	154	168	202	161	333
49	25.4	28.4	153	243	5230	153	155	172	201	163	334

TABLE 2

Condenser Maps with Coolant Flow an Independent Variable (Continued)

°F

Condenser Tube-Side Temperatures

Single Tubes at Distance from Exit

Point No.	2" T105-16	2" T111-23	3" T106-17	3" T110-21	4-1/2" T109-20	4-1/2" T104-27	5" T108-19	6" T107-18	7-1/2" T112-4	9" T103-26	11" T102-25	12" T101-24	Condensing Length - Fraction of Total Length (from Temp Plots)	Check Values: $\frac{BTU}{HR} \times 10^{-3}$ Q Power Loop	Check Values: $\frac{BTU}{HR} \times 10^{-3}$ Q Cond. Shell	Subcooled $\frac{UA}{(wC_p)_{PL}}$
1	181	184	165	220	220	219	216	169	262	183	220	284	0.817	260	252	1.20
2	170	171	163	222	184	190	216	166	259	178	223	286	0.770	260	252	1.41
3	173	175	169	223	190	190	210	170	243	168	218	250	0.741	263	258	1.58
4	164	164	160	183	170	186	222	160	230	173	197	294	0.697	262	258	1.76
6	162	170	158	178	168	178	190	158	226	165	178	236	0.575	263	257	2.28
7	155	162	156	165	162	169	183	157	200	158	170	215	0.525	265	257	2.49
8	157	154	157	173	163	170	174	157	185	157	170	212	0.416	264	262	2.90
9	194	203	166	248	216	236	216	173	258	186	270	280	0.875	259	258	0.87
10	208	212	168	242	250	243	216	216	259	190	270	276	0.924	257	252	0.56
11	207	210	173	246	247	242	212	212	256	210	270	274	1.000	253	248	0.10
12	205	209	171	220	249	239	210	253	256	266	272	270	1.000	254	253	0.070
13	203	210	167	220	249	240	211	211	257	266	273	273	0.980	255	253	0.020
15	173	183	160	221	205	220	217	175	254	195	222	285	0.795	260	253	1.24
16	167	174	159	223	173	220	218	179	230	190	225	288	0.750	262	261	1.40
17	161	164	155	183	184	186	221	160	230	180	187	290	0.670	264	263	1.82
18	158	163	155	183	170	188	200	167	232	176	181	293	0.625	265	263	1.96
19	156	160	150	176	180	180	185	161	215	170	183	294	0.562	263	258	2.30
20	158	158	151	180	170	186	200	164	229	171	174	293	0.624	264	263	2.04
21	154	160	154	180	168	176	219	167	225	174	190	290	0.705	263	264	1.72
22	166	176	156	220	181	219	215	167	240	186	220	285	0.764	263	263	1.34
23	174	183	156	216	216	218	212	170	248	201	218	280	0.824	261	258	1.14
24	202	209	156	242	248	239	210	202	258	266	272	279	0.916	258	253	0.35
25	203	206	158	210	249	238	208	209	255	266	270	275	0.925	258	248	0.84
26	162	169	179	185	174	191	225	174	232	179	190	289	0.709	266	257	1.72
27	170	173	177	220	175	210	221	184	240	185	229	287	0.766	263	257	1.43
28	180	193	225	225	225	235	218	183	261	196	272	285	0.829	262	257	1.17
29	205	217	220	248	222	248	218	184	261	218	255	279	0.904	261	257	0.756
31	212	219	238	250	258	252	220	189	266	272	280	283	0.965	255	247	0.252
32	216	218	243	240	256	252	218	260	264	272	278	280	1.000	254	252	0.053
33	200	222	225	230	222	252	222	176	265	223	277	282	0.886	258	256	0.734
34	187	197	229	228	228	232	224	173	261	207	230	287	0.824	260	246	1.13
39	157	158	163	175	170	172	172	161	182	162	175	218	0.454	267	259	3.10
40	161	164	171	182	170	187	187	164	193	172	180	254	0.504	264	254	3.02
41	171	185	173	183	215	160	219	164	226	224	232	283	0.742	263	260	1.40
42	180	217	214	180	213	160	218	165	254	270	276	278	0.800	264	255	1.03
43	165	216	171	220	220	166	213	172	248	267	273	271	0.895	260	259	0.57
46	157	154	157	163	192	169	166	163	246	190	275		0.490	265	259	2.12
47	156	164	156	157	178	158	160	160	214	165	180	256	0.445	265	258	2.33
48	156	162	156	168	162	164	161	157	218	191	193	254	0.434	264	257	2.44
49	160	167	162	172	158	164	162	160	247	201	193	251	0.504	261	251	2.12

TABLE 2

Condenser Maps with Coolant Flow an Independent Variable (Continued)

Point No.	PSIA Condenser Exit Pressure	PSIA Condenser Inlet Pressure	°F Condenser Shell Inlet Temp	Lb/Hr Power Loop Flow Rate	Lb/Hr Condenser Shell Flow Rate	°F Condenser Shell Temperatures Inlet	1/3 Dist.	2/3 Dist.	Exit	°F Condenser Tube-Side Temperatures Combined Exit	Combined Inlet
	P13	P9	T22	FM2	FM5	T22	T12	T11	T10	T13	T9
51	17.4	20.6	153	245	5260	153	160	179	201	173	338
52	16.1	19.4	153	245	5270	153	162	180	201	176	337
53	14.2	18.5	153	246	5260	153	174	183	202	181	335
54	13.3	17.2	153	246	5280	153	175	183	201	185	338
56	14.9	18.6	152.5	243	4750	152.5	167	187.5	206	185	334
57	18.1	21.2	153	243	4750	153	162	183	206	175	338
59	25.4	28.5	152.5	243	4770	152.5	157	176	207	167	336
60	30.5	33.7	152.5	243	4760	152.5	154.5	172.5	207	164	330
61	30.5	33.5	153	244	4500	153	155.5	175	210	165	334
62	25.3	28.2	153	243	4500	153	158	180	210	166	330
63	20.2	23.0	152.5	243	4500	152.5	162.5	184.5	209.5	175	335
64	20.2	22.8	153.5	246	4500	153.5	164	187	210.5	172	337
65	17.3	20.2	152	245	4500	152	166	188	209	178	342
66	16.2	19.0	152	245	4500	152	167	189	208	184	343
67	14.5	18.7	153	246	4500	153	170	191	209	194	344
68	13.5	16.5	153	233	5000	153	166	184	201	183	333
69	15.0	17.7	153	233	5000	153	162.5	181.5	200.5	175	333
70	16.4	19.1	153	232	5000	153	161	180.5	201	171	338
71	17.9	20.7	153	232	5000	153	159	178	201	169	338
72	20.2	22.2	153	232	5000	153	157	176	202	166	339
73	25.2	27.7	153	232	4990	153	155	171	202	162	331
74	30.5	33.2	153	232	4990	153	154	167	202	160	336
75	30.4	32.9	154	220	4990	154	155	166	200	159	338
76	25.4	27.8	153	220	4980	153	154	167	199	160	334
77	20.1	22.7	153	221	4980	153	156	172	199	162	330
78	18.0	20.7	153	221	4980	153	157	174	199	165	329
79	16.3	18.8	153	221	4980	153	160	177.5	199	168	331
80	14.6	17.5	153	220	4980	153	160.5	178.5	198	174	336
81	13.2	16.3	153	220	4980	153	163	180	198	179	335
83	11.8	15.3	153	220	4970	153	166	183	199	186	336
84	30.7	33.4	153	256	5000	153	156	174	208	165	329
85	25.2	27.9	153	256	5000	153	157	177	207	166	331
86	19.9	22.9	153	256	5000	153	161	182	207	173	328
87	18.0	20.9	153	256	5000	153	163	184	206	180	327
88	16.2	19.7	153	256	5000	154	166	186	206	186	340
89	14.9	18.6	153	256	5000	153	168	188	206	191	340
90	30.4	33.7	154	268	5000	154	158	178	211	167	317
92	20.1	23.3	153	268	5000	153	163	185	209	179	314
94	17.5	20.9	153	268	5000	153	166	188	208	187	317
95	16.3	19.8	153	268	5000	153	168	189	208	190	317

TABLE 2

Condenser Maps with Coolant Flow an Independent Variable (Continued)

Point No.	2" T105-16	2" T111-23	3" T106-17	3" T110-21	4-1/2" T109-20	4-1/2" T104-27	5" T108-19	6" T107-18	7-1/2" T112-4	9" T103-26	11" T102-25	12" T101-24	Condensing Length - Fraction of Total Length (from Temp Plots)	Check Values: $\frac{BTU}{HR} \times 10^{-3}$ Q Power Loop	Check Values: $\frac{BTU}{HR} \times 10^{-3}$ Q Cond. Shell	Check Values: Subcooled $\frac{UA}{(wC_p)_{PL}}$
	Condenser Tube-Side Temperatures °F, Single Tubes at Distance from Exit															
51	166	198	161	170	173	165	197	164	244	226	230	285	0.733	262	252	1.20
52	170	222	164	170	169	267	218	166	252	225	228	282	0.775	261	258	0.98
53	184	221	170	223	174	171	217	168	246	221	276	276	0.829	261	258	0.71
54	205	274	162	218	220	170	215	173	249		267	273	0.875	260	254	0.50
56	162	222	163	214	225	186	182	168	252	271	276	274	0.880	257	254	0.61
57	160	227	171	180	185	182	163	166	254	228	284	283	0.758	259	252	1.13
59	157	176	186	176	199	168	159	160	253	191	249	292	0.546	261	260	1.76
60	156	170	196	172	165	175	158	158	254	182	215	258	0.480	261	260	2.00
61	154	168	195	170	158	164	158	158	251	184	213	258	0.500	263	257	2.04
62	159	172	182	172	182	164	162	160	248	187	249	292	0.591	260	257	1.86
63	170	204	236	176	177	171	163	166	254	214	283	286	0.759	259	257	1.19
64	175	190	200	236	190	169	232	175	255	233	284	288	0.763	261	257	1.36
65	198	226	229	235	229	167	227	184	230	278	283	282	0.833	261	257	1.00
66	213	223	226	245	248	168	225	201	256	224	282	282	0.883	260	252	0.70
67	214	221	225	241	195	176	223	264	260	224	280	280	0.931	259	252	0.35
68	205	215	218	240	170	170	216	218	255	266	271	270	0.892	244	240	0.63
69	203	218	222	225	165	167	220	177	222	230	276	277	0.800	248	238	1.03
70	175	193	225	245	165	163	223	174	226	225	240	285	0.759	248	240	1.33
71	163	175	190	230	171	162	225	173	247	228	186	286	0.650	248	240	1.51
72	159	170	180	202	161	160	226	164	246	225	195	292	0.595	249	245	1.79
73	156	156	189	190	157	159	203	166	170	196	180	247	0.491	249	245	2.31
74	156	155	172	190	156	166	195	163	167	185	169	253	0.425	250	245	2.68
75	157	155	169	187	158	164	189	162	174	180	166	254	0.408	238	230	3.01
76	158	154	174	190	159	162	195	163	172	182	176	245	0.446	237	230	2.55
77	161	155	192	190	158	166	225	170	235	193	190	287	0.533	237	230	2.16
78	159	156	178	203	159	162	222	164	231	228	178	281	0.625	237	230	1.80
79	170	157	191	226	161	167	221	180	235	222	213	281	0.704	237	230	1.50
80	188	160	220	230	171	170	218	169	220	270	222	278	0.768	235	225	1.13
81	205	160	217	228	218	171	215	173	218	268	271	273	0.833	233	225	0.77
83	205	180	175	228	216	179	213	256	215	266	271	270	0.916	232	230	0.41
84	161	167	157	197	167	164	200	170	213	185	240	256	0.496	275	274	2.16
85	160	170	158	195	163	165	210	175	210	192	248	285	0.562	274	270	1.95
86	175	195	157	236	170	171	230	177	255	233	283	284	0.725	273	270	1.36
87	199	225	163	235	173	180	228	190	233	229	280	281	0.788	270	265	0.99
88	214	224	166	235	176	185	228	228	245	230	282	281	0.841	270	260	0.73
89	214	221	160	240	225	183	223	225	258	272	280	278	0.895	269	265	0.49
90	160	170	182	202	163	163	220	169	173	207	210	270	0.534	284	285	2.07
92	195	215	167	237	174	170	234	180	174	235	262	275	0.767	281	280	1.07
94	220	228	232	240	183	181	183	182	190	245	273	272	0.855	280	275	0.70
95	217	225	229	235	195	190	195	177	195	264	271	267	0.879	280	275	0.56

TABLE 3

Condenser Maps with Coolant Outlet Temperature Controlled

Point No.	PSIA Condenser Exit Pressure	PSIA Condenser Inlet Pressure	°F Condenser Shell Inlet Temp	Lb/Hr Power Loop Flow Rate	Lb/Hr Condenser Shell Flow Rate	°F Condenser Shell Temperature: Inlet	1/3 Dist.	2/3 Dist.	Exit	°F Condenser Tube-Side Temperatures: Combined Exit	Combined Inlet
	P13	P9	T22	FM2	FM5	T22	T12	T11	T10	T13	T9
1	15.9	18.8	153	244	5025	153	165.5	185.5	203.5	177	399
2	24.4	29.6	153	244	4975	152.5	154	172.5	204.5	159	343
3	22.4	25.9	152	244	5000	152.5	155.5	176	204	161	342
4	19.5	22.9	153	244	4965	153	158	180	204.5	164	341
5	16.1	18.3	153	244	4975	153	165	185.5	203.5	174	340
6	16.1	18.3	154	244	5215	154	165.5	185	203	174	340
7	29.4	31.6	147	244	4720	147	148	166	203	154	340
8	17.4	19.7	147	244	4625	147	157	180	202.5	165	342
9	16.0	18.4	147	244	4565	147	160	182.5	203	169	338
10	14.9	17.4	147	244	4520	147	162	184.5	203	178	342
11	13.4	16.3	147	244	4400	147	169	189	204	198	341
12	29.0	31.4	160	244	5880	160	160	174	204.5	164	338
13	19.1	21.5	160	244	6040	159.5	160	177.5	203	169	338
14	17.1	19.4	160	244	5880	159.5	167	186	203	172	340
15	15.6	18.2	159	244	5780	159	170	188	203	178	342
16	14.6	17.4	158	244	5610	158	171	189	203	184	342
17	17.4	20.2	135	244	3860	135	144	175	203.5	152	342
18	17.4	20.2	140	244	4225	140	149	177	203	156	340
19	17.5	20.2	146	244	4470	146	155	182	204	160	340
20	17.5	20.2	156	244	5440	156	163	184	204	169	340
21	17.4	20.2	160	244	5940	160	165	186	204	173	338
22	17.5	20.2	165	244	6650	165	172	189	204.5	178	338
23	30.2	32.5	153	220	4750	153	154	168.5	203.5	157	341
24	25.3	27.7	154	220	4720	154	154.5	173.5	203.5	159	337
25	25.3	27.7	154	220	4800	154	155	174	203	159	339
26	20.2	22.5	152	220	4620	152	155.5	178	203	161	340
27	18.0	20.5	153	220	4740	153	159	186	203	165	342
28	16.7	19.0	153	220	4630	153	164	187	203	169	343
29	15.7	18.3	153	220	4580	153	168	188.5	203	184	340
30	30.3	32.8	153	268	5690	153	154	171	203	160	338
31	25.3	28.0	153	268	5720	153	155	175	203	161	334
32	20.2	22.9	153	268	5720	153	160	182	203	168	336
33	18.0	20.7	153	268	5600	153	164	185.5	204	173	339
34	16.6	19.5	153	268	5630	153	167	187	203	180	333
35	15.8	18.6	153	268	5500	153	169	188	203	185	329

TABLE 3

Condenser Maps with Coolant Outlet Temperature Controlled (Continued)

Point No.	°F Condenser Tube - Side Temperatures, Single Tubes at Distance from Exit, Inches: 2	2	3	3	4-1/2	4-1/2	5	6	7-1/2	9	11	12	Condensing Length Fraction of Total Length	Check Values: BTU/Hr x 10^{-3}	BTU/Hr x 10^{-3}	Subcooled
	T105-16	T111-23	T106-17	T110-21	T109-20	T104-27	T108-19	T107-18	T112-4	T103-26	T102-25	T101-24	From (Temp. Plots)	Q Power Loop	Q Cond. Shell	$\frac{UA}{(wC_p)PL}$
1	167	196	158	242	223	162	167	177	255	271	196	277	0.843	260	254	0.947
2	153	157	168	171	168	153	154	158	187	175	160	225	0.496	264	259	2.63
3	154	159	160	187	173	154	155	164	193	193	170	244	0.562	264	259	2.16
4	155	162	160	185	172	154	157	168	220	202	171	292	0.667	263	256	1.85
5	158	196	171	238	224	163	224	174	256	271	275	225	0.820	261	251	1.09
6	171	196	165	236	224	163	224	176	255	274	276	224	0.825	261	256	1.12
7	151	153	168	176	168	149	169	165	182	185	182	206	0.464	265	264	2.59
8	165	176	186	226	179	156	219	173	246	229	229	226	0.762	263	256	1.37
9	168	189	222	223	224	160	217	170	251	274	275	221	0.825	262	256	1.12
10	192	215	221	243	221	163	218	174	231	272	276	220	0.867	260	253	0.738
11	208	214	230	223	250	170	214	246	256	216	221	219	1.000	255	251	0.170
12	161	164	174	179	172	160	176	166	184	188	183	222	0.450	262	259	3.01
13	166	170	181	194	179	163	203	172	232	229	199	287	0.674	262	262	1.80
14	170	179	179	226	179	166	219	183	249	224	203	283	0.758	261	256	1.50
15	181	170	221	236	222	167	217	176	259	272	223	280	0.844	260	254	1.06
16	208	171	218	234	220	169	216	183	260	270	270	276	0.870	259	252	0.715
17	150	151	180	175	175	143	220	159	230	227	230	285	0.712	266	264	1.56
18	152	156	166	180	166	148	220	164	229	227	230	286	0.725	265	266	1.56
19	161	161	170	186	170	153	220	167	230	227	230	286	0.733	264	259	1.62
20	166	173	178	195	178	161	225	173	233	230	230	286	0.742	262	261	1.56
21	170	177	190	197	192	165	220	172	238	226	230	285	0.750	261	261	1.50
22	175	180	192	228	195	170	220	182	282	227	230	285	0.770	260	263	1.42
23	154	156	165	169	165	166	164	156	175	177	171	207	0.432	239	240	3.10
24	155	157	169	176	170	170	173	157	183	184	182	240	0.505	238	234	2.78
25	155	158	166	173	168	170	172	157	185	183	183	240	0.520	238	235	2.78
26	155	160	180	175	176	180	192	162	220	197	190	285	0.629	238	236	2.04
27	165	166	173	175	190	180	218	169	232	222	226	282	0.709	238	237	1.71
28	167	175	185	222	193	221	213	183	255	270	274	278	0.792	237	232	1.37
29	180	190	218	218	218	219	213	170	257	267	271	274	0.875	233	229	0.680
30	155	158	172	180	169	172	172	160	186	186	190	250	0.475	289	285	2.56
31	155	157	173	183	177	180	190	164	210	193	186	238	0.555	289	286	2.32
32	164	170	175	192	177	164	223	173	235	230	233	285	0.738	287	286	1.43
33	173	182	220	225	220	166	220	190	240	230	280	282	0.819	287	286	1.22
34	190	218	222	230	223	169	218	180	245	269	274	275	0.876	284	282	0.855
35	208	217	220	230	222	168	216	195	237	267	272	272	0.924	282	275	0.655

TABLE 4

Boiler Map Around Design Point

Point No.	Variable	Data: °F Boiler Shell Inlet T2	°F Boiler Shell Exit T1	Lb/Hr Boiler Shell Flow FM1	°F Boiler Tube Inlet T6	°F Boiler Tube Exit T7	Lb/Hr Power Loop Flow FM2	PSIA Boiler Tube Inlet P6	PSIA Boiler Tube Exit P7	PSI ΔP Boiler ΔPM	°F T. S. Valve Exit T9	PSIA T. S. Valve Exit P9	Calculated Values: °F Boiler Exit °SH	Calculated Values: °F Boiler P. P. ΔT	Check Values (BTU/HR x 10^{-3}): Q Boiler Shell	Check Values (BTU/HR x 10^{-3}): Q Power Loop	Check Values (BTU/HR x 10^{-3}): Q Cond Shell	$\frac{W\sqrt{T}}{P}$ At TS Valve Inlet
1	T2	418	378	5980	172	367	243	151	119	31.9	346	19	50	28.1	258	261	261	59.4
2	T2	415	376	6050	171	356	243	150	118	31.2	329	19	33	26.6	255	259	261	59.0
3	T2	410	371	5960	172	337	244	145	114.5	29.0	294	19	1	24.4	252	256	255	59.9
4	T2	406	368	5970	173	336	242	142	112	27.3	258	19	-	22.9	245	251	240	-
5	T2	398	362	5970	172	333	246	135	109	25.4	222	19	-	20.8	232	-	230	-
6	T6	419	380	5960	200	384	244	154	120	33.9	345	19	49	27.6	251	255	256	59.0
7	T6	418	380	5980	189	382	243	154	120	33.3	342	19	46	28.0	245	256	255	59.0
8	T6	418	379	5960	179	381	244	153	120	32.9	340	19	44	27.9	251	260	260	59.0
9	T6	418	378	5970	173	378	244	152	119	32.4	341	19	45	27.6	258	262	255	59.3
10	T6	418	378	5980	162	375	244	151	119	32.1	340	19	44	28.6	258	264	257	59.2
11	T2	422	382	5980	173	394	243	156	120	34.1	353	19	57	29.5	258	262	257	59.6
12	T2	426	385	5970	172	402	243	157	120.5	36.3	363	19	63	32.1	263	263	252	59.5
13	T6	418	377	5970	150	358	245	151.5	120	31.7	330	19	32	27.3	265	266	262	58.9
14	FM2	418	378	5960	173	349	248	151	120	31.5	325	19	29	28.3	258	266	262	60.0
16	FM2	418	379	5960	173	374	242	150	117.5	32.0	344	19	47	29.5	252	258	261	59.7
17	FM2	418	376	5970	173	345	288	158	127	29.6	223	19	-	23.9	271	-	283	-
18	FM2	419	378	5950	173	344	258	156	123	30.8	304	19	6	26.0	264	272	276	59.7
19	FM2	419	380	5960	172	388	246	152	119	32.0	350	20	53	30.6	251	263	253	60.2
20	FM2	418	382	5960	172	402	213	142	106	35.0	371	19	80	36.1	232	232	235	59.2
21	FM2	418	381	5960	173	390	233	150	114	34.0	358	19	64	31.5	238	251	250	60.1
22 - Blowdown	T6	417	374	5960	84	342	249	149.5	121	28.0	318	20	22	29.9	283	286	-	59.3
24	T2	424	384	5940	172	402	242	154	119	34.7	367	19	71	32.6	257	261	258	60.0
25	FM2	417	376	5940	171	344	261	154	124	29.8	303	20	4	25.2	263	275	269	59.9
26	FM2	418	375	5950	172	346	273	156	127	27.8	252	21	-	23.6	271	281	277	-
27	FM2	419	385	5950	174	408	210	141	104	35.8	374	19	83	39.6	218	228	222	59.5
30	FM1	418	380	6230	172	383	245	151	120	32.4	348	19	52	28.9	256	263	259	59.6
31	FM1	418	381	6690	173	392	244	152	120	33.2	353	19	57	29.8	266	263	254	59.6
32	FM1	418	385	7060	172	401	244	157	121	34.7	362	19	66	32.0	252	264	258	59.4
33	FM1	419	388	7880	173	403	245	159	122	36.7	364	19	67	32.4	264	265	258	59.2
34	FM1	417	370	5100	173	336	244	142	114	27.5	276	20	-	26.1	256	254	249	-
35	FM2	418	375	5980	173	346	291	161	131	28.8	222	20	-	21.5	278	-	285	-
36	FM2	418	380	6010	172	398	230	143	113.5	33.7	363	19	69	33.9	247	249	240	59.6
37	FM1	418	368	4590	173	334	244	141	113	26.4	253	19	-	25.5	246	251	249	-
38	T6	418	378	6020	142	380	242	149	118	30.7	347	20	51	30.1	260	267	268	59.9
40	T2	430	390	6020	172	411	242	157	120	37.7	374	19	78	37.1	261	263	248	59.5
42	FM2	418	378	6020	175	365	246	153	120	31.7	345	19	49	27.0	260	263	259	59.6
43	T. S. Valve	419	380	6010	173	357	246	157	126.5	28.2	340	19	42	27.1	253	263	256	56.6
44	T. S. Valve	418	380	6010	172	348	246	160	133	26.7	310	19	10	25.7	247	260	255	52.9
45	T. S. Valve	418	380	6010	174	398	245	144	105	38.7	368	19	77	33.7	247	265	255	68.8
46	FM1	418	377	5610	173	340	244	149	119	30.0	325	19	29	28.4	249	259	250	59.0
47	FM1	418	374	5280	173	339	243	145.5	116	29.7	308	19	10	27.7	250	256	250	59.9

TABLE 4

Boiler Map Around Design Point (Continued)

°F

Data from Thermocouples on Boiler Shell - Distance from Boiler Shell Inlet, Inches

Point No.	Variable	4	8	12	16	20	24	28	32	36	40	44	48	52	56	60	64	68	72	76	80	84	88	92
1	T2	414	414	414	413	413	409	407	403	400	400	399	397	395	392	390	389	387	386	384	383	382	382	380
2	T2	413	413	413	413	412	407	406	402	398	398	396	396	393	392	389	388	386	386	382	382	380	380	379
3	T2	407	407	406	406	402	400	397	394	390	390	389	389	385	383	382	380	379	379	376	375	375	374	373
4	T2	403	403	400	400	397	396	393	389	385	385	385	383	382	380	379	376	376	373	372	372	371	371	369
5	T2	395	395	393	392	390	386	386	382	378	378	378	376	375	372	372	371	369	369	367	366	366	365	364
6	T6	417	417	416	416	416	413	412	407	402	402	402	402	398	396	394	392	392	389	388	386	386	385	382
7	T6	416	416	416	416	415	412	410	406	402	402	402	400	398	395	394	392	390	389	386	386	385	383	382
8	T6	418	418	416	416	416	412	411	407	403	402	402	400	399	396	395	392	392	388	386	386	385	384	382
9	T6	417	417	416	416	416	413	412	408	404	403	402	402	399	396	395	392	392	389	388	386	386	385	382
10	T6	415	415	415	415	413	410	408	406	401	401	400	400	396	395	392	390	389	387	386	385	382	382	380
11	T2	419	419	419	419	418	417	415	412	407	407	406	406	402	400	399	396	395	392	391	389	388	386	386
12	T2	422	422	422	422	422	421	420	417	412	412	410	409	406	405	403	400	400	396	394	392	392	390	388
13	T6	415	415	415	415	415	411	409	406	402	402	400	400	396	394	392	390	389	387	386	384	382	382	380
14	FM2	415	415	415	415	415	413	412	408	405	403	403	402	399	396	394	392	390	389	386	386	383	382	381
16	FM2	416	416	416	416	416	413	412	409	405	405	403	403	400	400	396	394	393	390	389	386	386	385	382
17	FM2	415	415	411	410	409	405	403	400	396	396	396	395	393	392	389	389	386	386	383	382	381	381	379
18	FM2	417	417	416	416	416	413	410	407	403	403	402	402	400	397	396	394	392	389	386	386	383	383	382
19	FM2	418	418	418	418	418	416	413	412	406	406	406	406	402	400	399	397	394	392	390	389	386	386	385
20	FM2	415	415	415	415	415	415	414	412	408	408	407	406	404	402	400	398	396	394	392	390	389	386	386
21	FM2	416	416	416	416	416	415	413	411	406	406	406	405	402	400	399	397	395	392	390	389	386	386	384
22 - Blowdown	T6	415	415	415	415	415	413	-	407	404	404	403	402	400	398	396	394	392	390	389	386	386	384	382
24	T2	422	421	421	421	421	421	-	-	414	414	413	412	410	408	406	403	402	400	396	395	393	392	390
25	FM2	415	415	415	415	412	409	-	-	400	400	400	399	396	394	392	392	388	386	386	383	382	382	380
26	FM2	415	415	415	415	411	408	-	-	398	398	398	396	394	392	390	389	386	386	383	382	382	380	379
27	FM2	416	416	416	416	416	416	-	-	410	409	409	409	406	405	403	401	399	396	394	392	390	389	388
30	FM1	415	415	415	415	415	415	-	-	407	407	407	406	406	402	402	400	396	395	392	390	389	389	386
31	FM1	414	415	415	415	415	415	-	-	405	405	405	405	405	402	400	396	395	393	390	389	389	386	385
32	FM1	416	416	416	416	416	416	-	-	408	408	408	408	408	405	403	402	399	397	395	393	392	392	390
33	FM1	417	417	417	417	417	417	-	-	409	409	409	409	409	406	406	403	402	400	396	395	393	393	390
34	FM1	412	412	412	412	412	410	-	-	400	400	400	399	398	395	393	390	388	385	383	381	380	379	376
35	FM2	416	416	413	413	410	406	-	-	397	397	397	397	396	394	392	389	388	386	385	382	382	382	380
36	FM2	415	415	415	415	415	415	-	-	408	408	408	408	406	403	402	400	399	396	392	390	389	388	386
37	FM1	414	414	414	414	413	412	-	-	403	403	402	402	400	398	397	392	389	386	385	382	379	378	376
38	T6	416	416	416	416	416	415	-	-	407	407	407	406	405	402	400	398	395	393	391	389	388	386	385
40	T2	427	427	427	427	427	427	-	-	419	419	419	419	416	413	413	410	408	406	402	400	400	399	396
42	FM2	416	416	415	415	415	413	-	-	405	405	405	405	403	398	398	398	395	393	390	389	386	386	385
43	T.S. Valve	417	417	417	417	416	416	-	-	408	408	408	408	405	403	400	400	396	395	393	390	389	389	386
44	T.S. Valve	416	416	416	416	416	413	-	-	404	404	404	404	402	402	400	396	394	393	390	389	388	386	386
45	T.S. Valve	417	417	417	417	417	416	-	-	409	409	409	409	406	406	402	400	398	396	393	392	389	388	386
46	FM1	415	415	415	415	415	415	-	-	405	405	405	406	403	403	402	400	397	396	392	389	387	386	384
47	FM1	415	415	415	415	415	415	-	-	405	405	405	405	403	403	400	399	395	393	390	388	386	385	382

TABLE 5

Extrapolated Values at Frequency at Which a 180-Degree Phase Shift Existed Between Boiler Inlet Pressure and Flow Rate

Test No. (Fig. No.)	$\frac{\Delta P_{boiler\ in}}{\Delta w_{boiler\ in}}$, psi/lb hr	Frequency, cps	Normalized $\frac{\delta P_{boiler\ in}}{\delta w_{boiler\ in}}$	$\frac{\delta P_{boiler\ in}}{\delta w_{boiler\ in}}$, psi/lb hr
1 (51, 52, 53)	0.233	0.30	0.24	0.056
2 (54, 55, 56)	0.103	0.27	0.09	0.009
3 (57, 58, 59)	0.373	0.31	0.13	0.048
4 (60, 61, 62)	0.116	0.27	0.05	0.005
5 (63, 64, 65)	0.200	0.32	0.25	0.051

TABLE 6

Exploratory Boiler Mapping Data

	Data									Calculated Values	
Point No.	°F Boiler Shell Inlet	°F Boiler Shell Exit	Lb/Hr Boiler Shell Flow	°F Boiler Tube Inlet	°F Boiler Tube Exit	Lb/Hr Power Loop Flow	PSIA Boiler Tube Inlet	PSIA Boiler Tube Exit	Position	°F Boiler Exit °SH	°F Boiler PP ΔT
	T2	T1	FM1	T6	T7	FM2	P6	P7	T. S. Valve		
1	428	384	5950	184	353	263	162	130	C_1 Defined	27	29
2	428	376	4420	164	336	235	143	115	C_1	25	33
3	427	390	7820	178	360	289	175	141	C_1	22	28
5	428	387	5890	162	400	236	155	119	C_1	62	35
6	428	391	5950	152	415	210	146	108	C_1	79	44
9	428	385	5950	179	362	263	163	130	C_1	38	30
10	427	374	4420	160	337	234	143	115	C_1	26	34
11	429	378	4490	160	377	213	137	107	C_1	66	39
12	427	371	4490	167	338	250	141	116	C_1	0	31
13	428	370	4490	170	340	269	146	123	C_1	0	27
14	428	379	5060	173	340	244	148	119	C_1	28	33
15	423	377	5060	168	348	243	143	117	C_1	24	34
16	418	372	5060	169	341	244	143	116	C_1	0	29
17	433	384	4980	170	386	243	154	121	C_1	58	35
18	428	380	5060	173	380	244	144	109	C_{18} Defined	56	36
19	428	376	5140	178	337	270	148	116	C_{18}	18	30
20	428	381	4980	165	400	243	140	100	C_{20} Defined	69	39
21	428	377	5060	175	344	268	143	107	C_{20}	37	34
22	428	373	5060	177	334	291	145	113	C_{20}	0	30
24	428	383	5950	179	345	263	162	130	C_1	26	29
25	428	385	5950	173	373	243	157	124	C_1	53	32
27	433	388	5890	163	375	235	160	124	C_1	62	35
28	423	381	5950	160	375	235	152	119	C_1	51	32
29	418	378	5950	173	358	242	150	120	C_1	34	29
30	413	375	5950	170	349	242	148	119	C_1	23	27
31	413	369	5070	167	337	243	140	115	C_1	0	27
33	428	385	5950	170	395	243	151	115	C_{33} Defined	66	36
34	423	380	5950	162	366	243	148	113	C_{33}	53	33
35	418	378	5950	165	367	243	146	112	C_{33}	50	32
36	428	380	5060	169	356	244	151	119	C_1	51	32
37	428	379	5140	173	341	258	152	124	C_1	0	40
38	428	387	5140	166	411	213	139	104	C_1	74	45

TABLE 7

Exploratory System Mapping Data with Pump Speed Set to give Design Conditions with the Pump Throttling Valve Wide Open

		Data																Calculated Values		Check Values BTU/Hr x 10^{-3}		
		Lb/Hr Boiler Shell Flow	°F Boiler Shell Inlet	°F Boiler Shell Exit	Lb/Hr Power Loop Flow	PSIA Pump Exit	PSIA Boiler Tube Inlet	PSIA Boiler Tube Exit	°F Boiler Tube Inlet	°F Boiler Tube Exit	°F T. S. Valve Exit	Lb/Hr Condenser Shell Flow	PSIA Condenser Tube Inlet	PSIA Condenser Tube Exit	°F Condenser Shell Inlet	°F Condenser Shell Exit	°F Condenser Tube Exit	°F Boiler Exit Superheat	°F Boiler PP ΔT	Q Boiler Shell	Q Power Loop	Q Condenser Shell
Point No.	Variable	FM1	T2	T1	FM2	P10	P6	P7	T6	T7	T9	FM5	P9	P13	T22	T10	T13					
1	T2	6080	423	385	238	154	150	115	176	397	365	5000	19.8	16.0	153	205	180	66.0	35.21	250	256	260
2	T2	6080	411	372	260	150	146	118	183	339	235	4940	20.1	15.8	153	205	190	--	24.68	256	--	257
3	T2	6080	418	378	249	152	149	118	178	347	335	4960	20.7	16.5	154	207	184	36.4	28.94	263	263	263
4	T2	6080	425	388	224	154	150	112	176	410	376	5000	18.3	14.4	154	203	.190	77.8	37.91	243	240	245
5	T2	6080	430	394	218	154	151	108	178	418	385	4960	17.3	13.5	153	201	190	87.8	43.07	236	234	238
7	FM1	5080	420	374	249	150	146	116	193	337	373	5000	18.7	14.0	153	205	203	73.8	27.18	253	263	260
8	FM1	5530	420	378	244	150	146	115	193	347	334	5030	18.1	13.5	153	203	204	36.8	30.48	251	253	252
9	FM1	6570	418	382	235	151	147	113	191	379	356	5030	18.0	13.5	153	203	204	58.6	32.73	256	246	252
10	FM5	5590	419	380	246	154	150	120	173	340	311	4970	19.9	16.2	153	205	179	13.4	30.71	252	258	258
11	FM5	6020	419	380	239	153	149	118	168	339	334	6050	17.7	15.7	153	195	173	36.6	31.14	254	255	254
12	FM5	6010	419	380	236	154	150	119	168	381	350	5550	19.0	15.4	154	200	175	51.0	30.61	254	253	255
13	FM5	5970	418	378	238	156	153	119	174	377	350	4450	22.6	18.7	153	210	182	49.8	26.91	258	253	254
14	FM5	6010	419	380	250	156	153	122	183	341	311	4000	24.2	20.3	154	220	190	10.4	28.81	257	260	264
15	FM5	6000	419	380	240	154	151	119	173	340	333	4970	20.0	16.3	153	205	180	34.4	29.97	253	254	258
17	T22	5960	419	379	251	155	151	121	183	341	300	5000	22.7	18.7	160	212	183	1.2	28.97	256	261	260
18	T22	6010	419	380	240	155	151	119	178	351	339	5000	20.7	16.9	156	207	178	40.2	29.77	254	255	255
19	T22	5940	419	380	238	153	150	118	173	351	340	5000	18.9	15.3	150	201	173	42.0	30.51	250	255	255
20	T22	6000	419	380	237	153	150	118	171	352	335	5000	18.5	14.4	147	198	171	37.0	30.51	253	254	255
21	T22	6000	418	378	237	152	144	118	161	340	330	5000	16.0	12.6	140	192	161	33.4	31.98	259	255	260
22	INV	6080	419	381	239	156	151	118	175	388	356	5000	20.0	16.2	154	205	181	56.6	30.77	256	255	255
24	INV	6100	420	380	249	159	154	123	167	344	322	5070	23.8	19.8	154	207	168	21.2	28.78	264	265	269
26	INV	6100	420	382	235	156	152	119	174	388	356	5040	20.0	17.2	154	205	182	56.4	31.14	250	251	257
27	INV	6020	420	383	227	155	151	117	170	382	358	5160	19.8	15.7	153	200	170	58.8	32.67	241	245	243
28	INV	6020	420	382	231	152	148	115	182	386	354	5130	16.7	14.5	154	201	192	56.6	32.99	247	244	241
29	FM2	5990	419	380	242	154	150	120	177	341	330	5000	20.0	16.3	153	205	177	31.2	30.41	252	257	260
30	FM2	5990	419	385	210	158	142	108	166	405	370	5000	17.8	14.5	154	199	166	73.6	39.09	219	229	225
31	FM2	5990	420	388	196	160	134	99	163	411	379	5000	15.7	13.5	154	198	163	86.0	46.28	207	215	220

TABLE 8

Exploratory System Mapping Data with Pump Speed Set to give a Pump Exit Pressure of 203 PSIA at Design Flow

		Data															Calculated Values		Check Values BTU/Hr x 10^{-3}		
Point No.	Variable	Lb/Hr Boiler Shell Flow	°F Boiler Shell Inlet	°F Boiler Shell Exit	Lb/Hr Power Loop Flow	PSIA Pump Exit	PSIA Boiler Tube Inlet	PSIA Boiler Tube Exit	°F Boiler Tube Inlet	°F Boiler Tube Exit	°F T.S. Valve Exit	Lb/Hr Condenser Shell Flow	PSIA Condenser Tube Inlet	PSIA Condenser Tube Exit	°F Condenser Shell Inlet	°F Condenser Shell Exit	°F Condenser Tube Exit	°F Boiler Exit Superheat	°F Boiler P.P. ΔT	Q Boiler Shell	Q Power Loop	Q Condenser Shell
		FM1	T2	T1	FM2	P10	P6	P7	T6	T7	T9	FM5	P9	P13	T22	T10	T13					
1	T2	6000	421	381	246	202	151	121	185	341	324	4960	20.6	16.2	153	206	191	25.2	30.67	259	259	263
2	T2	6000	414	373	256	199	150	119	190	339	220	4950	19.6	15.0	152	205	196	--	23.31	266	--	262
3	T2	6000	418	377	250	200	148	119	190	340	388	4960	19.9	15.6	153	206	196	87.4	28.19	266	267	263
4	T2	6000	423	383	243	202	152	121	187	340	343	4980	20.6	16.2	154	207	192	43.2	32.04	259	256	264
5	FM1	7050	423	389	234	203	156	118	185	402	367	4960	19.8	15.8	153	205	189	67.2	34.94	259	250	258
6	FM1	6400	423	385	244	202	153	120	186	370	355	5000	20.6	16.2	153	206	190	54.8	33.11	263	258	265
7	FM1	5450	423	378	254	201	148	120	186	340	282	4980	20.2	15.7	153	206	191	--	29.99	265	360	264
8	FM1	4940	423	375	254	200	145	119	188	339	221	4960	19.6	15.1	152	204	192	--	29.33	256	--	258
9	FM5	6080	422	382	247	202	151	121	186	340	324	4980	20.8	16.2	153	206	191	25.2	31.57	263	258	264
10	FM5	6080	422	382	250	205	153	122	195	340	319	3920	24.9	20.8	154	221	200	18.4	30.31	263	258	263
11	FM5	6000	424	383	245	205	152	121	190	340	333	4470	22.8	18.2	153	212	195	33.0	31.94	266	259	264
12	FM5	6080	423	383	241	202	152	120	183	341	341	5450	19.0	14.7	152	200	185	42.0	32.04	263	255	262
13	FM5	6080	423	382	243	202	152	121	177	341	333	5950	17.9	13.7	153	197	183	35.0	31.34	269	257	262
14	T22	6000	423	383	245	203	153	121	183	340	332	5000	20.7	16.3	153	205	190	32.8	31.71	259	257	260
15	T22	6080	423	383	245	202	152	120	180	340	333	5000	18.9	14.6	147	200	183	34.8	32.24	263	259	265
16	T22	6000	423	383	245	204	152	121	181	340	333	5000	20.0	15.7	150	203	186	33.8	32.34	259	258	264
17	T22	6000	423	383	245	204	153	122	191	340	329	4980	22.8	18.4	159	211	196	28.8	31.41	259	255	259
18	T22	6000	423	383	245	203	153	121	189	340	333	4980	21.5	17.0	156	208	192	33.2	31.51	259	257	259
19	INV	6000	423	381	254	209	154	123	169	341	307	4980	25.3	21.0	152	207	170	5.8	29.98	272	268	274
20	INV	6080	423	380	262	213	155	125	160	342	269	4980	31.9	27.9	152	209	160	--	28.96	283	274	284
21	INV	6080	424	385	240	202	154	120	188	384	352	4980	19.5	14.8	153	205	193	52.4	32.78	256	254	259
22	T2	6080	427	387	240	206	157	120	176	390	360	4980	20.7	16.8	152	205	179	59.6	33.72	263	258	264
23	T2	6080	424	384	245	205	154	121	176	350	341	4980	20.6	16.2	153	206	188	41.4	32.38	263	259	264
24	FM2	6040	419	379	244	211	151	121	175	340	320	4980	19.7	16.2	153	206	177	21.6	28.97	260	258	264
25	FM2	6040	417	381	208	218	141	107	157	395	366	5000	19.3	16.2	146	193	154	69.6	35.85	234	229	235
26	FM2	6040	418	378	238	215	147	115	162	376	347	5020	20.6	17.0	150	202	163	48.6	30.03	261	258	261
27	FM2	6040	419	377	259	207	152	113	184	341	273	5000	19.8	16.2	154	208	190	--	26.54	274	265	270
28	FM2	6040	419	377	277	203	156	126	193	344	225	5020	19.9	16.2	156	210	199	--	24.64	274	--	272

APPENDIX E

Nomenclature

Nomenclature for Body of Report

A	flow cross-sectional area, ft^2
A_s	heat transfer surface area, ft^2
C_p	specific heat of fluid, Btu/lb °F
d	disturbance
G_1	transfer function between boiler-inlet flow rate and pressure
G_2	transfer function between pump exit pressure and flow rate
H_{fg}	heat of vaporization, Btu/lb
I	position (length) of vapor-liquid interface
K	specific heat ratio
l	length, ft
NTU	number of heat transfer units
P	pressure, lb/in^2
R	gas constant
T	temperature, °F
T_{sat}	saturation temperature, °F
ΔT_m	mean temperature difference between two fluids in heat exchanger, °F
ΔT_{pp}	temperature difference between two fluids at boiler pinch point, °F
U	overall heat transfer coefficient between two fluids, Btu/hr ft^2 °F
w	flow rate, lb/hr
X	quality (per cent vapor)
ρ	fluid density, lb/ft^3
ϕ	heat transfer perimeter, ft
ω	frequency, sec^{-1}

Subscripts

cf	condensing fluid
cool	condenser coolant fluid
sc	subcooled fluid

Nomenclature for Appendix B

I	electrical current
K	proportionality constant
R	electrical resistance
V	voltage
δ	mechanical position of potentiometer (0 to 1, end to end)

Subscripts

p	"process" input to controller
ref	reference voltage
sig	electrical signal from measuring device
sp	"set point" input to controller

Nomenclature for Appendix F

fv	friction factor of vapor
G_M	average mass flow rate
h	heat transfer coefficient between fluid and surface, Btu/hr ft^2 °F
N_{PR}	Prandtl Number
N_R	Reynolds Number
N_{ST}	Stanton Number
V	fluid velocity

Subscripts

o	steady-state design values
L	liquid

APPENDIX F

Linearized Condenser Variable Relationships

Approximate expressions for the rate of change of interface position in the condenser with condensing pressure, coolant flow rate, power-loop flow rate and coolant inlet temperature may be derived starting with an approximate equation for overall heat transfer in the condenser:

$$(w\,H_{fg})_{\text{condensing fluid}} = U_{\text{mean}}\left(T_{\substack{\text{saturation,}\\\text{condensing}\\\text{fluid}}} - T_{\text{coolant}}\right)_{\text{mean}} \phi\, I$$

where ϕ is the heat transfer perimeter and I is the distance of the interface from the entrance to the condensing tubes, i.e. the condensing length.

This equation may be differentiated to obtain the following partial derivatives at the nominal design operating point. The subscript o designates the steady-state design value of a variable.

$$\frac{\partial I}{\partial T_{sat}} = -\frac{I_o}{(T_{sat} - T_{coolant})_{mean,\ o}}$$

$$\frac{\partial I}{\partial T_{\substack{\text{coolant}\\\text{mean}}}} = \frac{I_o}{(T_{sat} - T_{coolant})_{mean,\ o}}$$

$$\frac{\partial I}{\partial U_{mean}} = -\frac{I_o}{U_{mean,\ o}}$$

$$\frac{\partial I}{\partial w_{cf}} = \frac{I_o}{w_{cf}}$$

Additional partial derivatives which will be required are evaluated below.

$$\frac{\partial T_{\text{coolant mean}}}{\partial T_{\text{coolant in}}} \approx 1$$

$$\frac{\partial T_{\text{coolant mean}}}{\partial w_{\text{coolant}}} \approx \frac{1}{2} \quad \frac{(T_{\text{coolant in}} - T_{\text{coolant out}})_o}{w_{\text{coolant, o}}}$$

Employing the relationship $U = \dfrac{h_{cf}\, h_{\text{coolant}}}{h_{cf} + h_{\text{coolant}}}$

$$\frac{\partial U}{\partial h_{cf}} = \frac{U - h_{\text{coolant}}}{h_{cf} + h_{\text{coolant}}}$$

$$\frac{\partial U}{\partial h_{\text{coolant}}} = \frac{U - h_{cf}}{h_{cf} + h_{\text{coolant}}}$$

Assuming that the shell-side coefficient varies with the six-tenths power of the shell flow rate [1], as is typical for flow across staggered tubes

$$\frac{\partial h_{\text{mean, coolant}}}{\partial w_{\text{coolant}}} \approx 0.60 \quad \frac{h_{\text{mean, coolant}}}{w_{\text{coolant}}}$$

Assuming a variation of the condensing coefficient with the 0.85 power of flow rate, which is the approximate value obtained from the simplified correlation of Carpenter and Colburn [2]

$$\frac{\partial h_{\text{mean, cf}}}{\partial w_{cf}} \approx 0.85 \quad \frac{h_{\text{mean, cf}}}{w_{cf}}$$

---

[1] Kays, W. M., and A. L. London, Compact Heat Exchangers, p. 60. From the equation $N_{ST}\, N_{PR}^{\,2/3} = C_h\, N_R^{\,-0.4}$, it follows that $h \propto V^{0.6}$

[2] Carpenter and Colburn, The Effect of Vapor Velocity on Condensation Inside Tubes, Proc. of the Gen. Disc. of Heat Transfer, the Inst. of Mech. Eng. and the Am. Soc. of Mech. Eng., July 1951, pg. 6

From the equation $h_c = 0.065\left(\dfrac{C_p K f_v}{2 \mu \rho_v}\right)^{1/2} G_M$, (since f_v is approximately proportional to $N_R^{\,-0.3}$ at the nominal design point), it follows that $h_c \propto G_M^{\,0.85}$

The flow rates, temperatures, heat transfer coefficients, and condensing fluid properties at the design point are

$w_{\text{condensing fluid}}$ = 244 lb/hr

w_{coolant} = 5000 lb/hr

$T_{\text{coolant in}}$ = 153°F

$T_{\text{coolant out}}$ = 203°F

T_{sat} = 216°F

U_{mean} = 1126 Btu/hr ft^2 °F

$h_{\text{mean, cf}}$ = 1800 Btu/hr ft^2 °F

$h_{\text{mean, coolant}}$ = 3000 Btu/hr ft^2 °F

ρ_L = 60 lb/ft^3

H_{fg} = 968 Btu/lb

The design interface location is

$I = 1.7$ ft = 85 per cent of condenser length from inlet

The condenser geometrical constants are

$\phi = 3.0$ ft

$A = 0.0122$ ft^2

The vapor pressure curve of water at the design point yields

$$\frac{\partial T_{sat,\ cf}}{\partial P} = 3.2°F/psi$$

The desired partial derivatives may now be evaluated

$$\frac{\partial I}{\partial P_{sat}} = \frac{\partial I}{\partial T_{sat}} \frac{\partial T_{sat}}{\partial P_{sat}} = -\frac{I_o}{(T_{sat} - T_{coolant})_o} \frac{\partial T_{sat}}{\partial P_{sat}} = 0.071 \frac{\text{\% Cond. Length}}{\text{psi}}$$

$$\frac{\partial I}{\partial w_{coolant}} = \left.\frac{\partial I}{\partial T_{coolant\ mean}}\right)_{\substack{constant \\ U}} \frac{\partial T_{coolant\ mean}}{\partial w_{coolant}} + \left.\frac{\partial I}{\partial U}\right)_{\substack{constant \\ T_{coolant\ mean}}} \frac{\partial U}{\partial w_{coolant}}$$

$$= \frac{I_o}{(T_{sat} - T_{coolant})_{mean,\ o}} \times \frac{1}{2} \frac{(T_{coolant\ in} - T_{coolant\ out})_o}{w_{coolant,\ o}}$$

$$- \frac{I_o}{U_{mean,\ o}} \times \frac{U_o - h_{cf,\ o}}{h_{cf,\ o} + h_{coolant,o}} \times \frac{0.60\ h_{mean,\ coolant,o}}{w_{coolant,o}}$$

$$= -\ 0.00015 \frac{\text{\% Cond. Length}}{\text{lb/hr}}$$

$$\frac{\partial I}{\partial w_{cf}} = \left.\frac{\partial I}{\partial w_{cf}}\right)_{\substack{constant \\ U}} + \frac{\partial I}{\partial U} \frac{\partial U}{\partial w_{cf}}$$

$$= \frac{I_o}{w_{cf,o}} - \frac{I_o}{U_o} \times \frac{U_o - h_{coolant,o}}{h_{cf,o} + h_{coolant,o}} \times \frac{0.85\ h_{cf,o}}{w_{cf,o}}$$

$$= 0.0056 \frac{\text{\% Cond. Length}}{\text{lb/hr}}$$

$$\frac{\partial I}{\partial T_{\substack{coolant\\in}}} = \frac{\partial I}{\partial T_{\substack{coolant\\mean}}} \; \frac{\partial T_{\substack{coolant\\mean}}}{\partial T_{\substack{coolant\\in}}} = \frac{I_o}{(T_{sat} - T_{coolant})_{mean,\,o}} \times 1$$

$$= 0.019 \; \frac{\%\ \text{Cond. Length}}{{}^{\circ}\text{F}}$$

These calculated values for rate of change of condenser interface portion are compared on page 17 to values obtained from data plots.

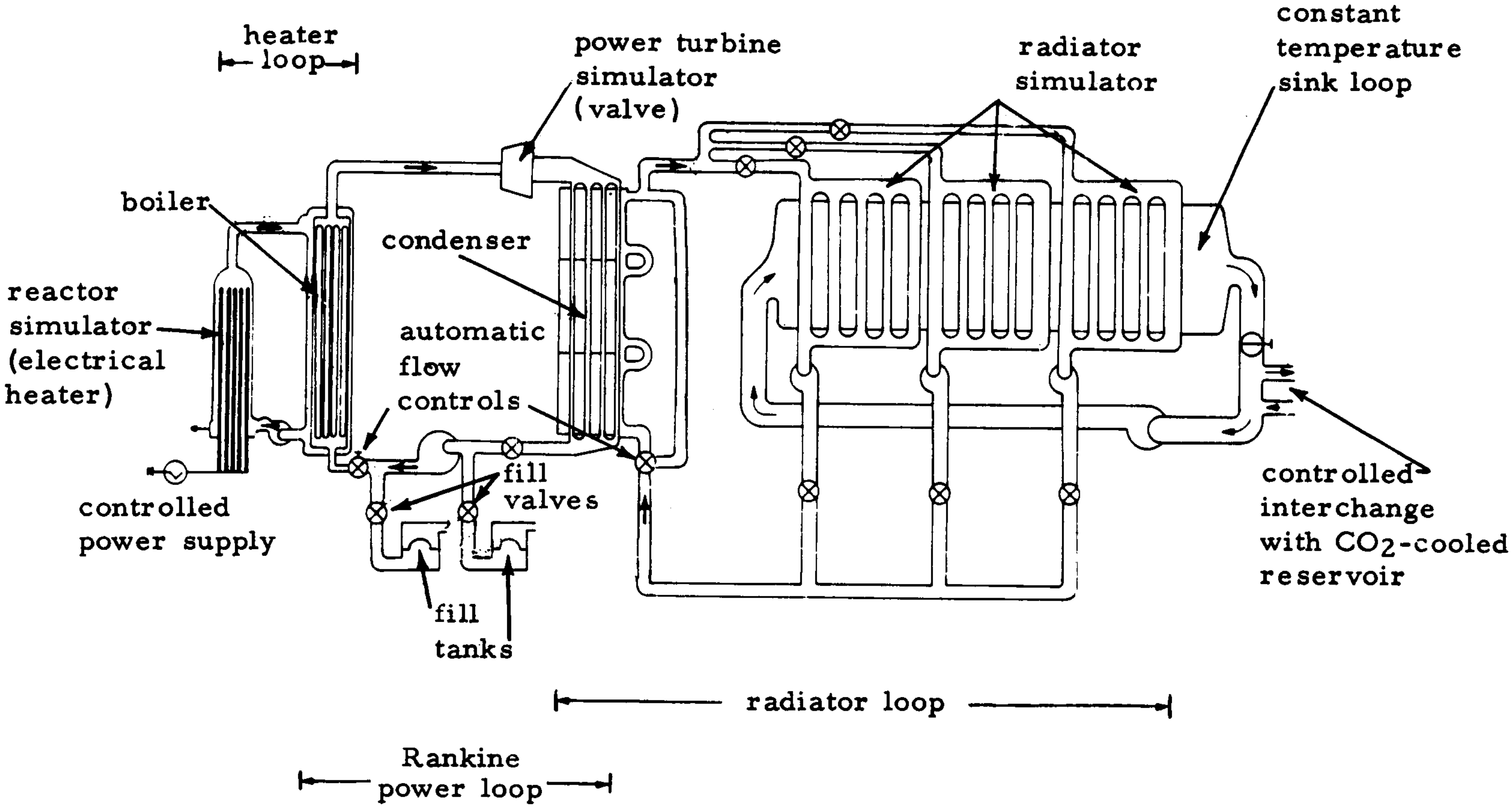

Figure 1 Schematic Diagram of Powerplant Simulator

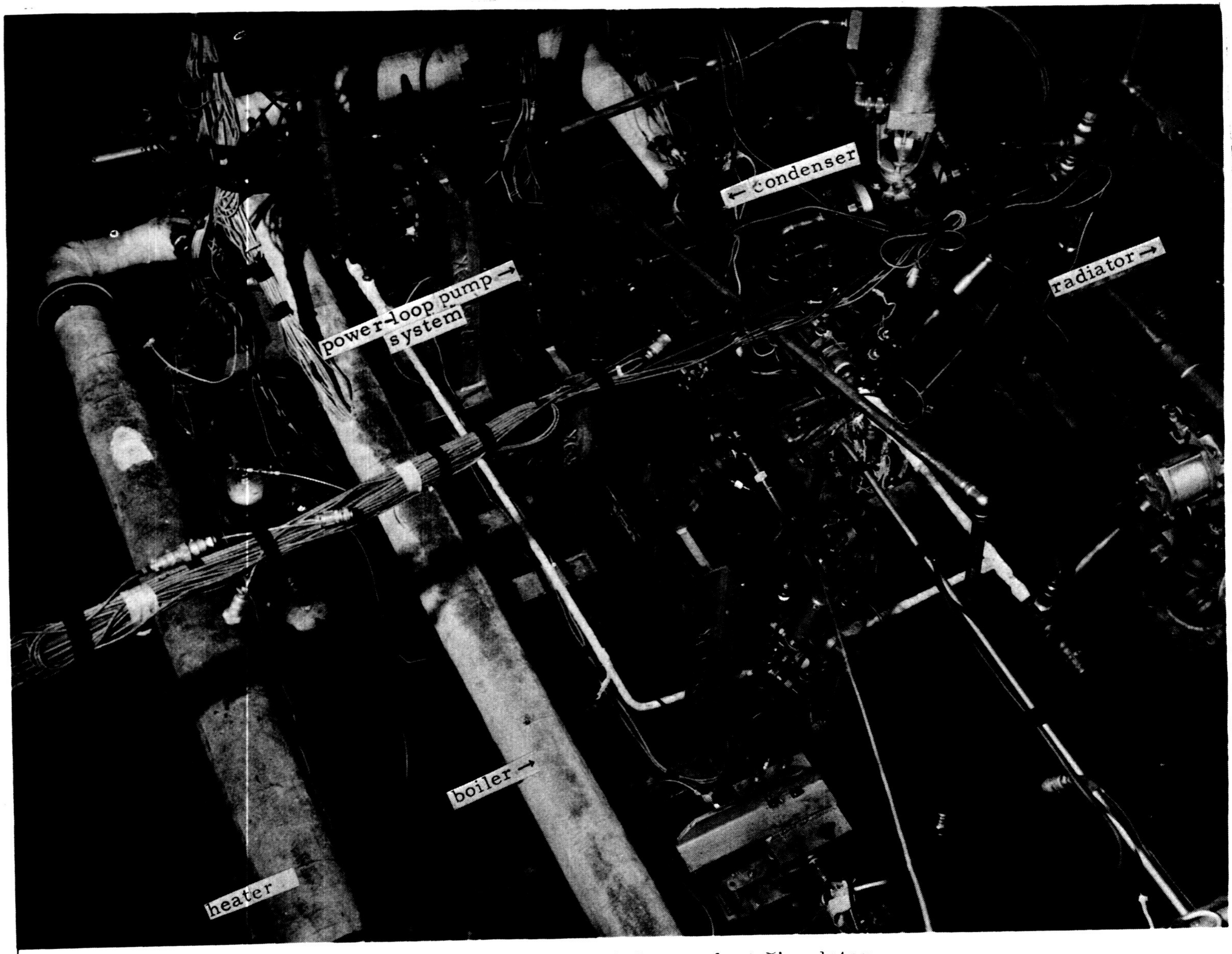

Figure 2 Photograph of Powerplant Simulator

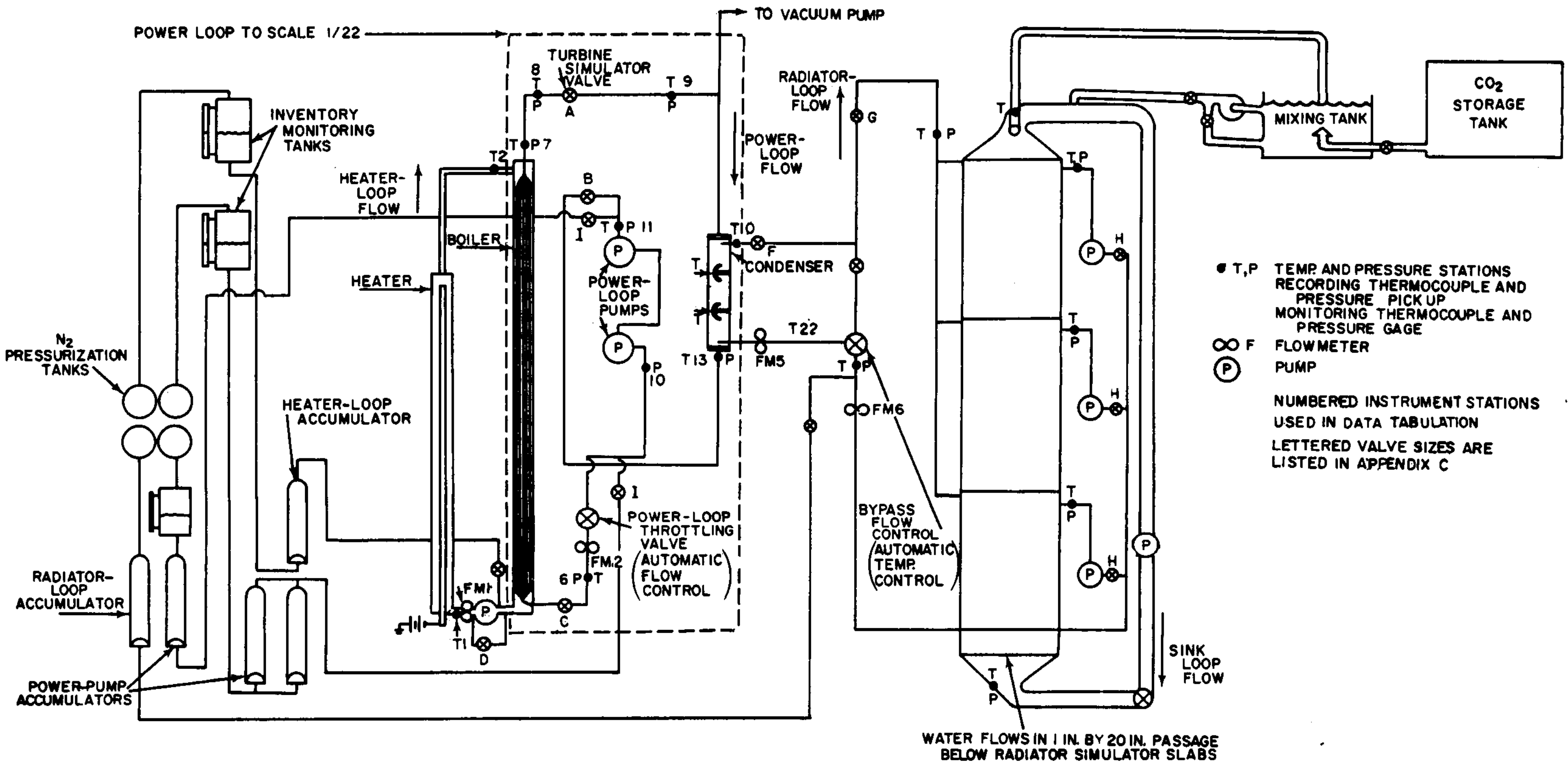

Figure 3 Three-Loop Powerplant Simulator Arrangement

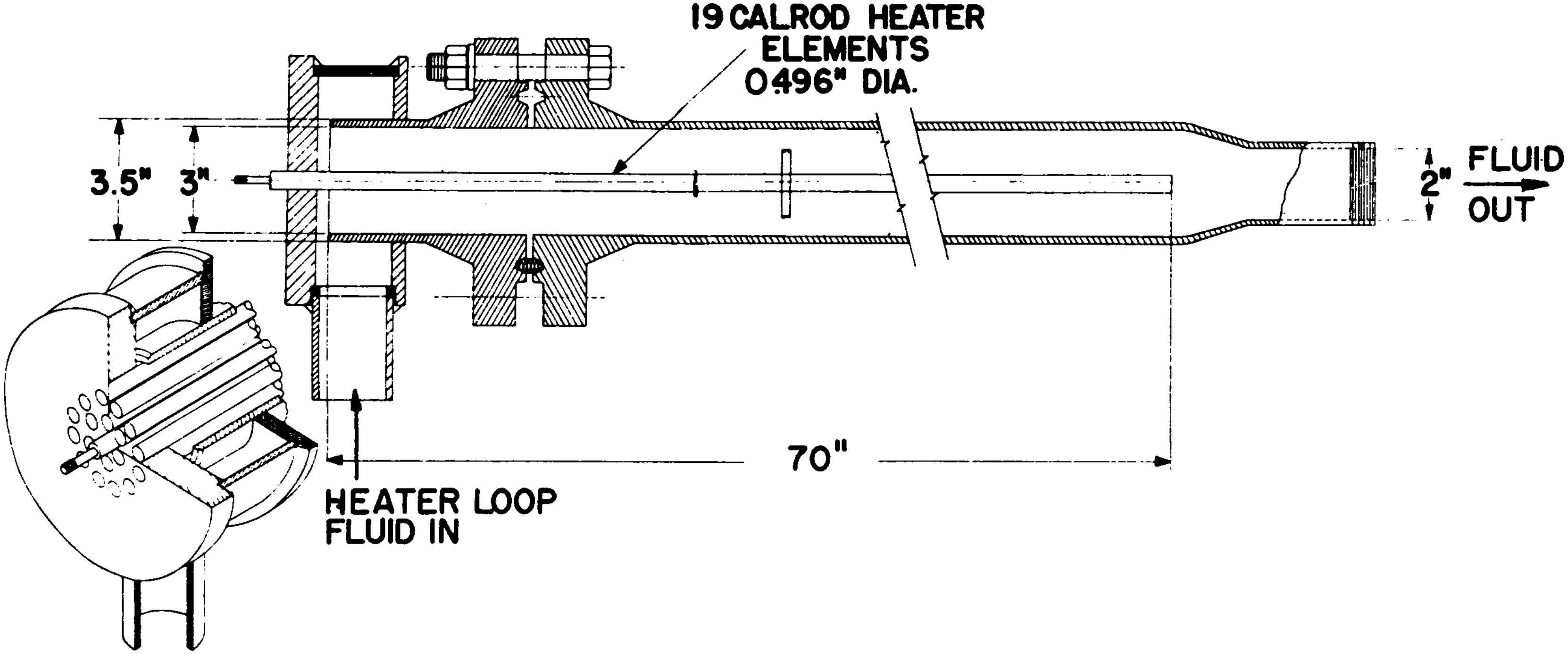

Figure 4 Calrod Heater

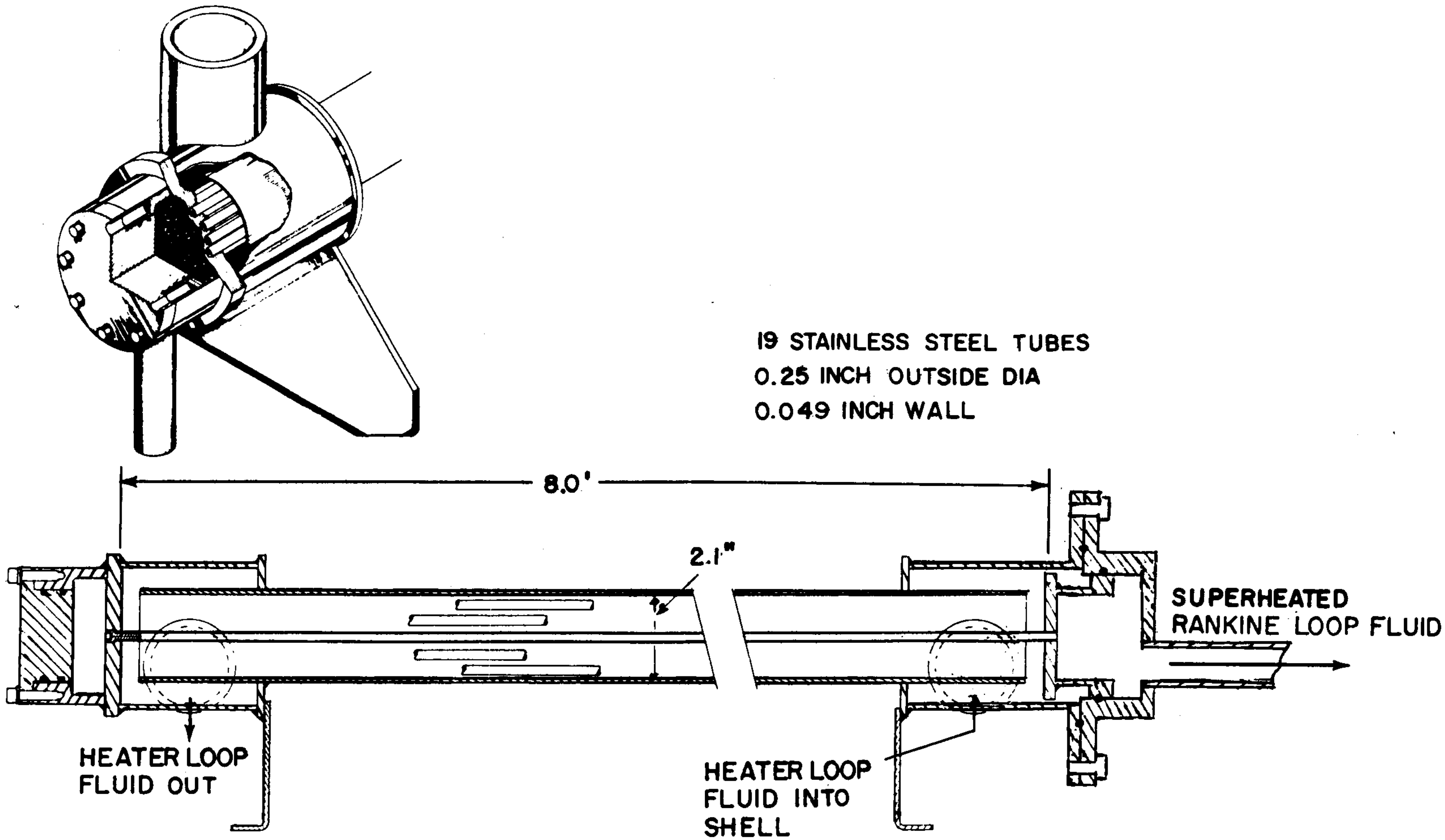

Figure 5 Rankine-Loop Boiler

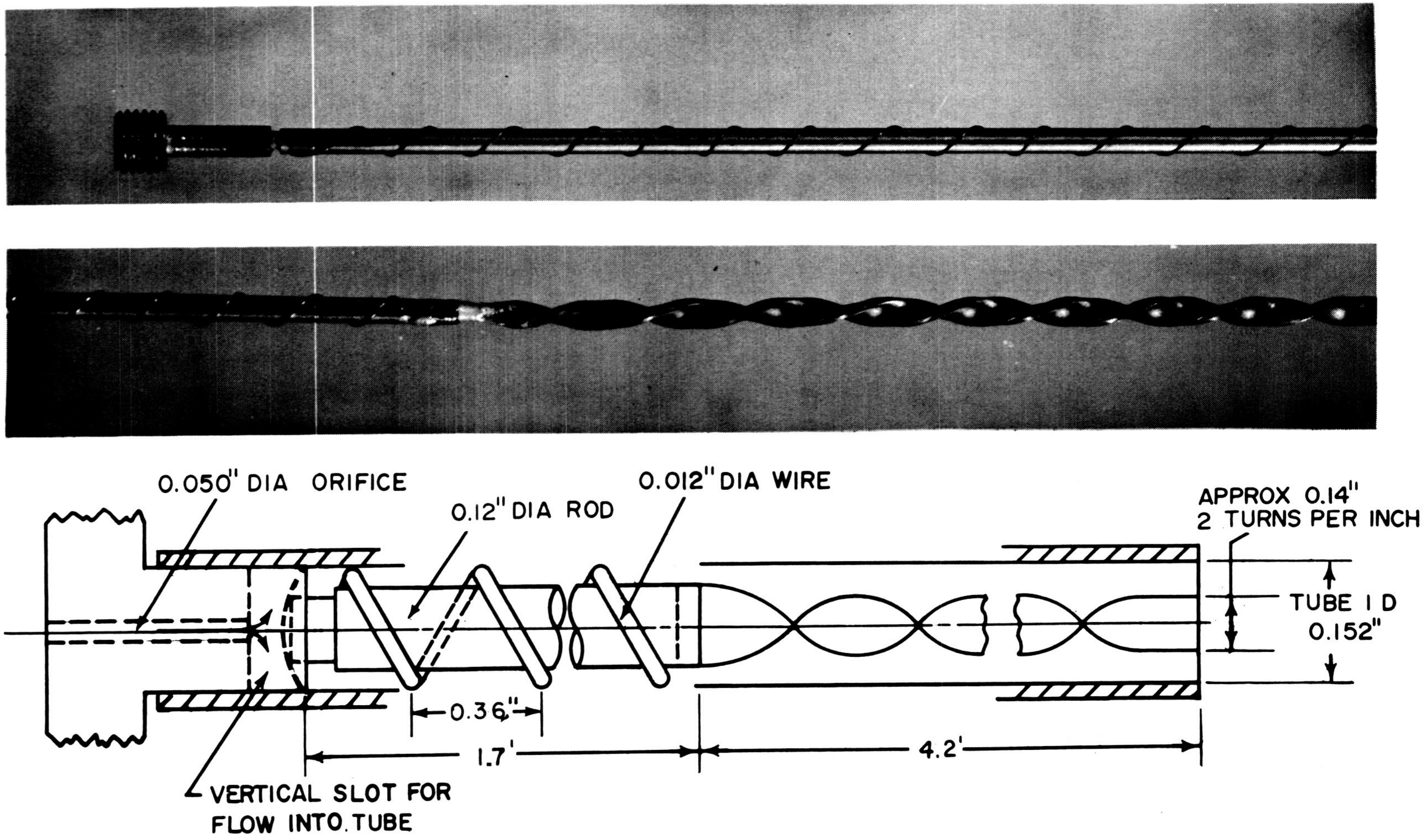

Figure 6 Boiler Inserts

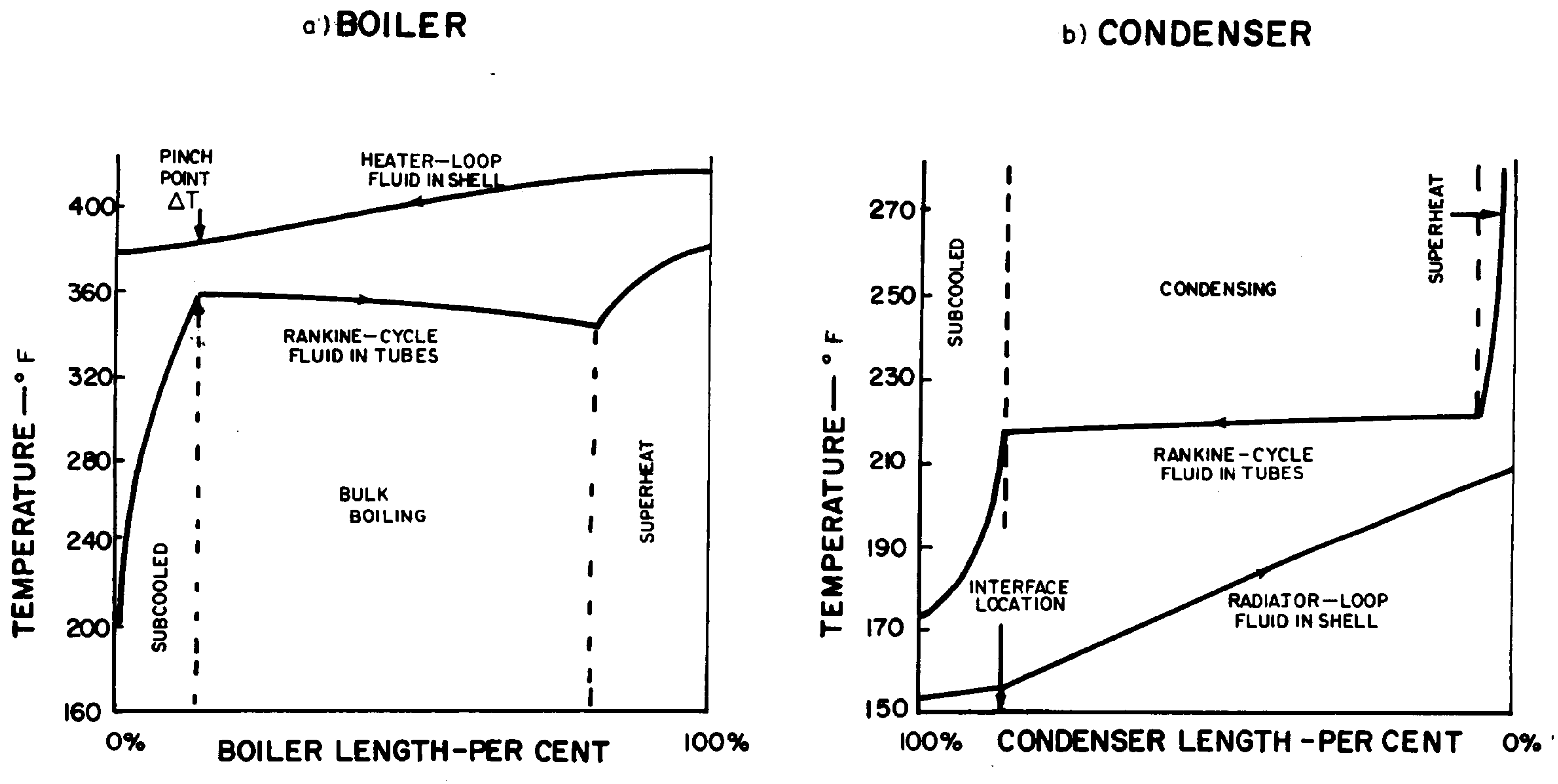

Figure 7 Idealized Bulk Temperature Distribution in Boiler and Condenser

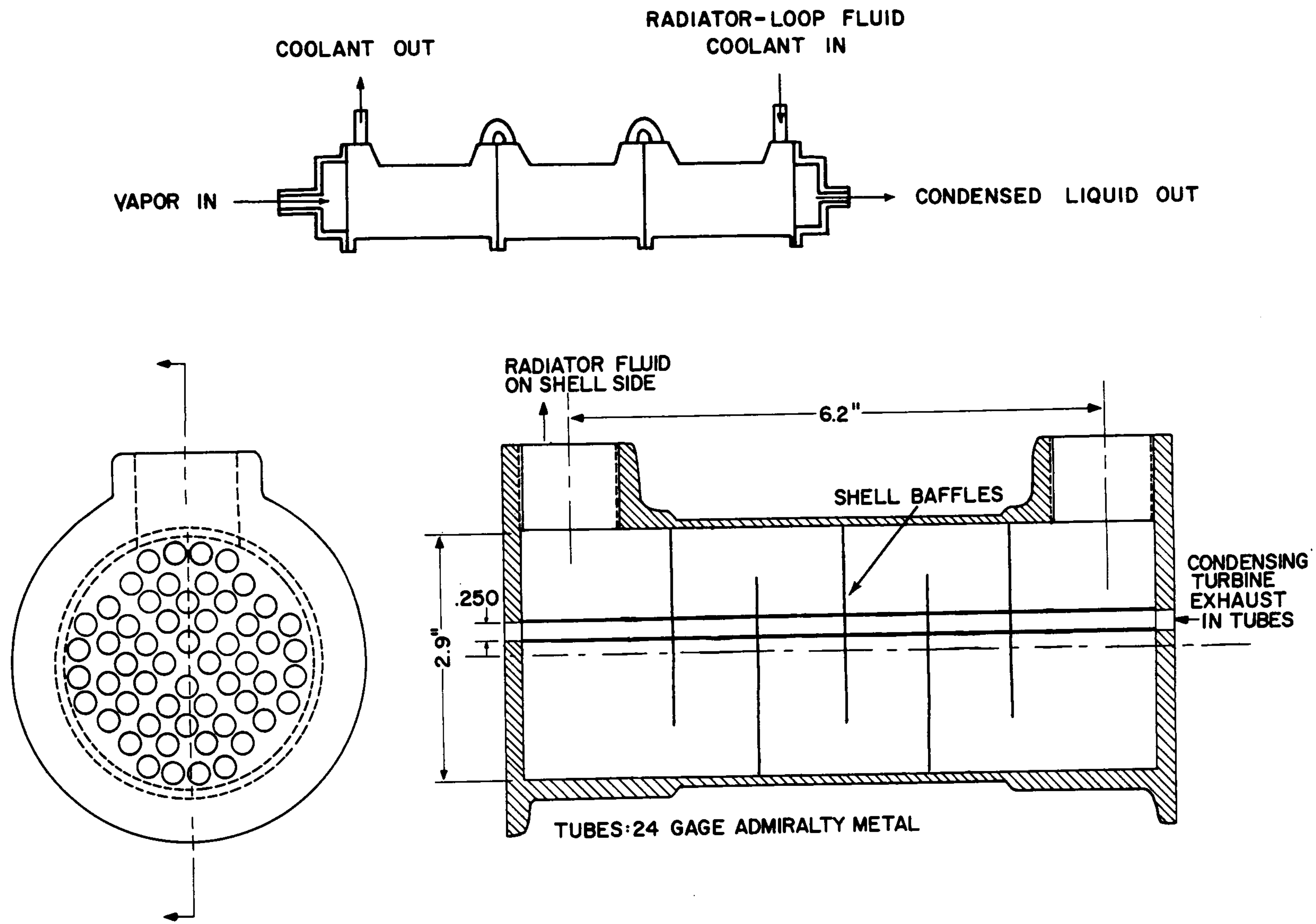

Figure 8 Condenser (Three Ross BCF-7M300 Heat Exchangers Connected in Series)

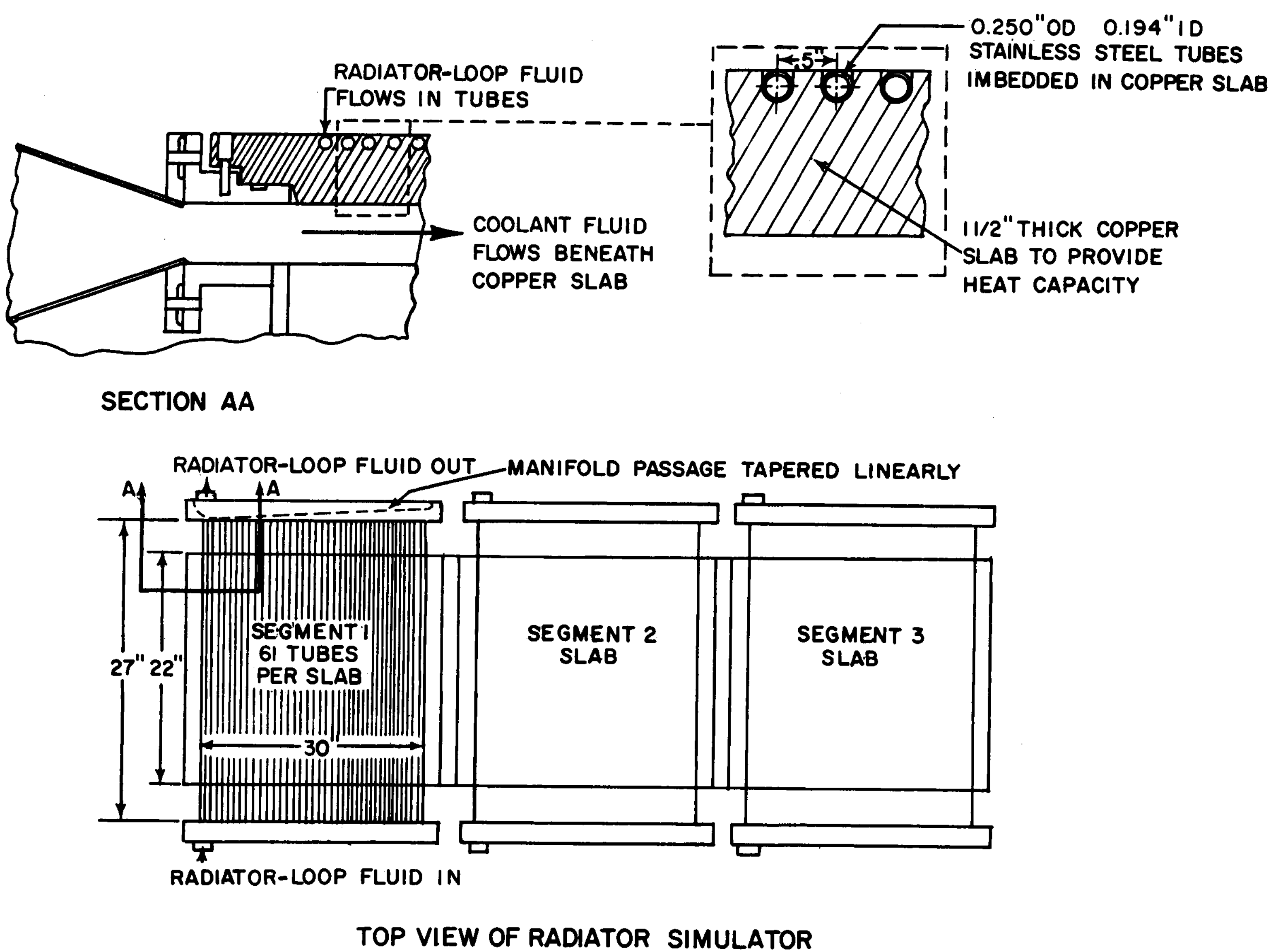

Figure 9 Radiator Simulator

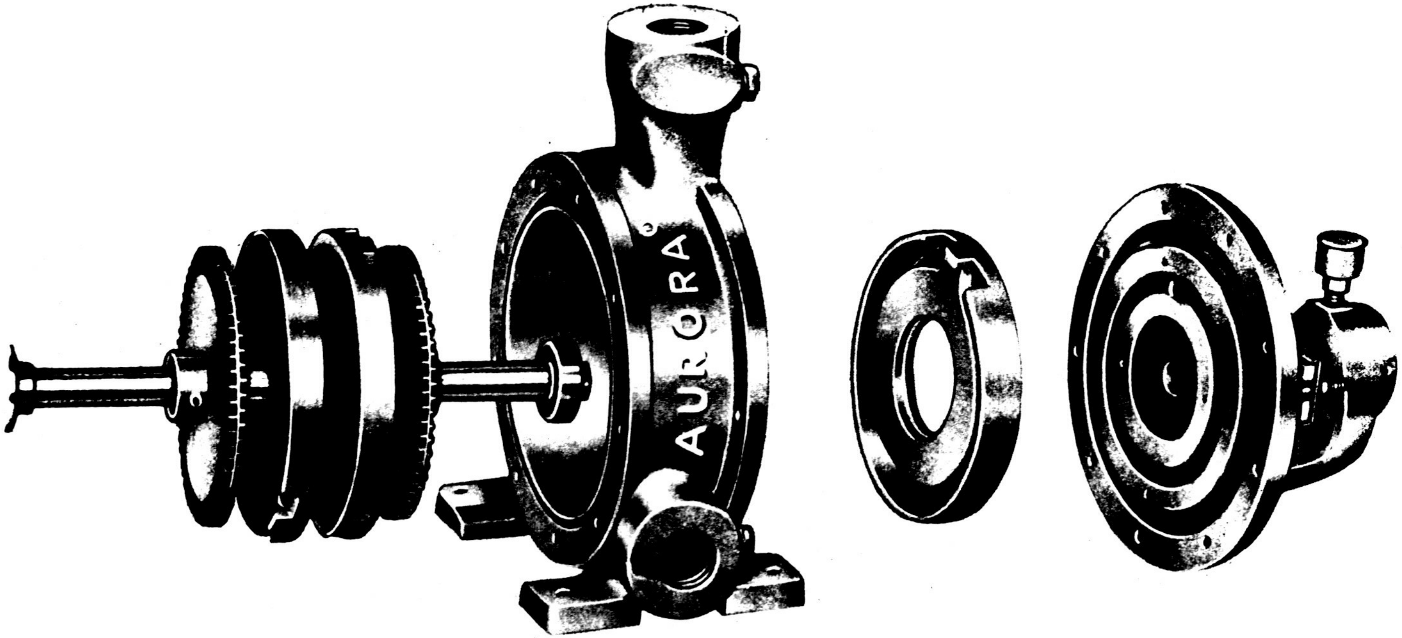

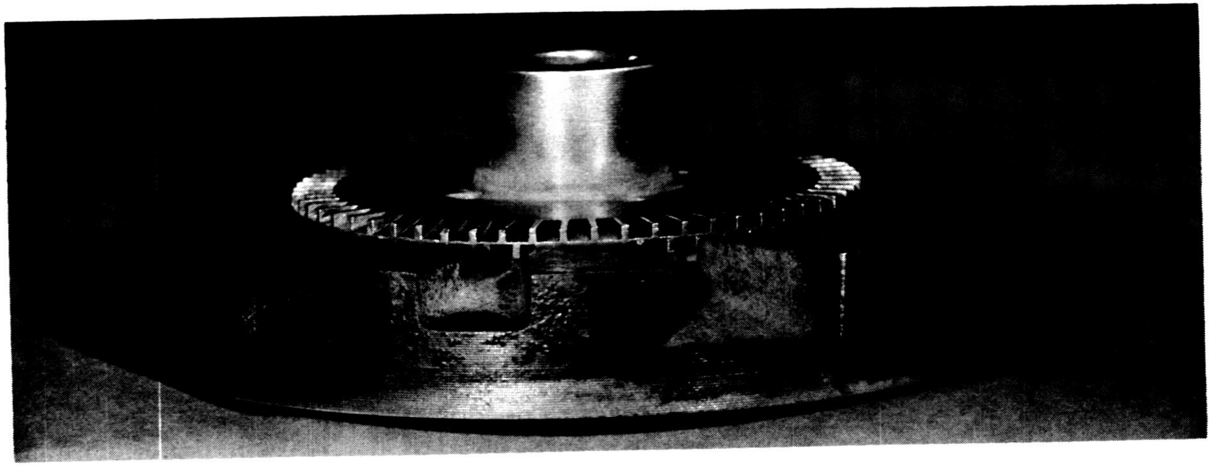

Figure 10 Aurora Type B-4-T Turbine Pump

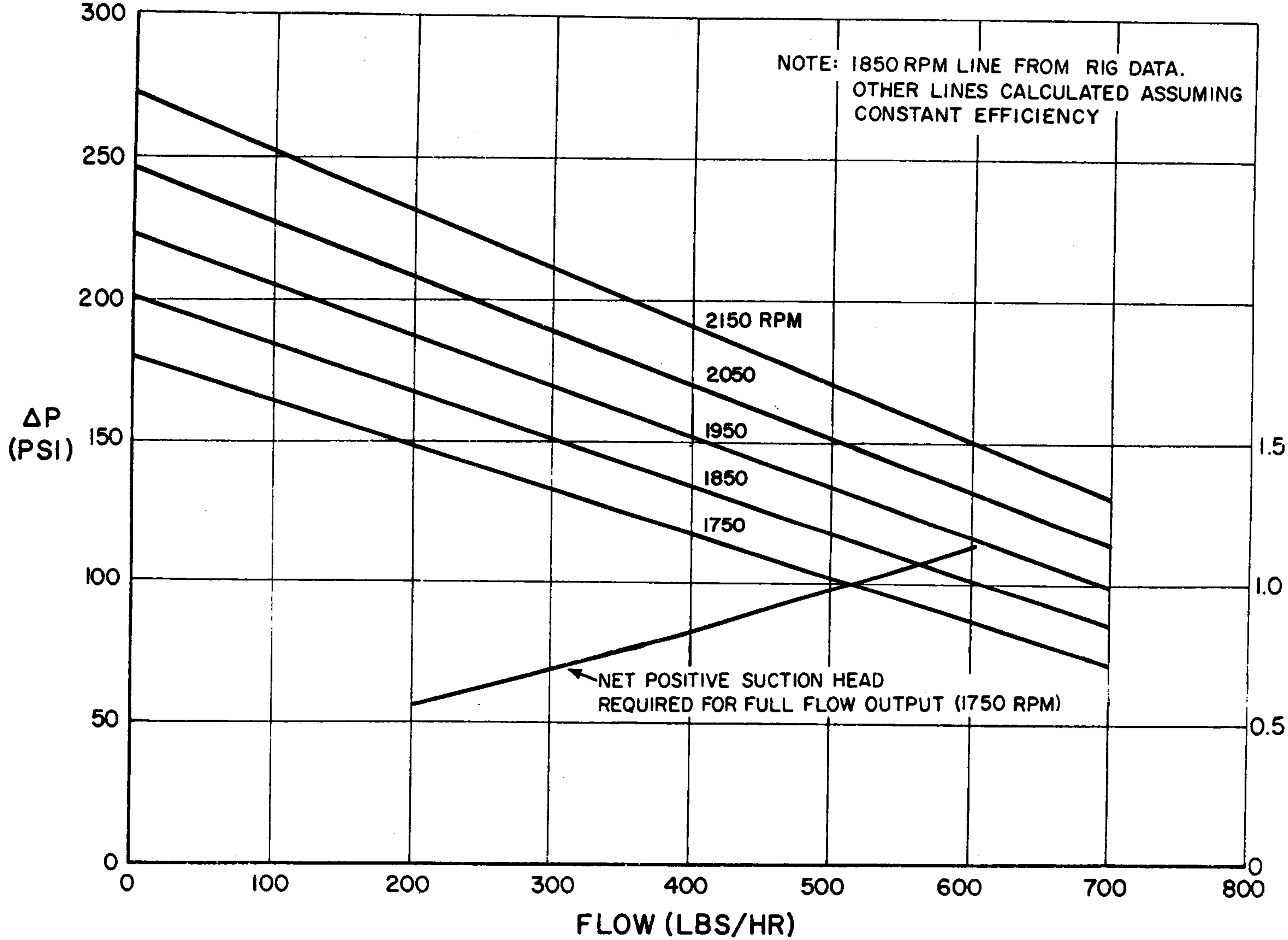

Figure 11 Power-Loop Pump System (2 Aurora Type B-4-T in Series). Head-Flow Relationship at Different Pump Speeds for Two Pumps in Series

Design Conditions

$W_{\text{power loop}}$ = 244 lbs/hr
$W_{\text{cond. shell}}$ = 5000 lbs/hr
$P_{\text{cond. inlet}}$ = 18.4 psia
$P_{\text{cond. exit}}$ = 16.0 psia
$T_{\text{cond. shell inlet}}$ = 153°F

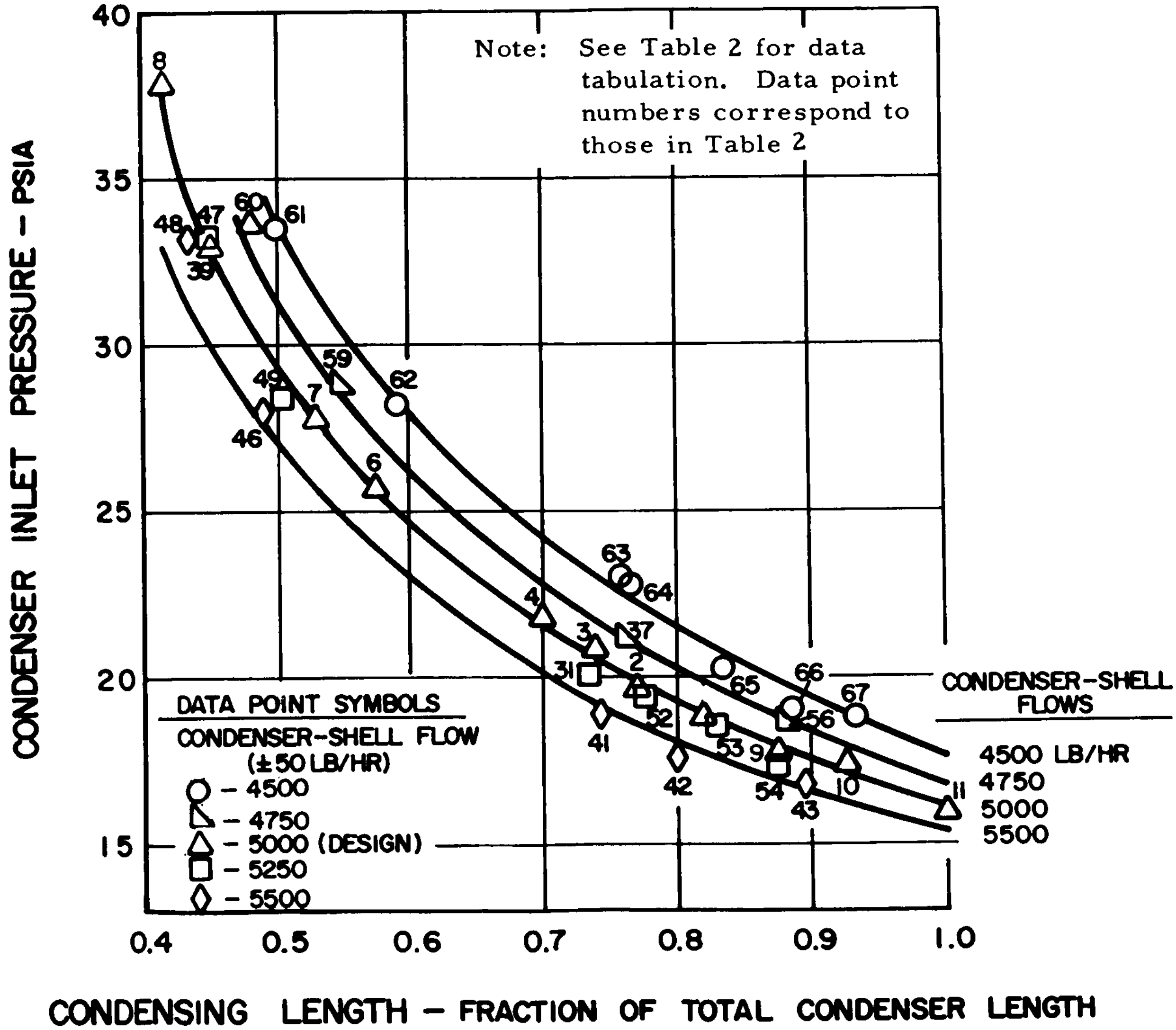

Figure 12 Variation of Condenser Inlet Pressure With Condensing Length at Several Condenser-Shell Flow Rates (With Conditions Otherwise at Design)

Design Conditions

$W_{power\ loop}$ = 244 lbs/hr
$W_{cond.\ shell}$ = 5000 lbs/hr
$P_{cond.\ inlet}$ = 18.4 psia
$P_{cond.\ exit}$ = 16.0 psia
$T_{cond.\ shell\ inlet}$ = 153°F

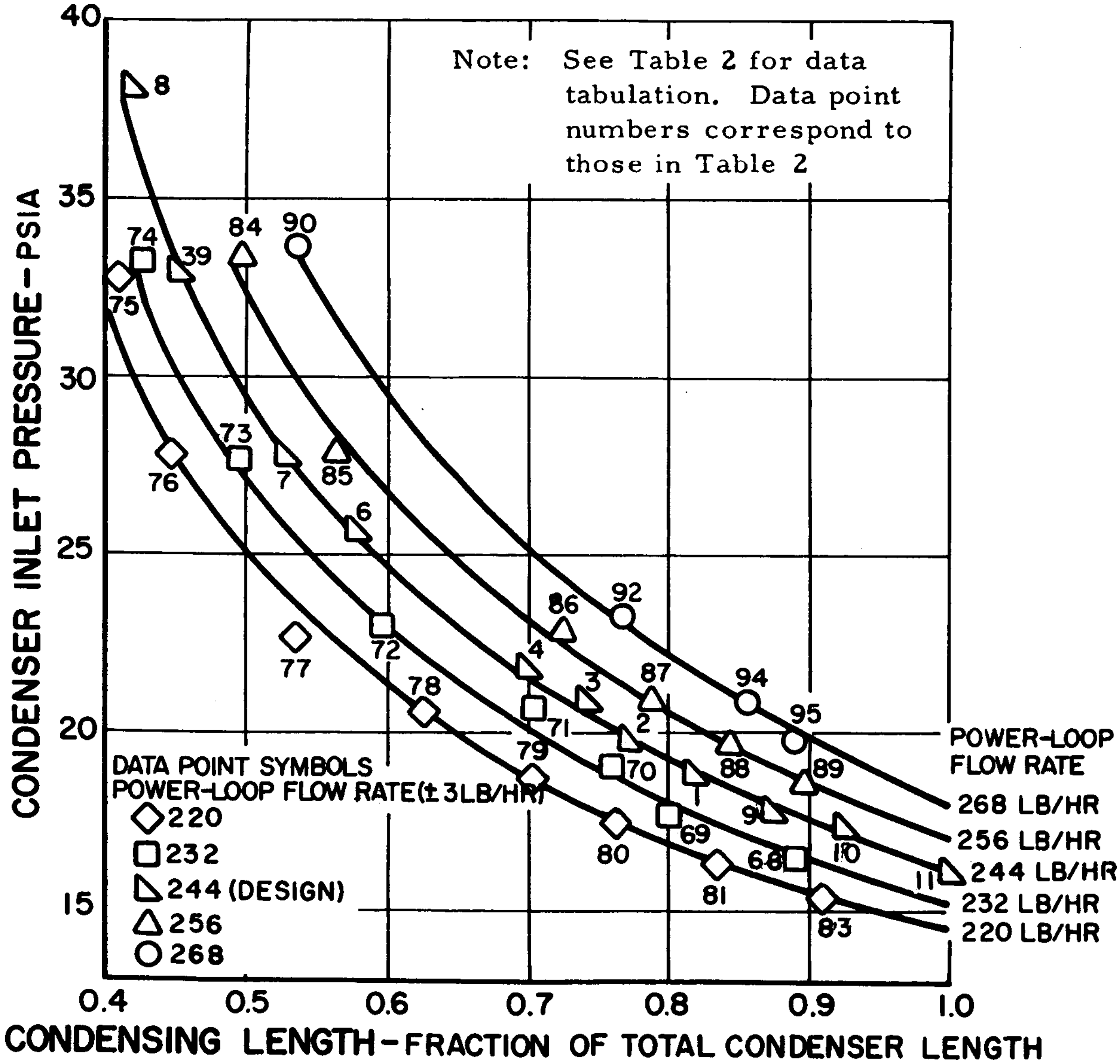

Figure 13 Variation of Condenser Inlet Pressure With Condensing Length at Several Power-Loop Flow Rates (with conditions otherwise at design)

Design Conditions

$W_{\text{power loop}} = 244$ lbs/hr
$W_{\text{cond. shell}} = 5000$ lbs/hr
$P_{\text{cond. inlet}} = 18.4$ psia
$P_{\text{cond. exit}} = 16.0$ psia
$T_{\text{cond. shell inlet}} = 153°F$

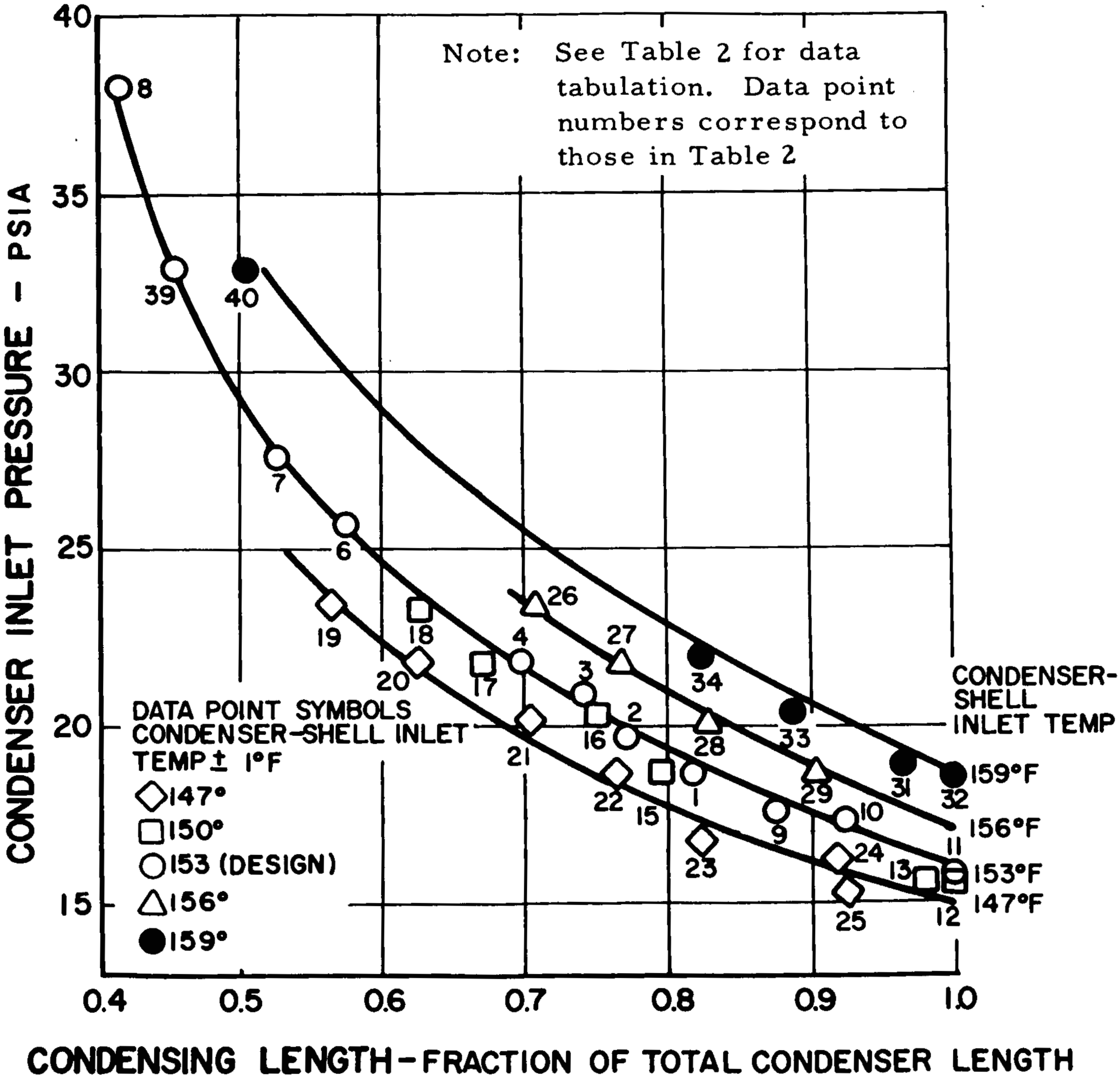

Figure 14 Variation of Condenser Inlet Pressure With Condensing Length at Several Condenser-Shell Inlet Temperatures (with conditions otherwise at design).

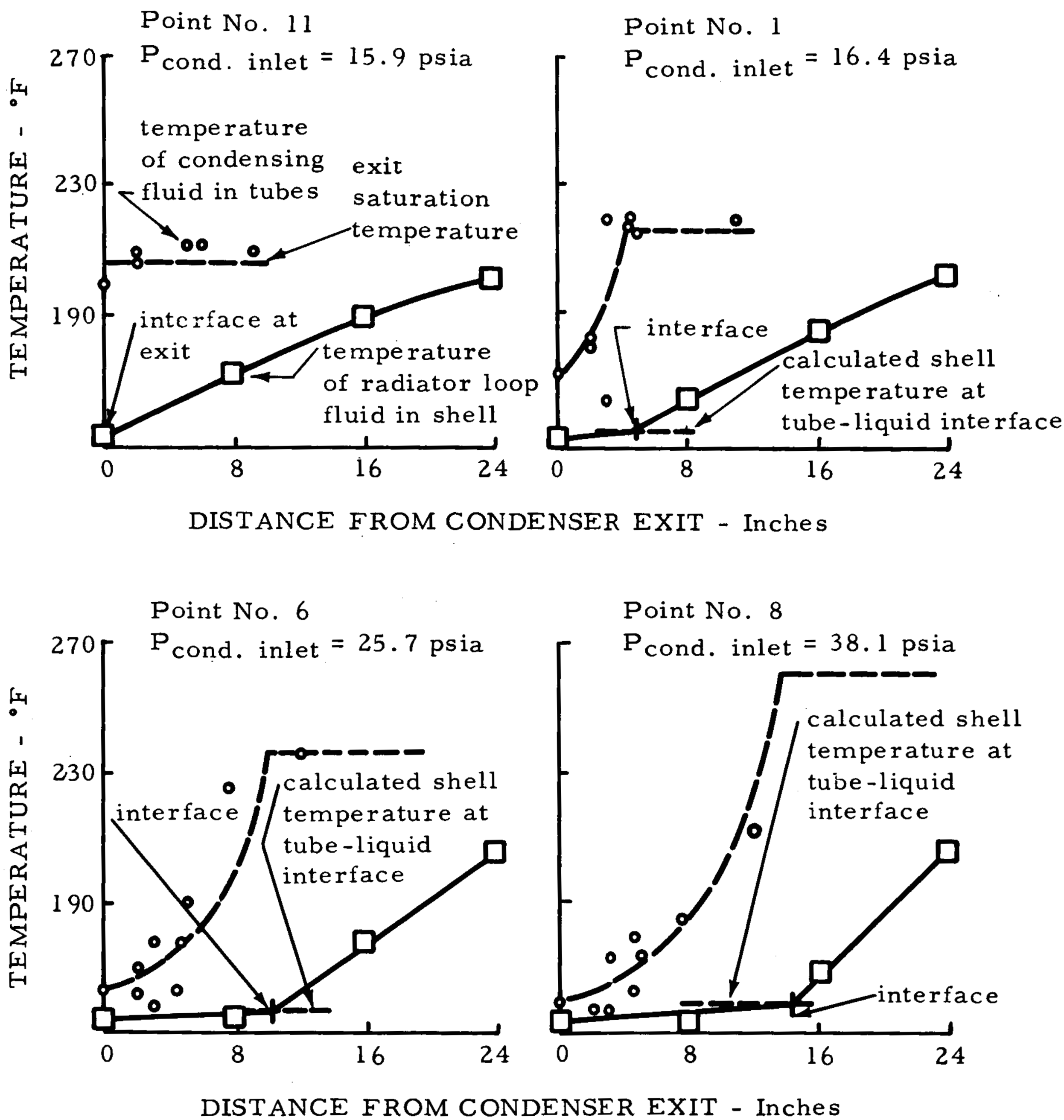

Figure 15 Plots of Condenser Temperature Data Showing Measured Temperatures and Calculated Location of Interface. (Data Points Were Selected to Show Interface Progressively Farther From Exit).

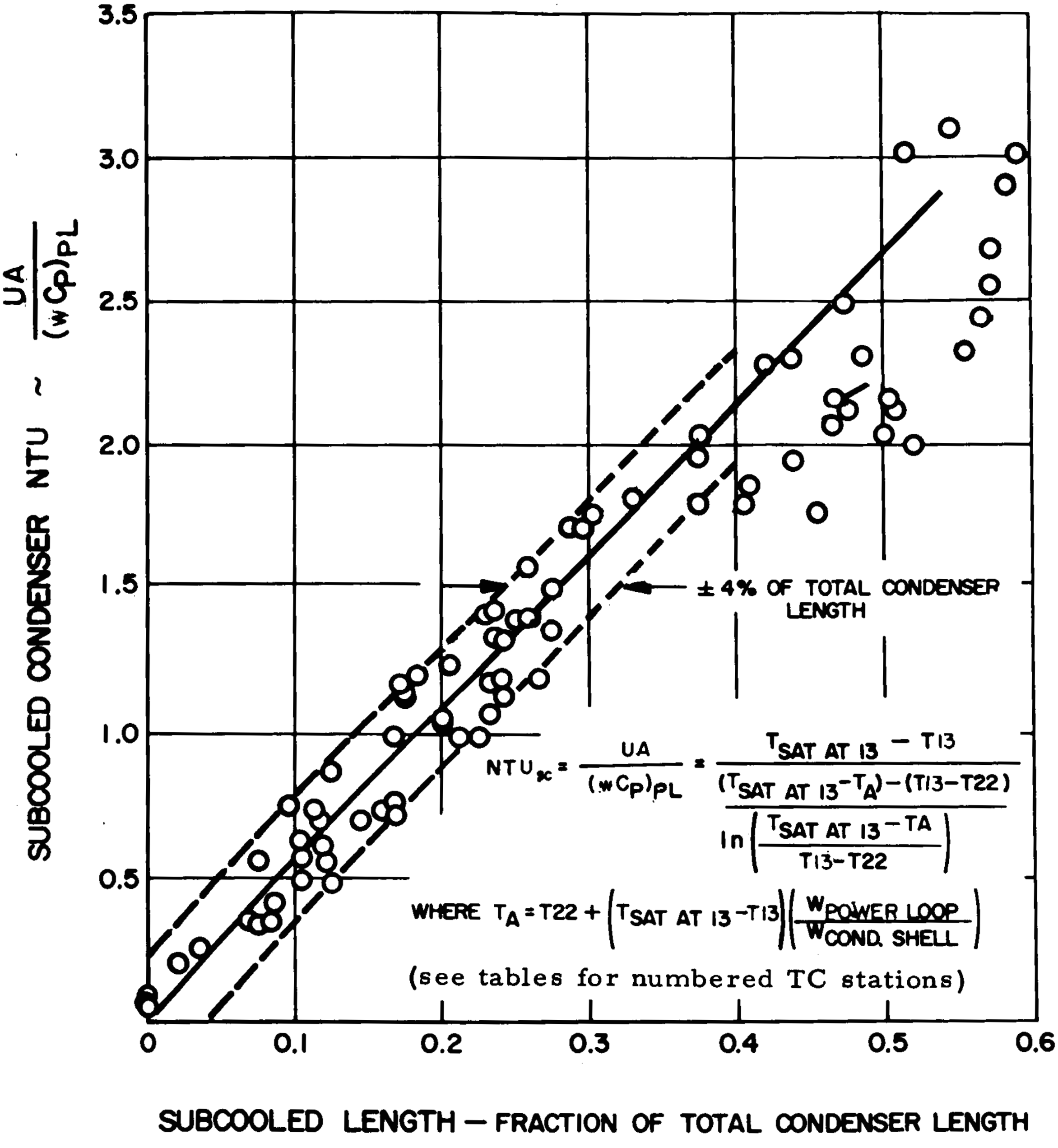

Figure 16 Subcooled NTU vs Subcooled Length from Shell Temperature Plots for Data with Condenser-Shell Flow an Independent Variable

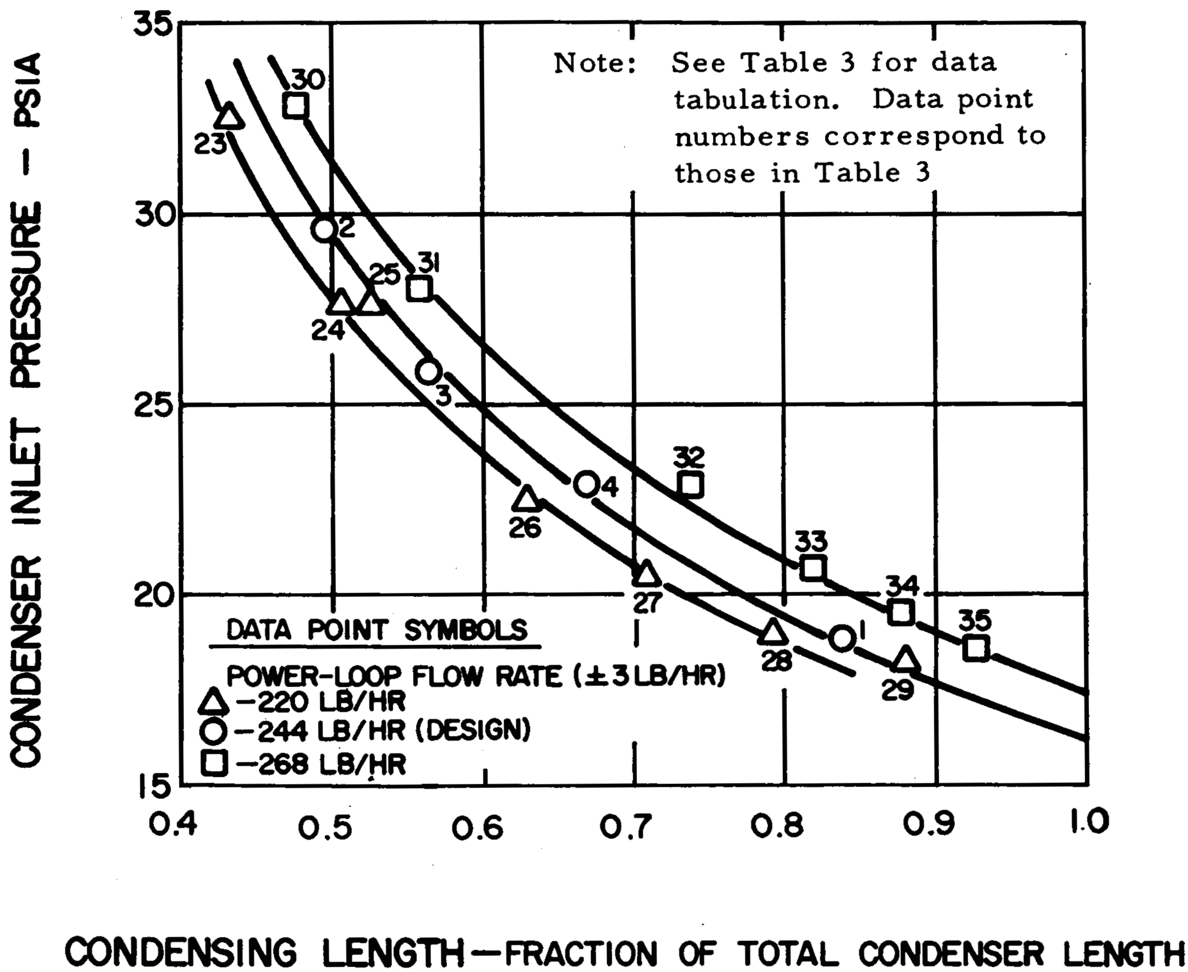

Figure 17 Variation of Condenser Inlet Pressure With Condensing Length at Three Power-Loop Flow Rates. Condenser-Shell Outlet Temperature Controlled at 203°F

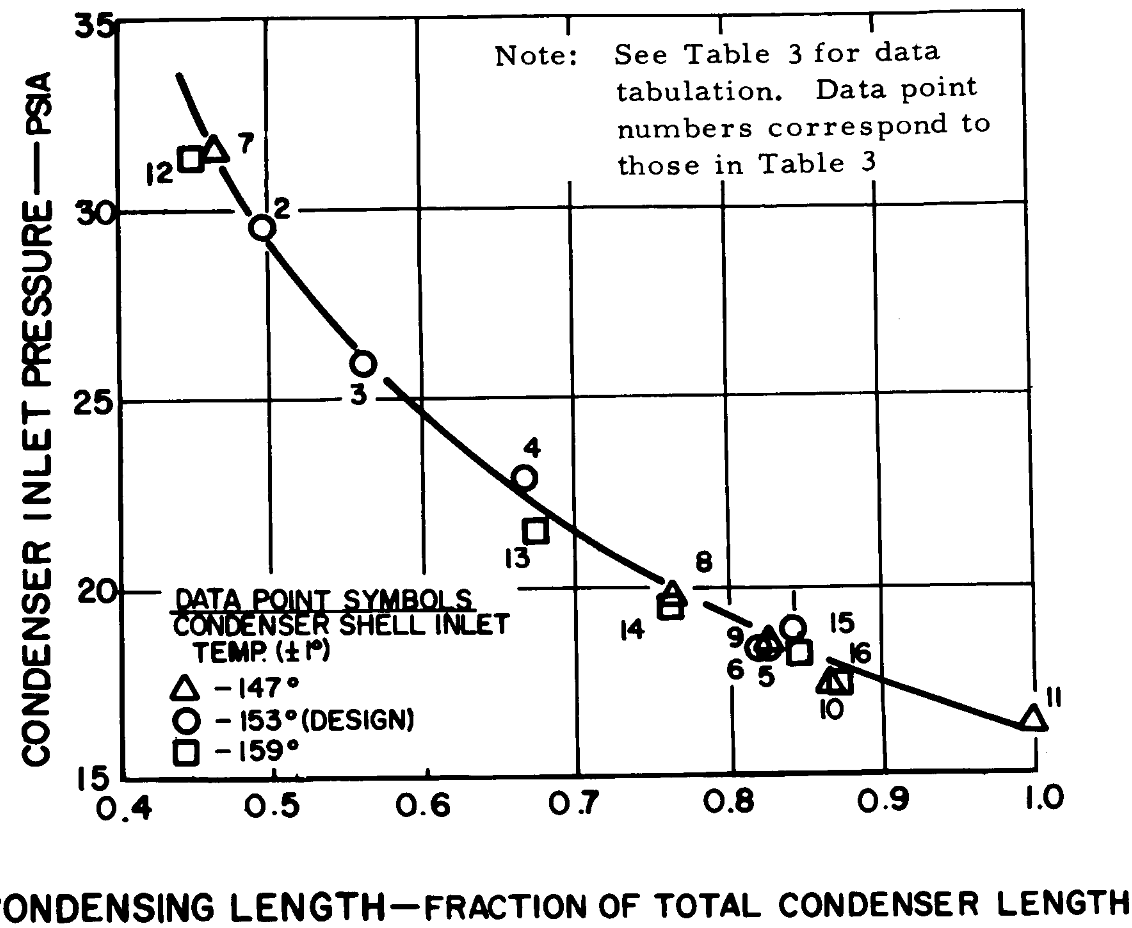

Figure 18 Variation of Condenser Inlet Pressure With Condensing Length at Three Condenser-Shell Inlet Temperatures. Condenser-Shell Outlet Temperature Controlled at 203°F

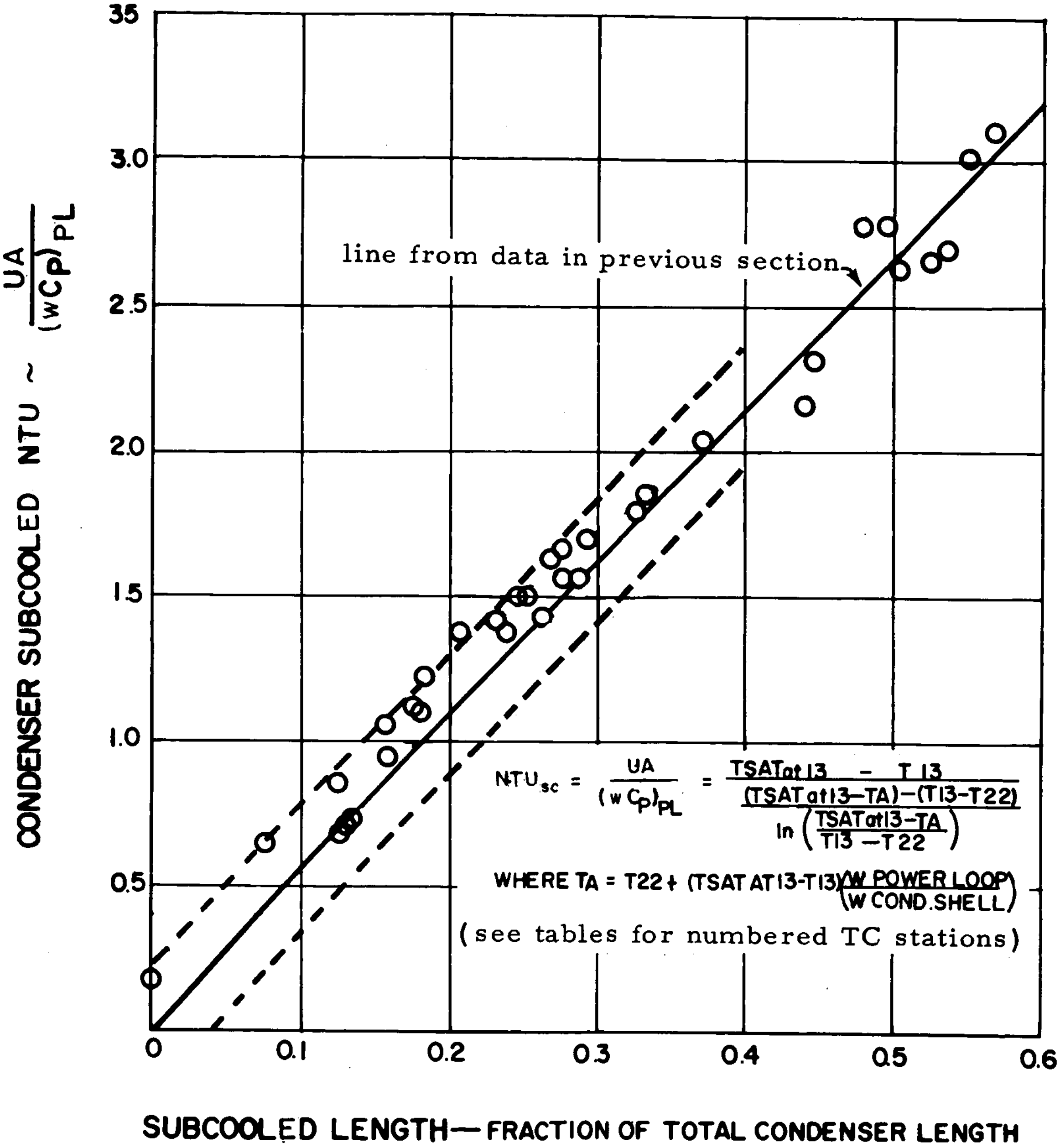

Figure 19 Subcooled NTU vs Subcooled Length from Shell Temperature Plots for Data with Condenser-Shell Outlet Temperature Controlled at 203 °F

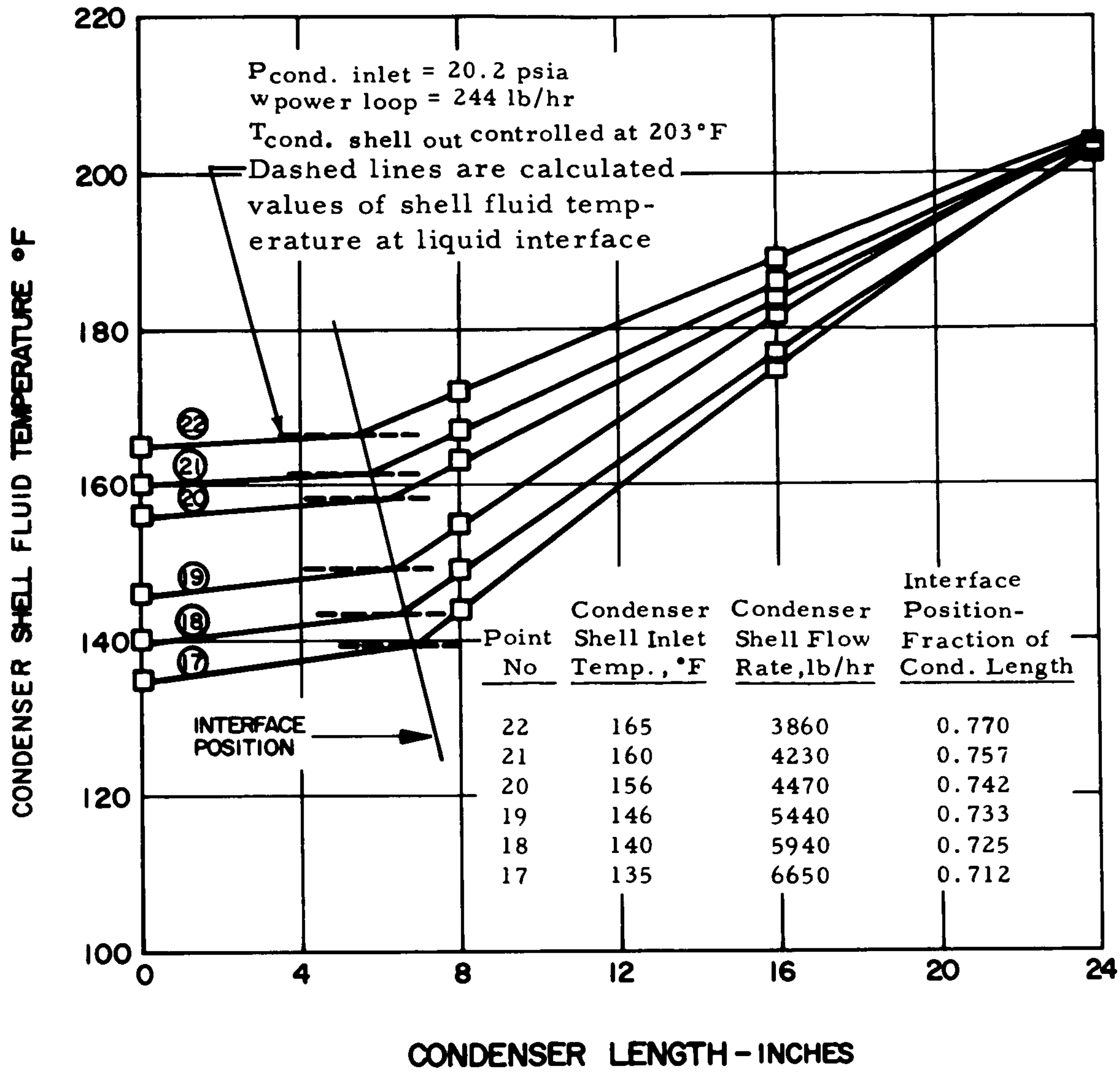

Point No	Condenser Shell Inlet Temp., °F	Condenser Shell Flow Rate, lb/hr	Interface Position-Fraction of Cond. Length
22	165	3860	0.770
21	160	4230	0.757
20	156	4470	0.742
19	146	5440	0.733
18	140	5940	0.725
17	135	6650	0.712

Figure 20 Condenser-Shell Fluid Temperature Profiles vs Condenser Length at Six Inlet Temperatures With Outlet Temperature Controlled at 203°F and Condensing Pressure Held Constant

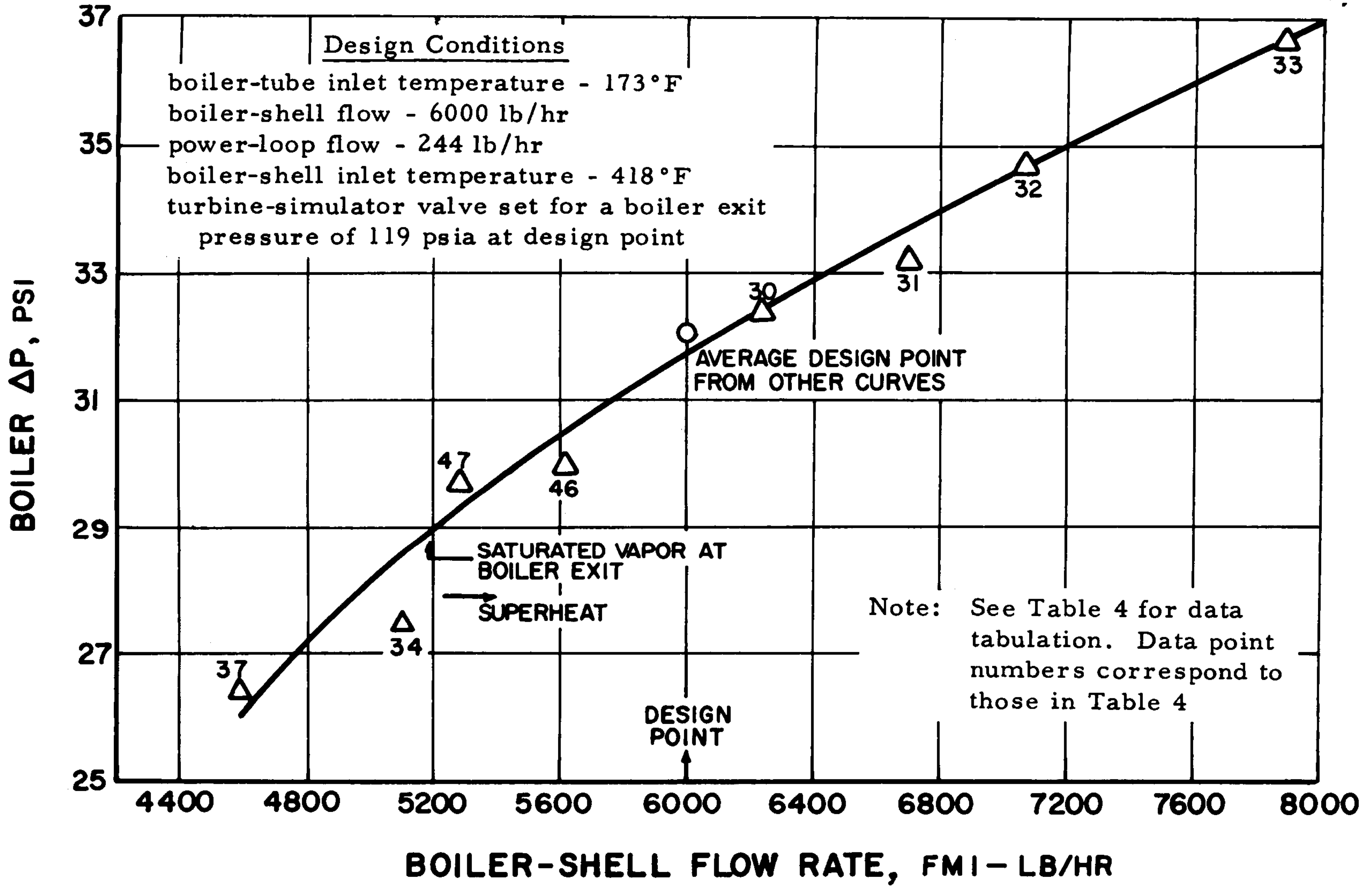

Figure 21 Boiler ΔP vs Boiler-Shell Flow Rate (with conditions otherwise at design)

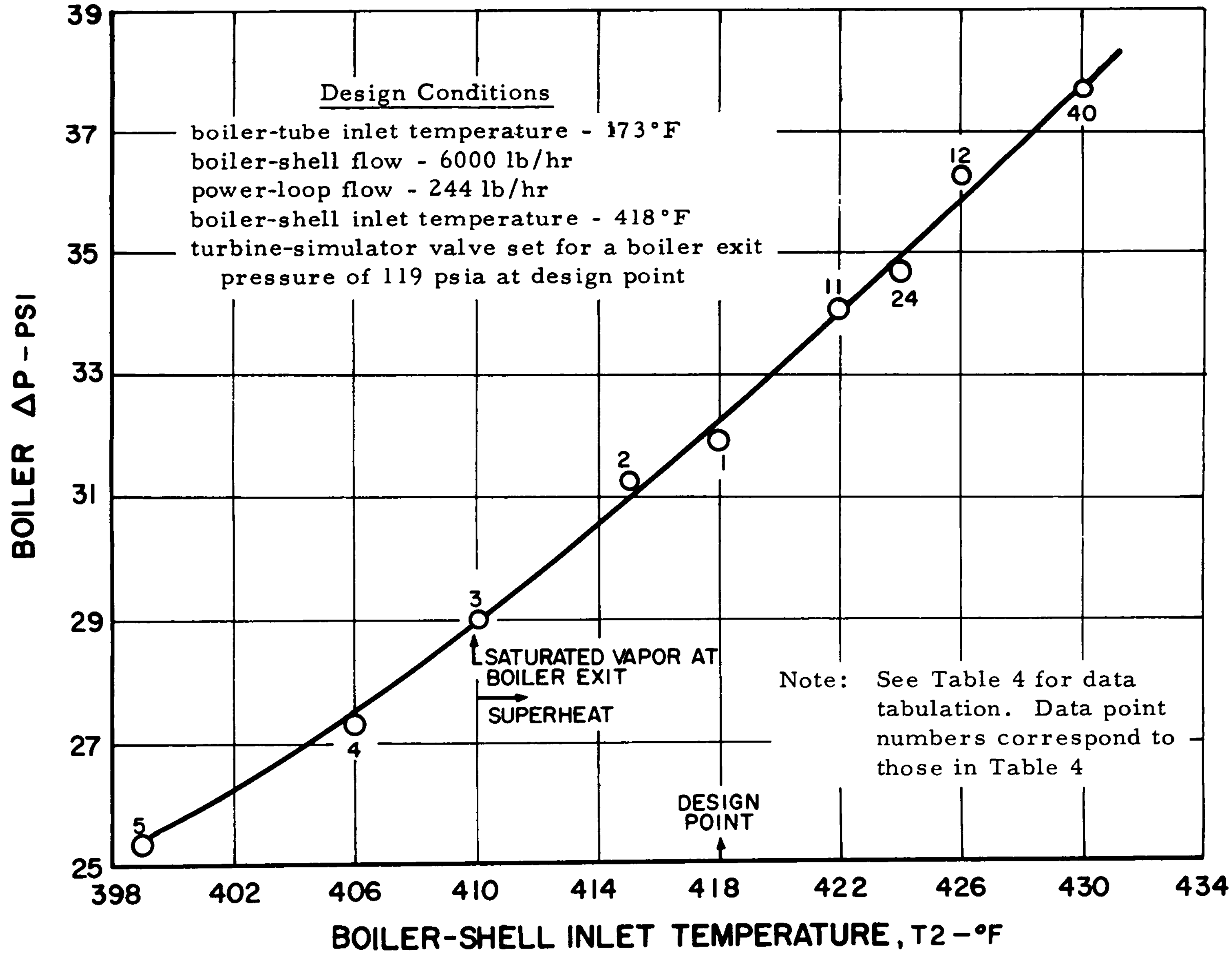

Figure 22 Boiler ΔP vs Boiler-Shell Inlet Temperature (with conditions otherwise at design)

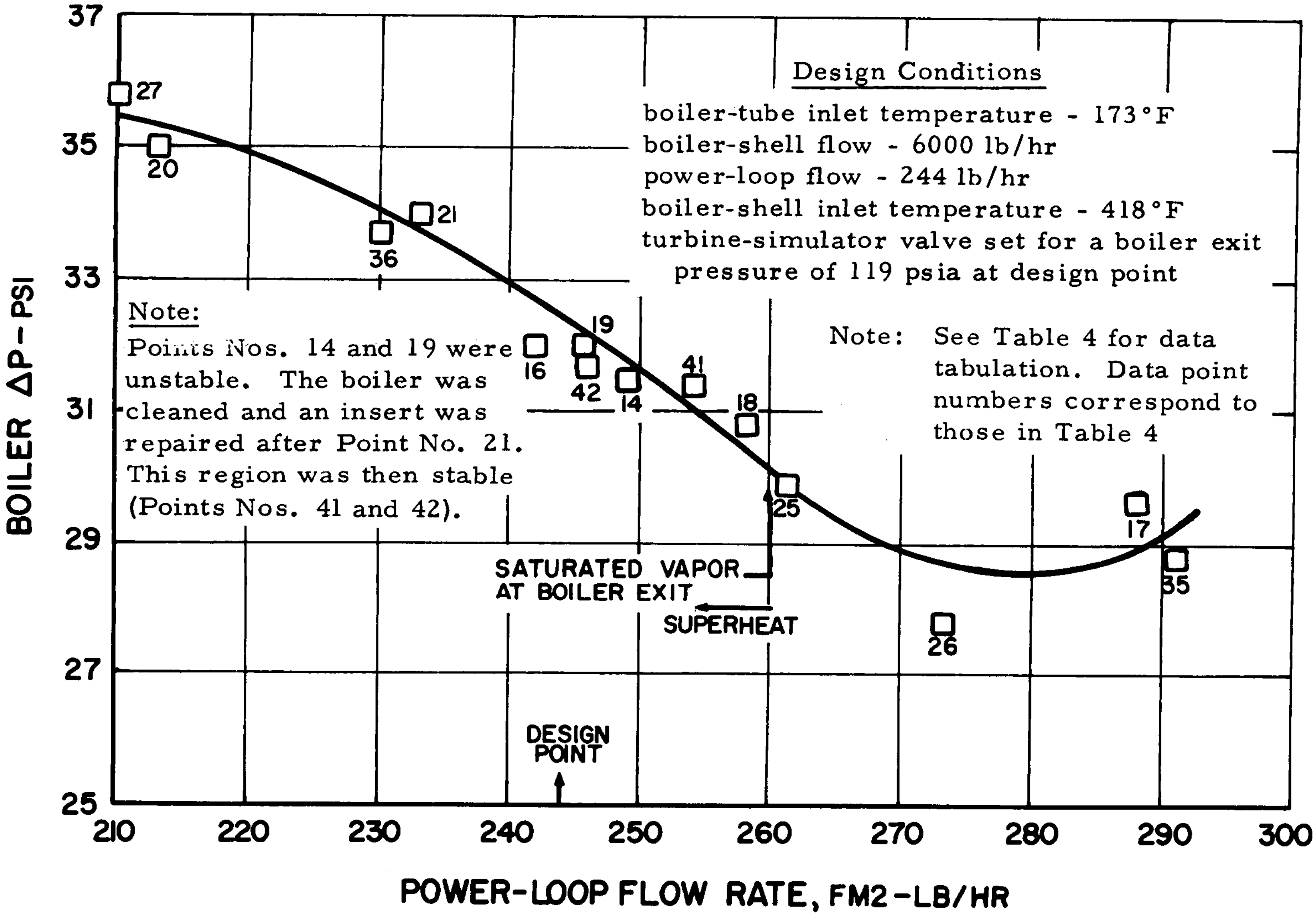

Figure 23 Boiler ΔP vs Power-Loop Flow Rate (with conditions otherwise at design)

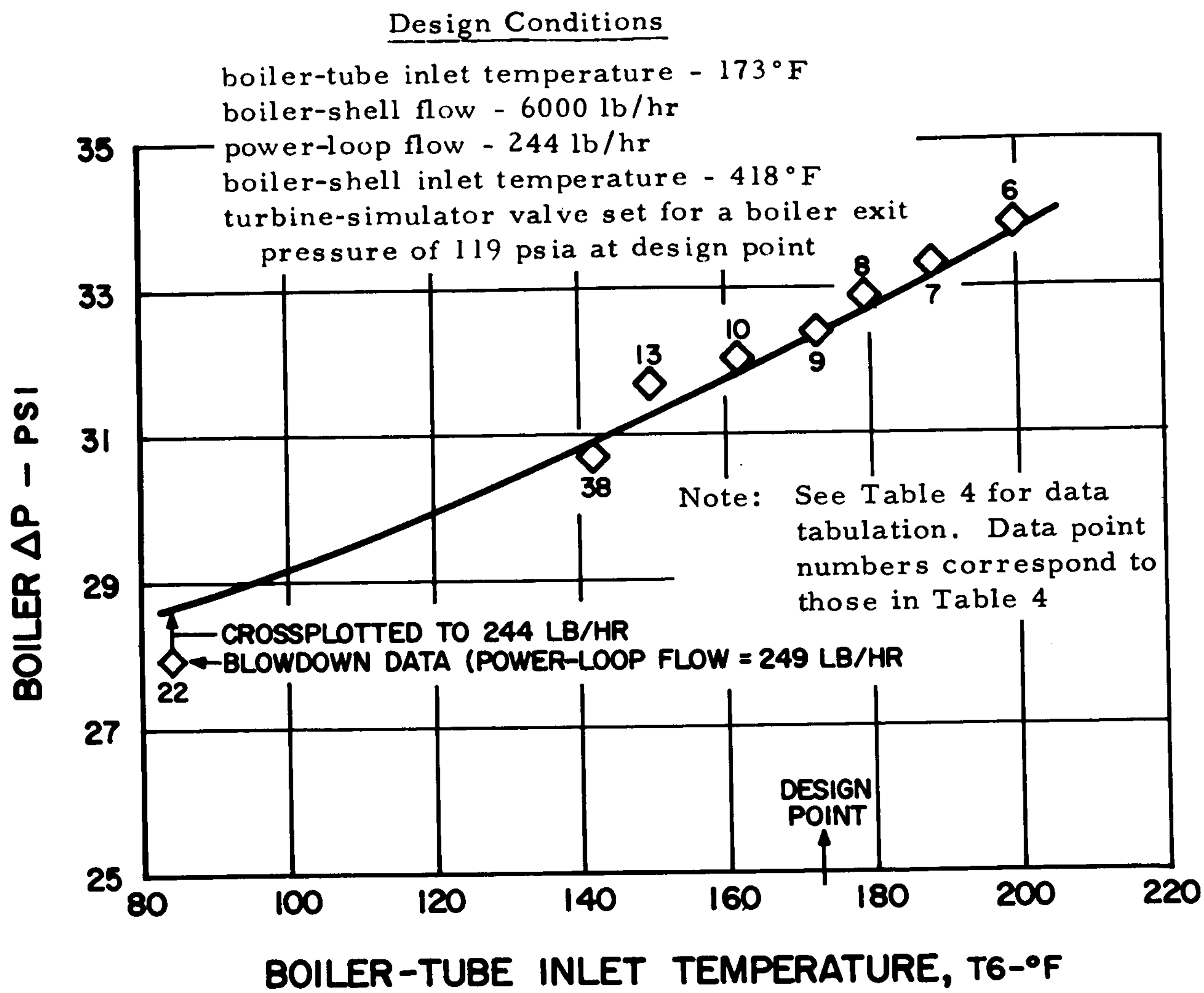

Figure 24 Boiler ΔP vs Boiler-Tube Inlet Temperature (with conditions otherwise at design)

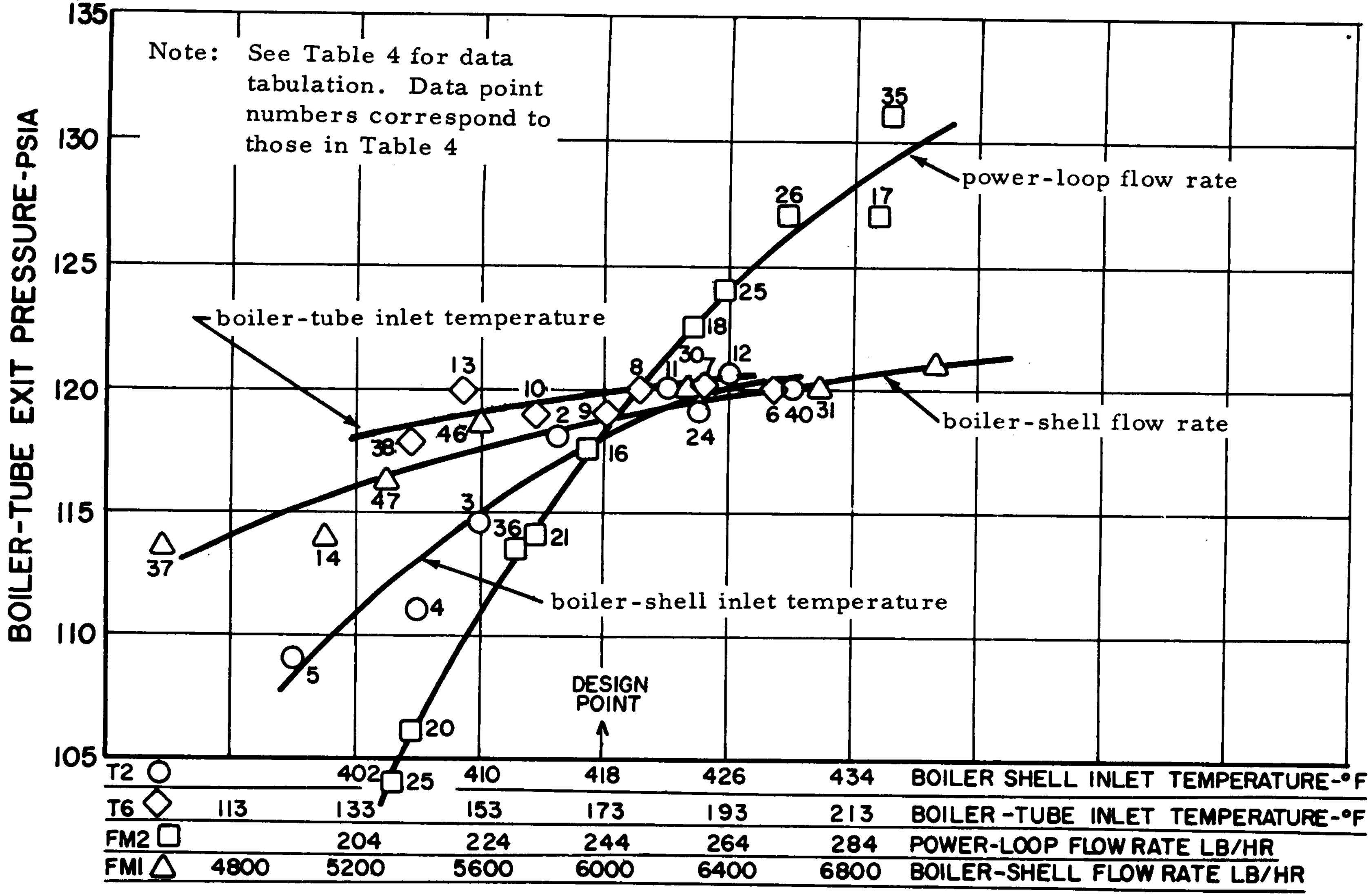

Figure 25 Variation of Boiler Exit Pressure around Design Point with Variation of:

○ Boiler-Shell Inlet Temperature □ Power-Loop Flow Rate
◇ Boiler-Tube Inlet Temperature △ Boiler-Shell Flow Rate

Design Conditions

boiler-tube inlet temperature - 173°F
boiler-shell flow - 6000 lb/hr
power-loop flow - 244 lb/hr
boiler-shell inlet temperature - 418°F
turbine simulator valve set for a boiler exit
pressure of 119 psia at design point

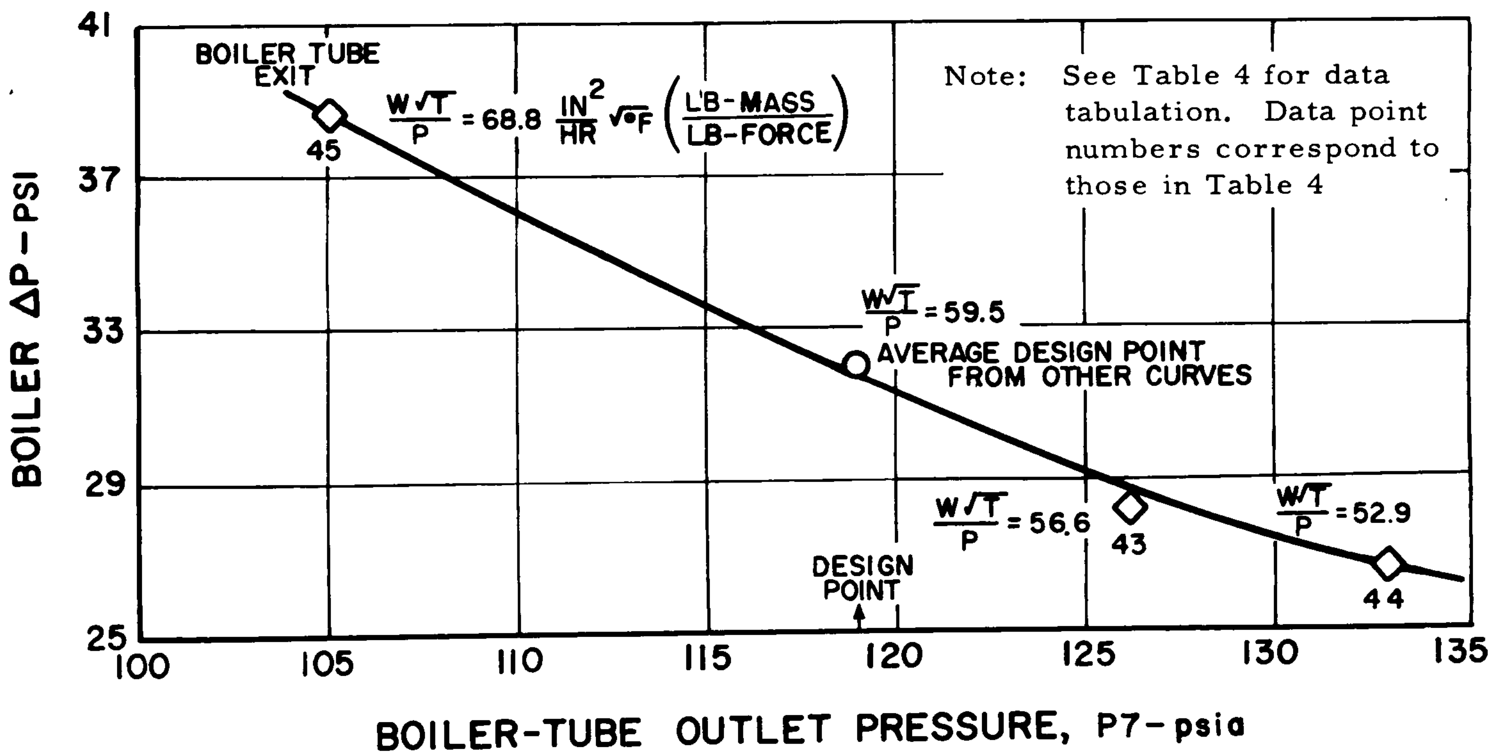

Figure 26 Boiler ΔP vs Boiler-Tube Outlet Pressure (with conditions otherwise at design). Boiler-Tube Outlet Pressure Was Varied by Changing Setting of Choked Turbine Simulator Valve.

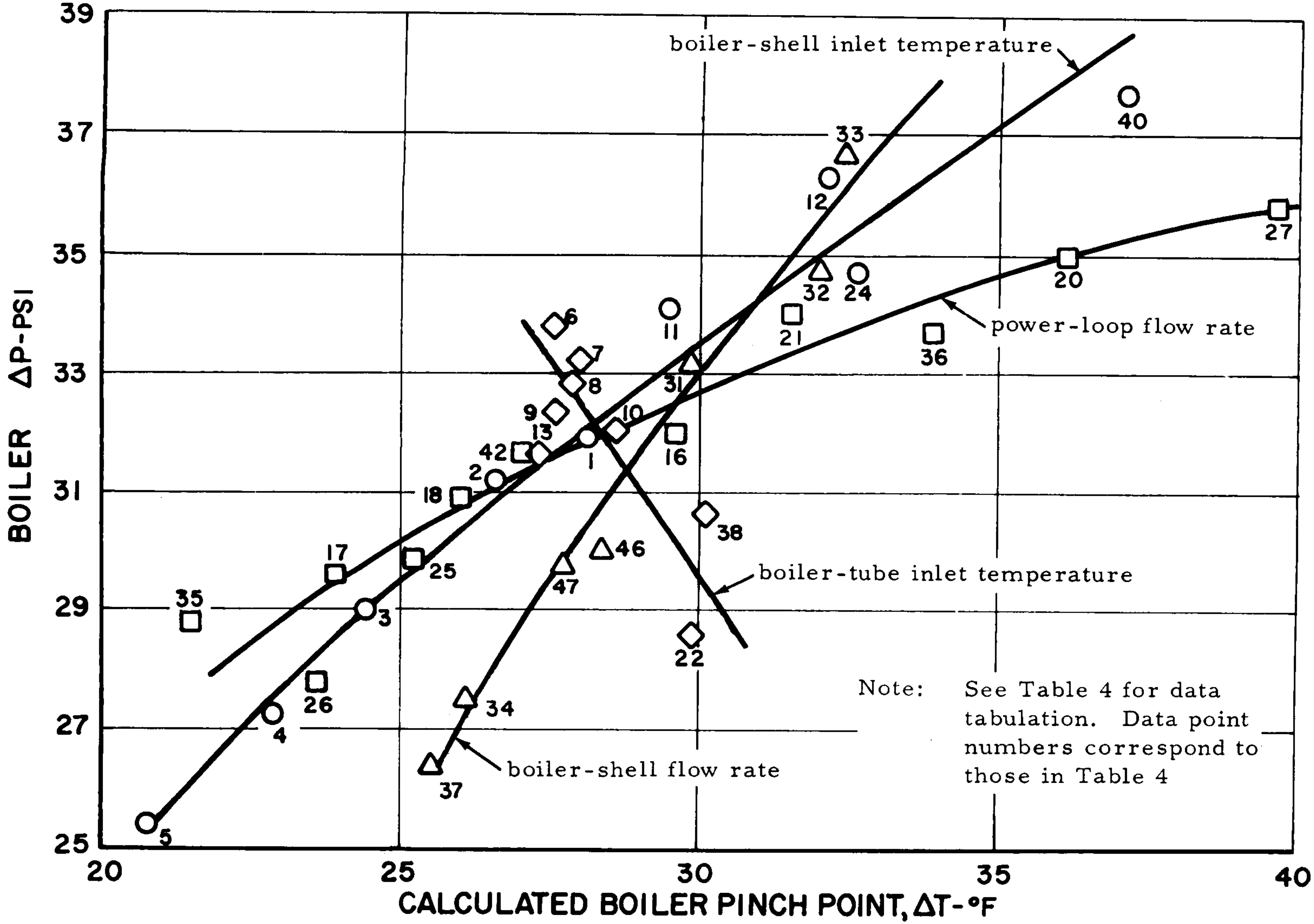

Figure 27 Boiler ΔP vs Calculated Boiler Pinch-Point ΔT with Variation of:
○ Boiler-Shell Inlet Temperature
◇ Boiler-Tube Inlet Temperature
□ Power-Loop Flow Rate
△ Boiler-Shell Flow Rate

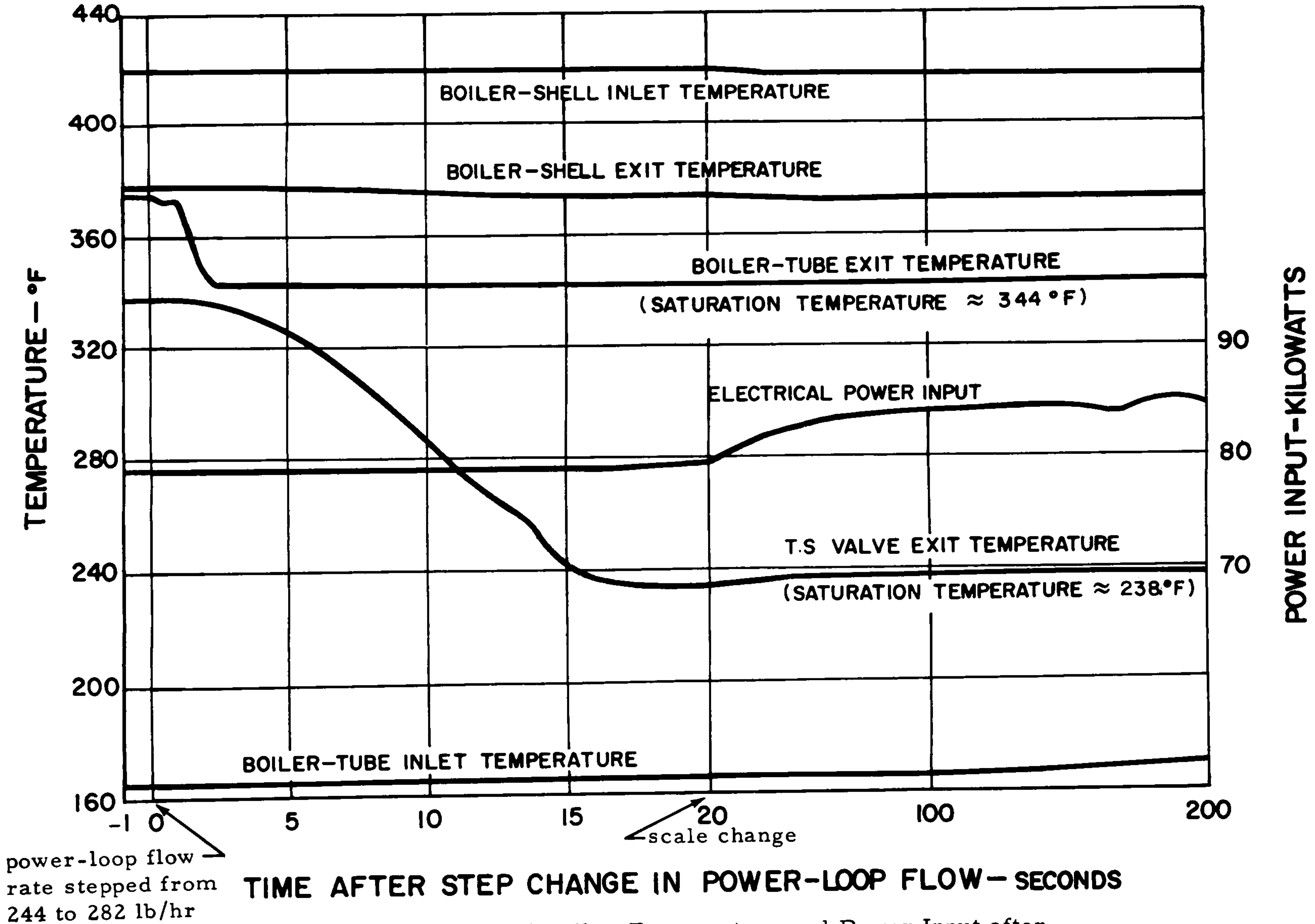

Figure 28 Variation of Boiler Temperature and Power Input after Power-Loop Flow Rate Was Stepped from 244 to 282 lb/hr at Time Zero. Constant Inventory at Design + 120 ml

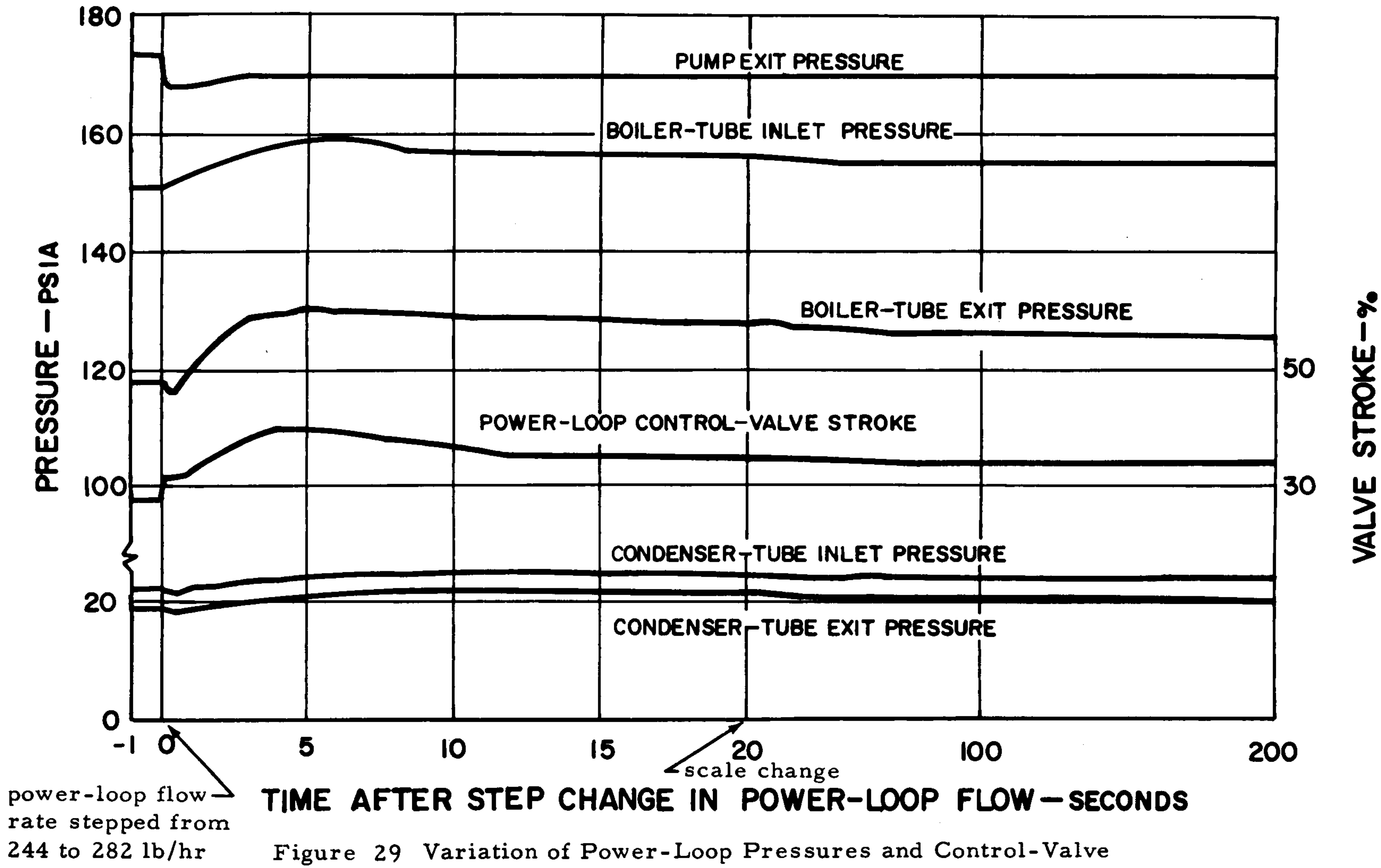

Figure 29 Variation of Power-Loop Pressures and Control-Valve Stroke after Power-Loop Flow Rate Was Stepped from 244 to 282 lb/hr at Time Zero. Constant Inventory at Design + 120 ml

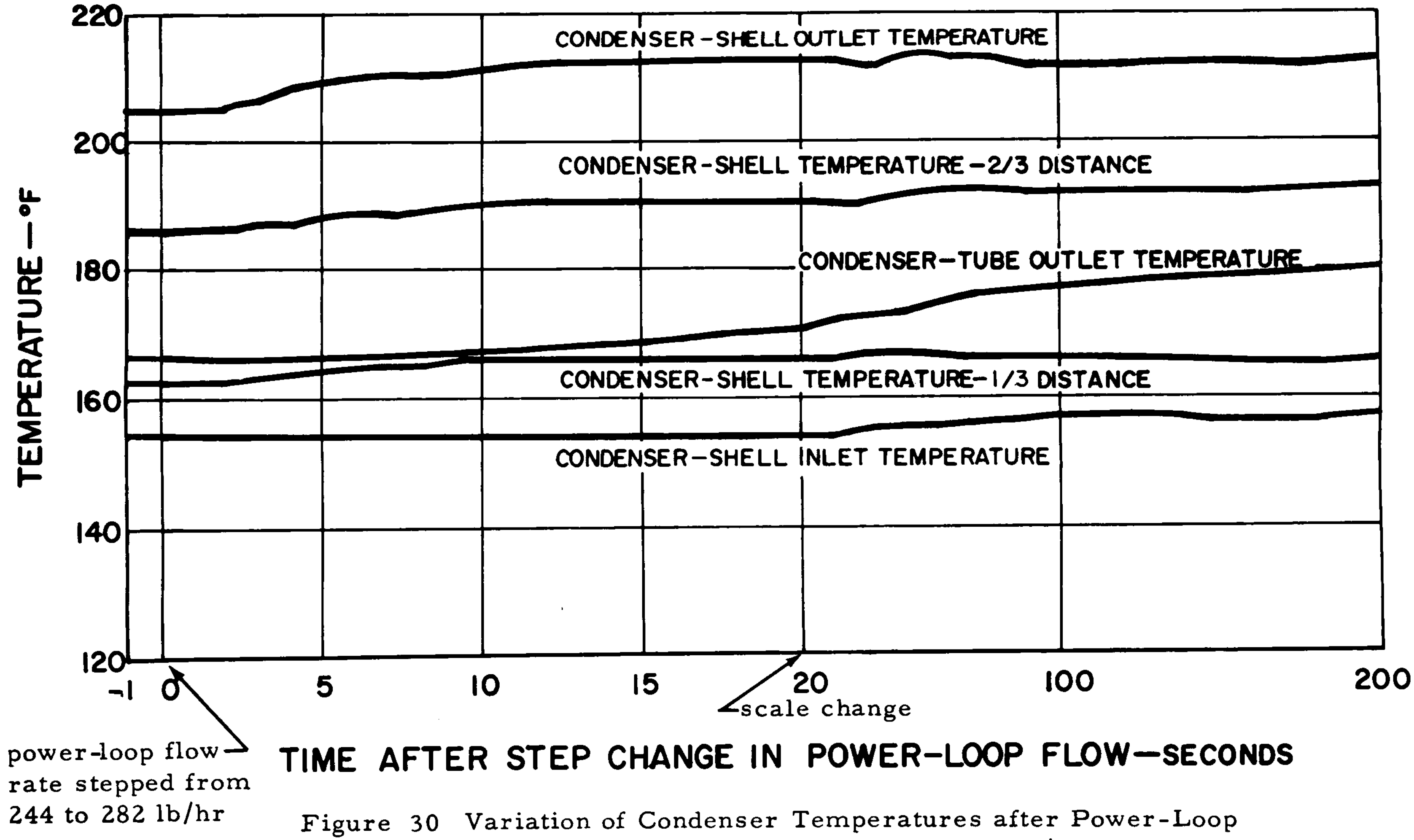

Figure 30 Variation of Condenser Temperatures after Power-Loop Flow Rate Was Stepped from 244 to 282 lb/hr at Time Zero. Constant Inventory at Design + 120 ml

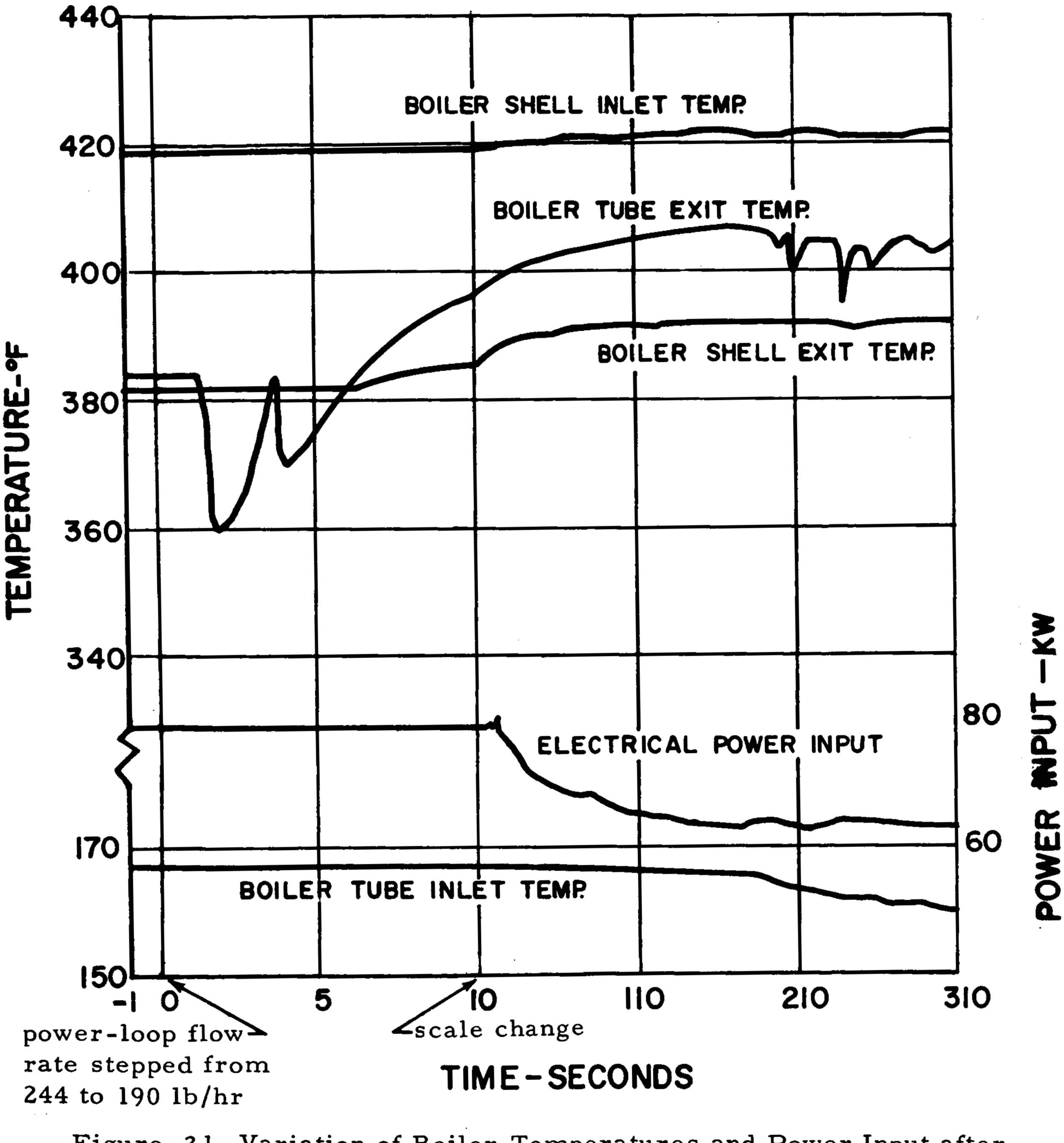

Figure 31 Variation of Boiler Temperatures and Power Input after Power-Loop Flow Rate Was Stepped from 244 to 190 lb/hr at Time Zero. Constant Inventory at Design Value

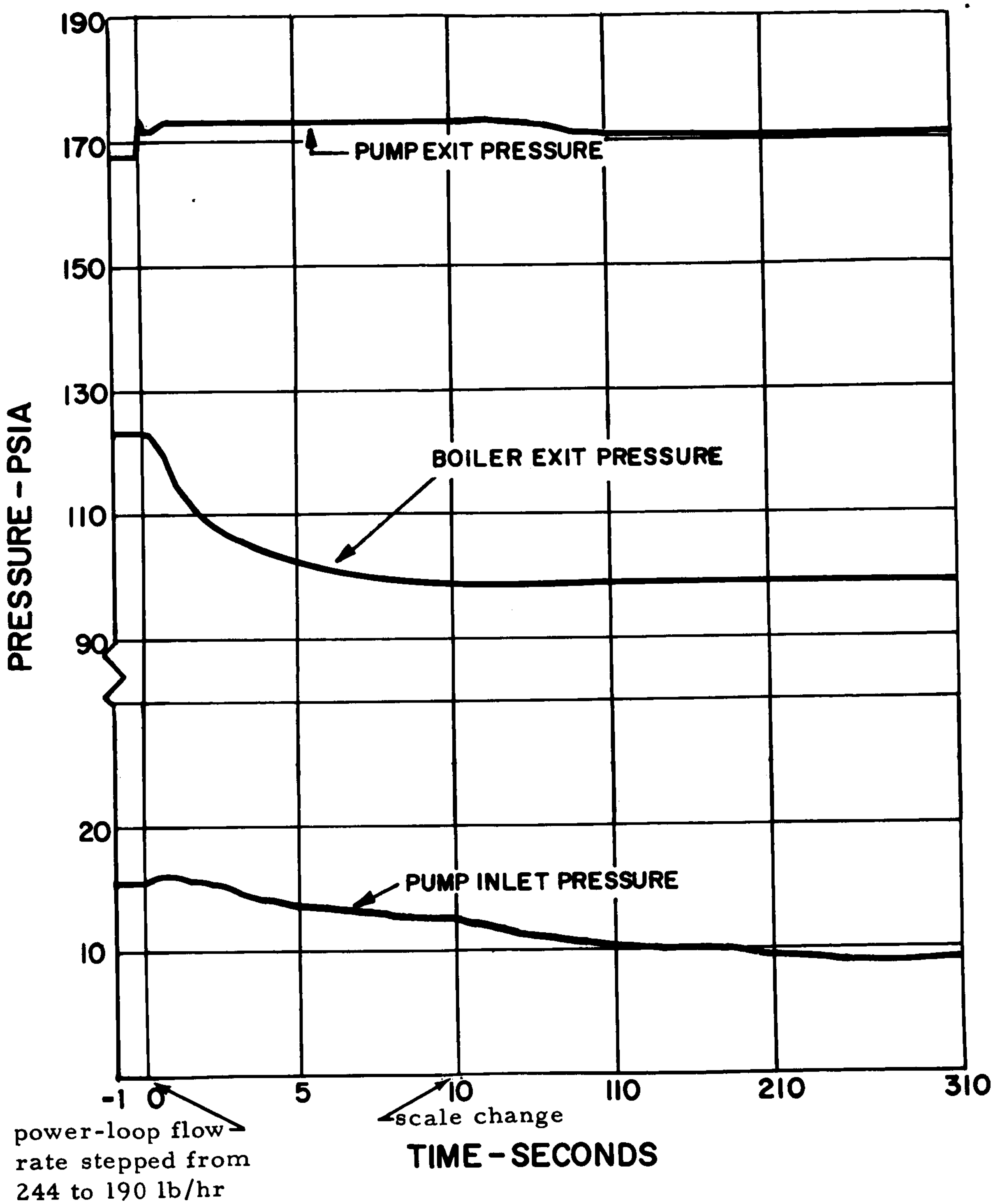

Figure 32 Variation of Power-Loop Pressures after Power-Loop Flow Rate Was Stepped from 244 to 190 lb/hr at Time Zero. Constant Inventory at Design Value

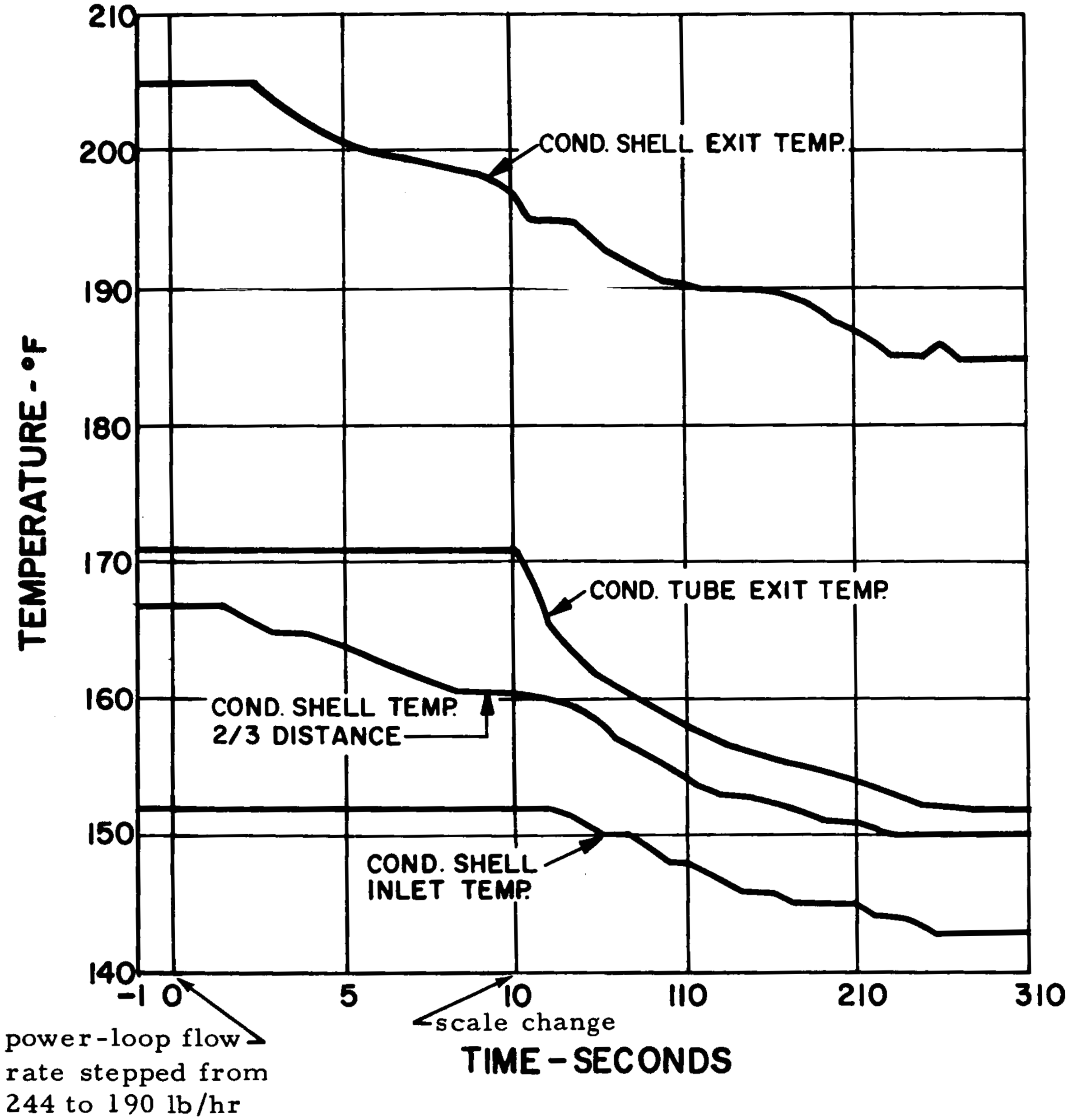

Figure 33 Variation of Condenser Temperatures after Power-Loop Flow Rate Was Stepped from 244 to 190 lb/hr at Time Zero. Constant Inventory at Design Value

38 - power-loop flow rate at boiler inlet
36 - control valve stroke
34 - power-loop pump exit pressure
28 - condenser-tube exit pressure
22 - boiler exit pressure
21 - boiler inlet pressure

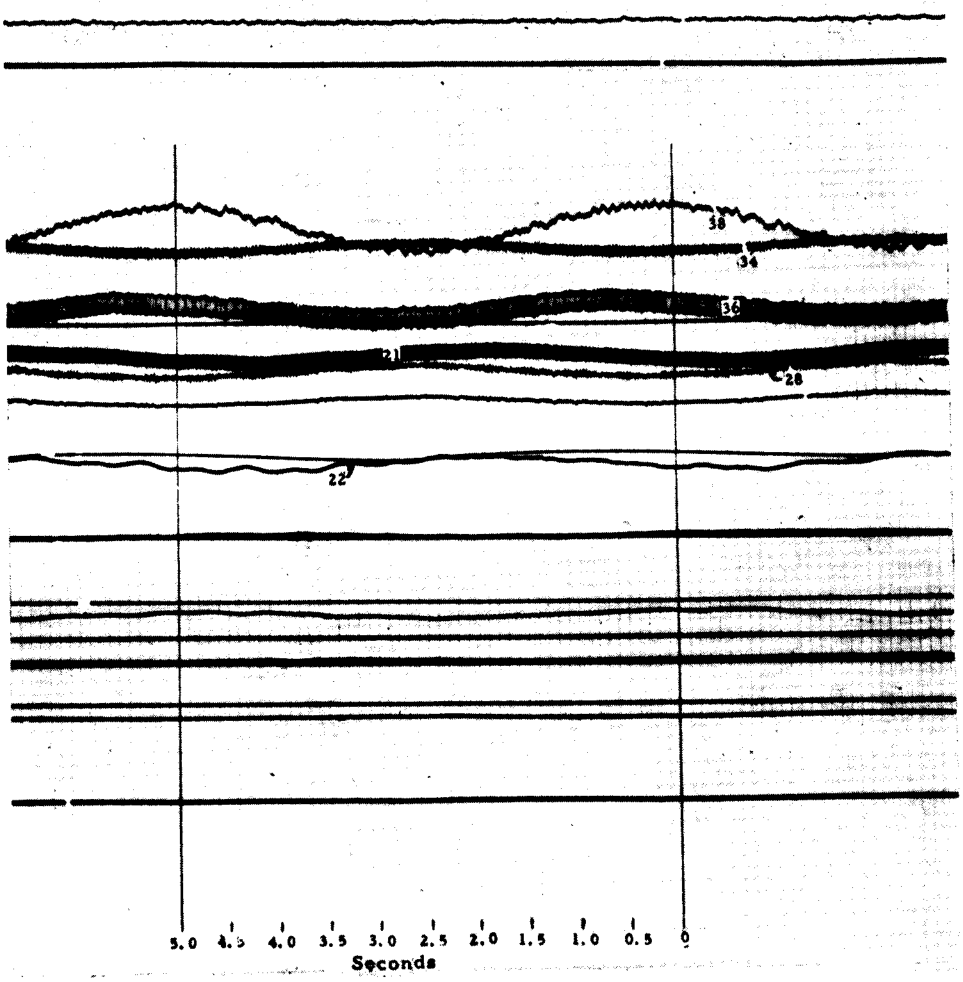

Figure 34 Oscillograph Recording of 0.2 cps Sine-Wave Power-Loop Flow Rate Variation

O boiler inlet pressure
□ boiler exit pressure
◇ boiler-tube exit temperature
Δ boiler-shell exit temperature
∇ electrical power input

<u>constant conditions</u>

boiler-shell inlet temperature - 415°F
boiler-shell flow rate - 6000 lb/hr
turbine simulating valve at design setting
calculated boiler pinch point ΔT at mean flow rate - 28°F

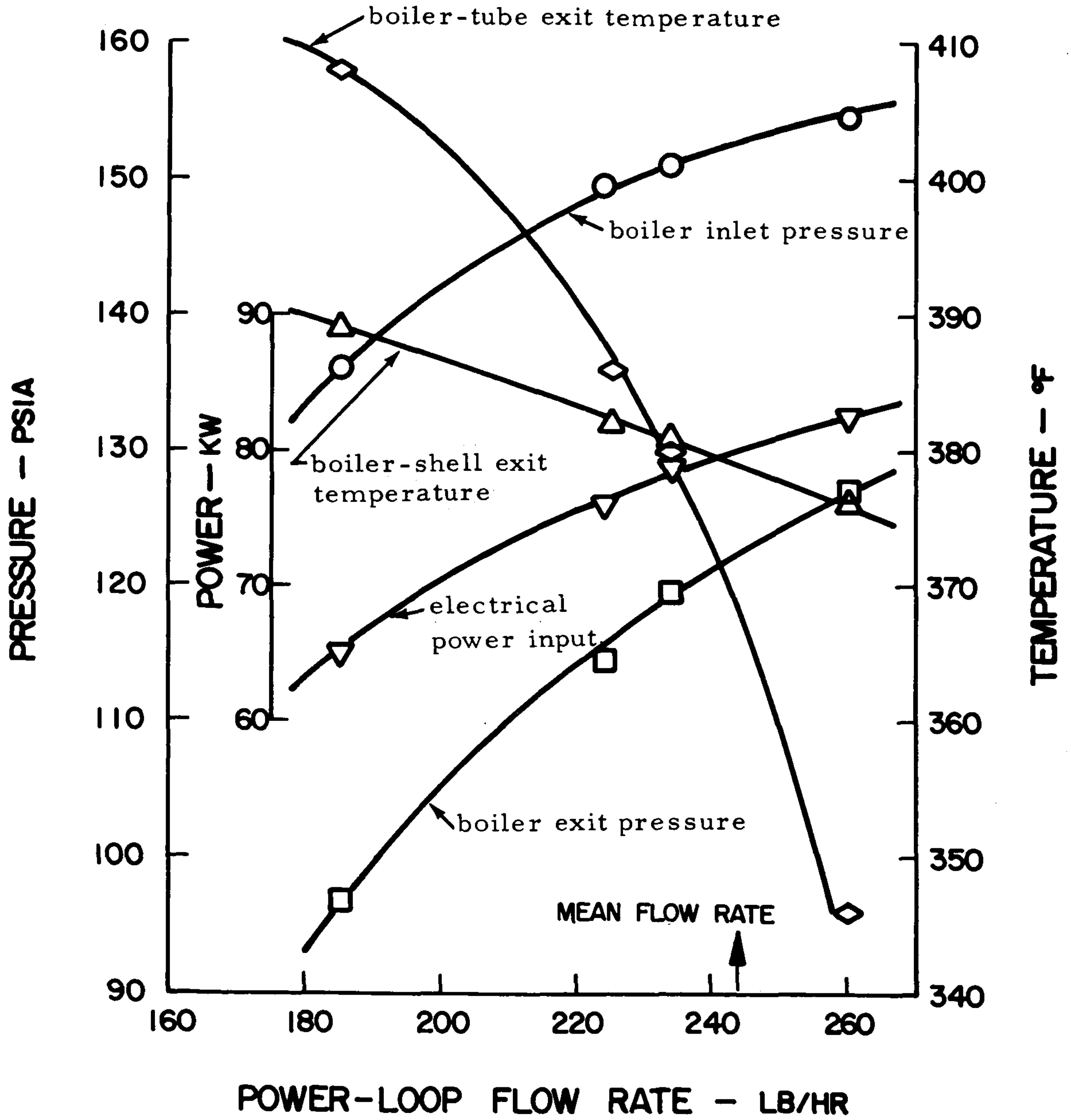

Figure 35 System Dynamic Response Test. Steady-State Variation of Dependent Boiler Variables with Power-Loop Flow Rate

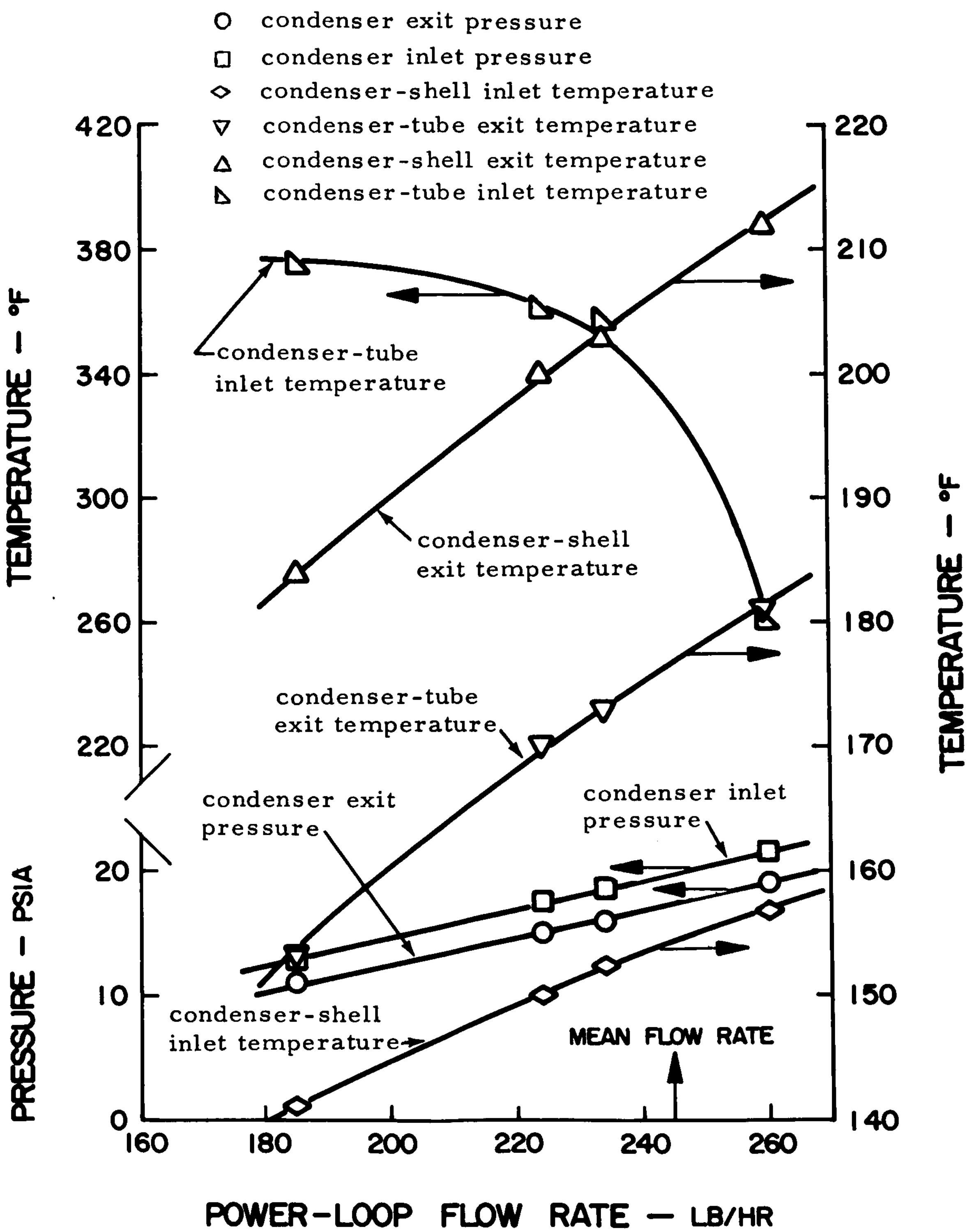

Figure 36 System Dynamic Response Test. Steady-State Variation of Dependent Condenser Variables with Power-Loop Flow Rate

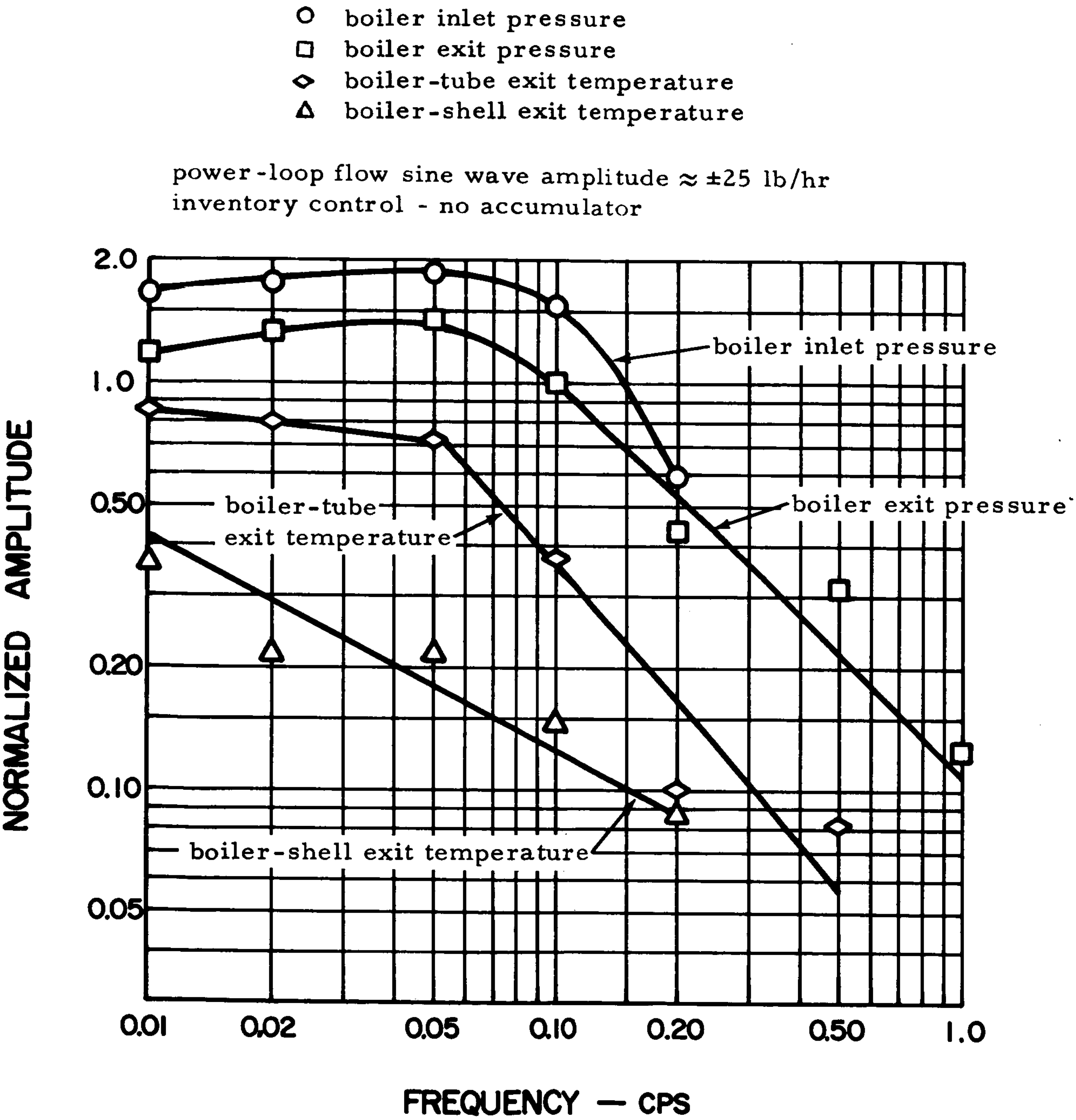

Figure 37 System Dynamic Response Test. Frequency Response - Amplitude Normalized to Steady State

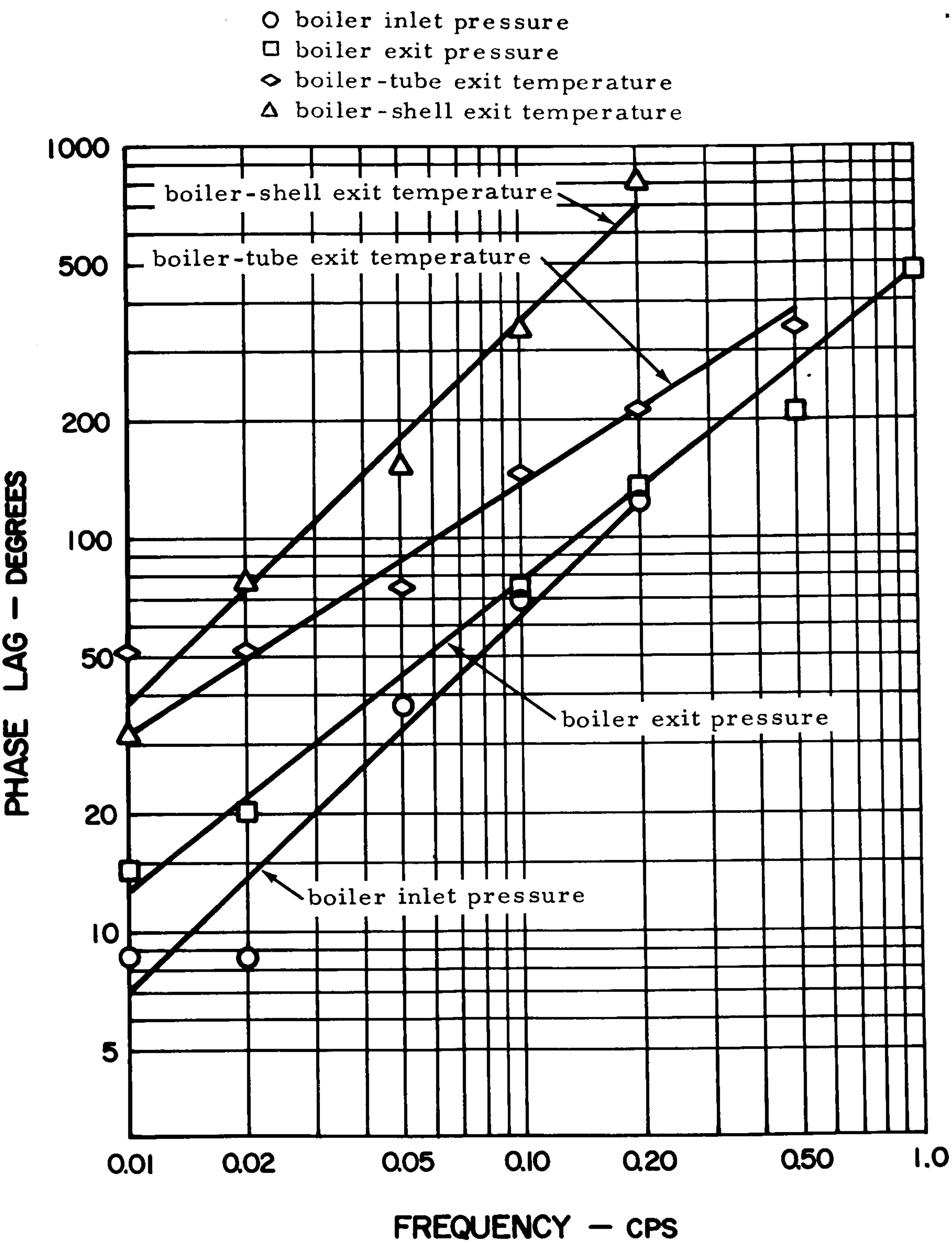

Figure 38 System Dynamic Response Test. Frequency Response - Phase Shift

O condenser exit pressure
□ condenser inlet pressure
Δ condenser-shell exit temperature
∇ condenser-tube inlet temperature

power-loop flow sine wave amplitude ≈ ±25 lb/hr
inventory control - no accumulator

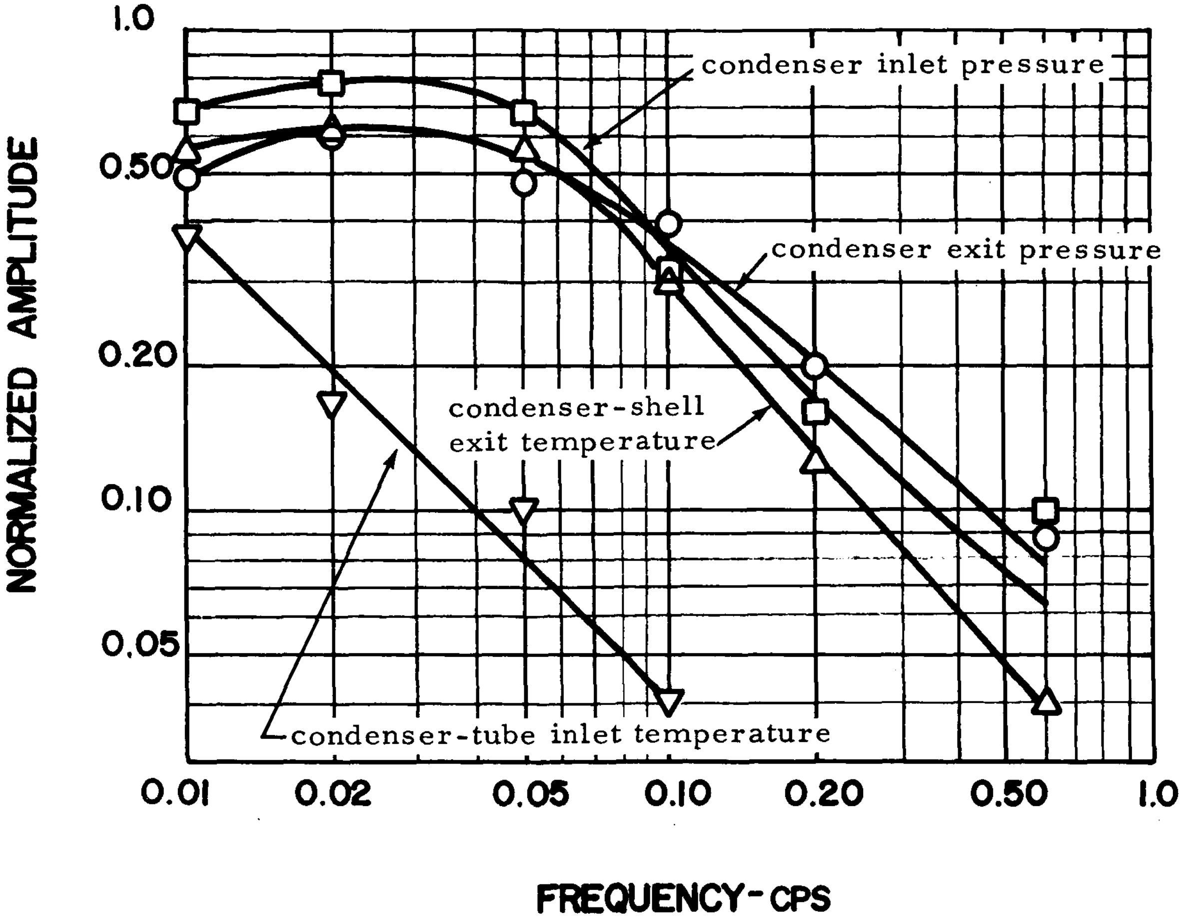

Figure 39 System Dynamic Response Test. Frequency Response - Amplitude Normalized to Steady State

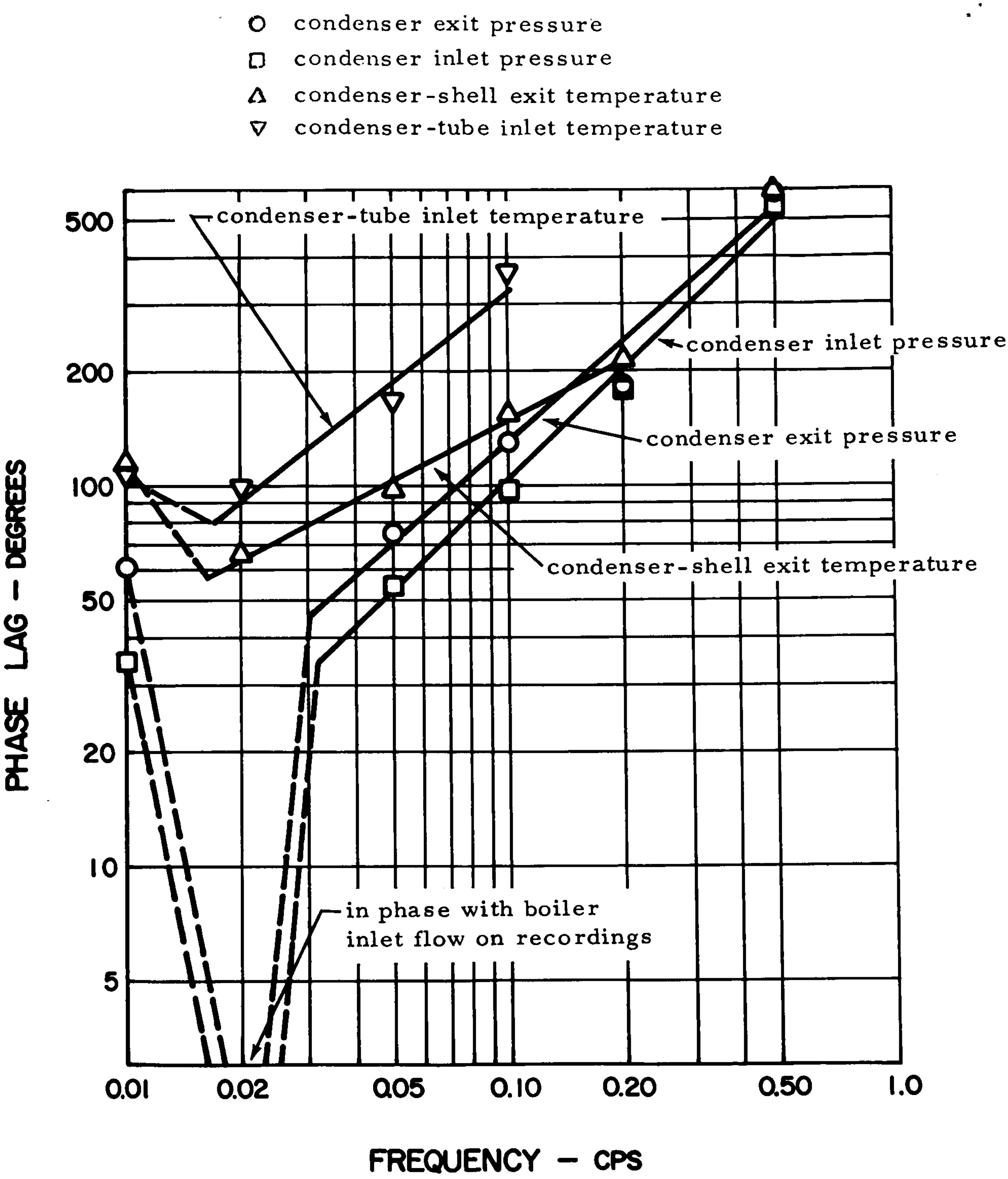

Figure 40 System Dynamic Response Test. Frequency Response - Phase Shift

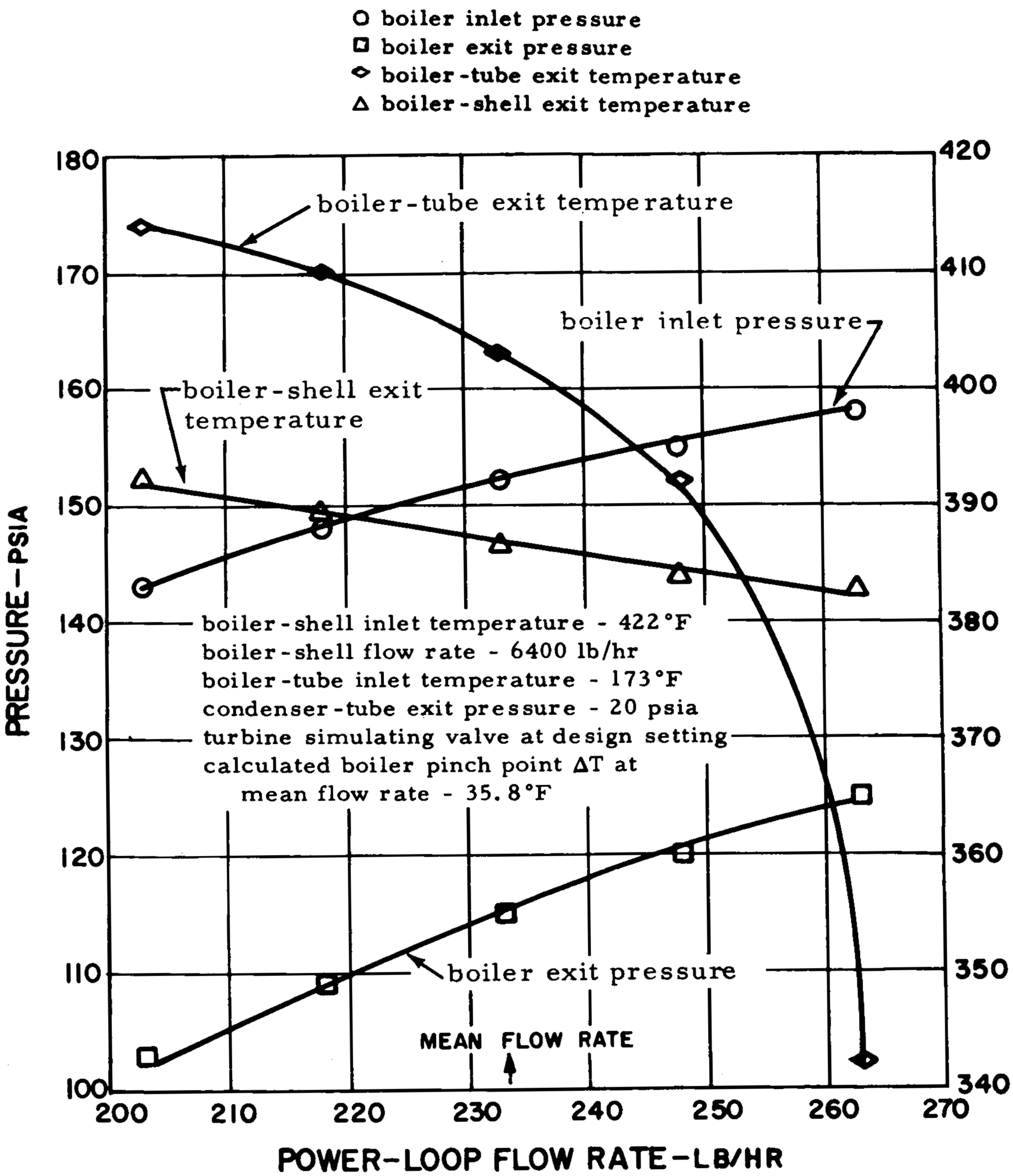

Figure 41 Boiler Dynamic Response Test No. 1. Steady-State Variation of Dependent Boiler Variables with Power-Loop Flow Rate

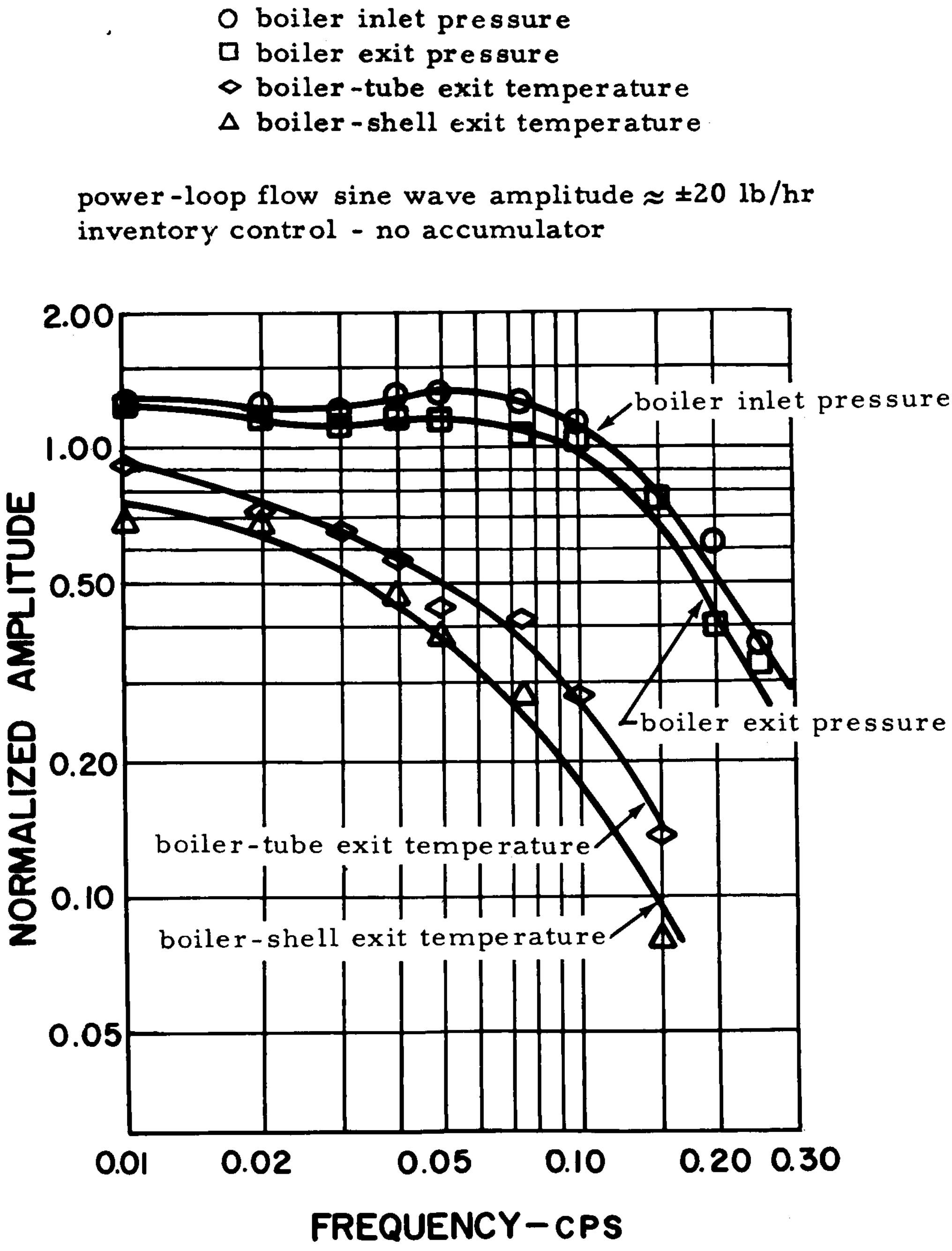

Figure 42 Boiler Dynamic Response Test No. 1. Frequency Response-Amplitude Normalized to Steady State

O boiler inlet pressure
□ boiler exit pressure
◇ boiler-tube exit temperature
Δ boiler-shell exit temperature

power-loop flow sine wave amplitude ≈ ±20 lb/hr
inventory control - no accumulator

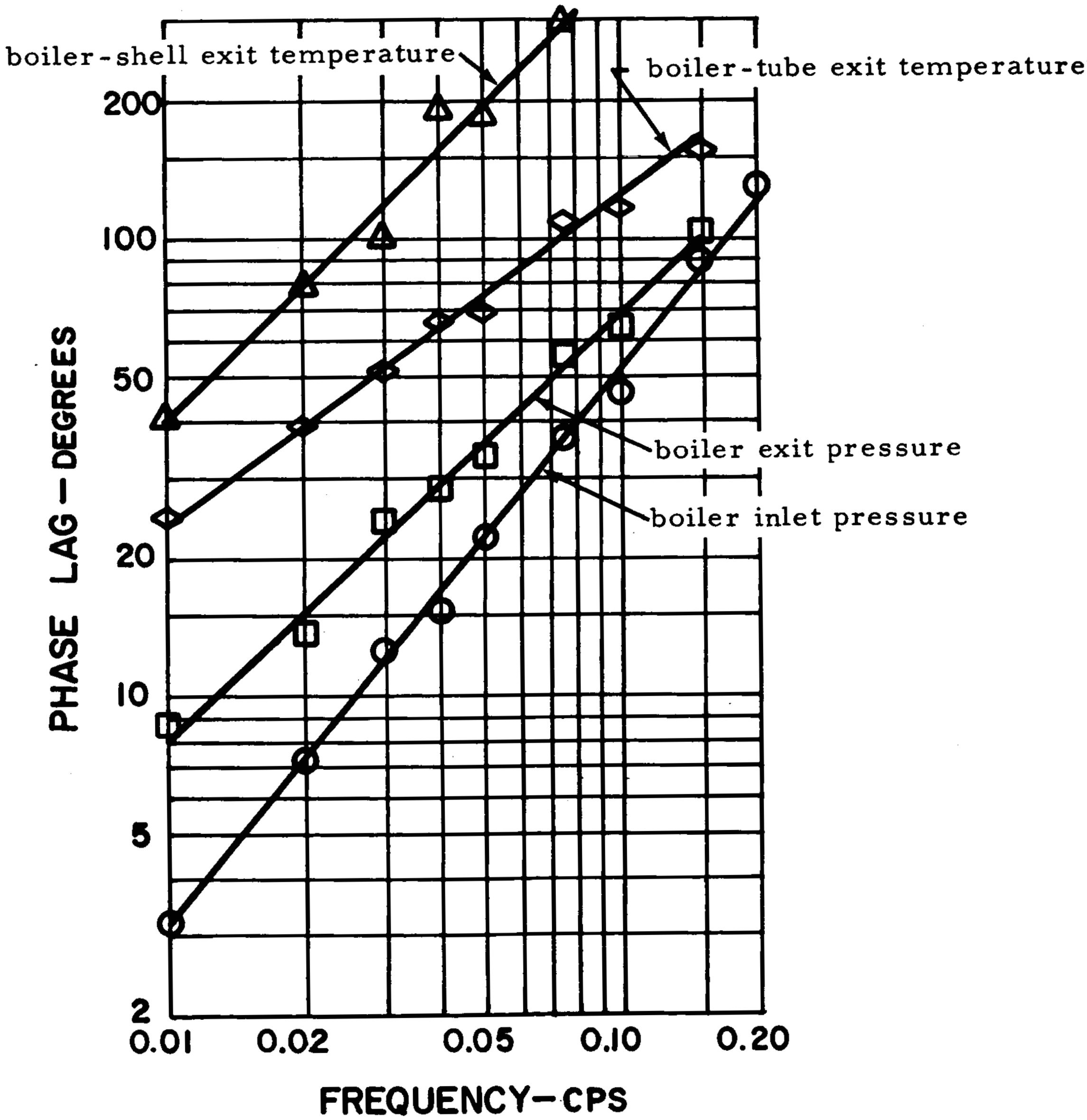

Figure 43 Boiler Dynamic Response Test No. 1. Frequency Response-Phase Shift

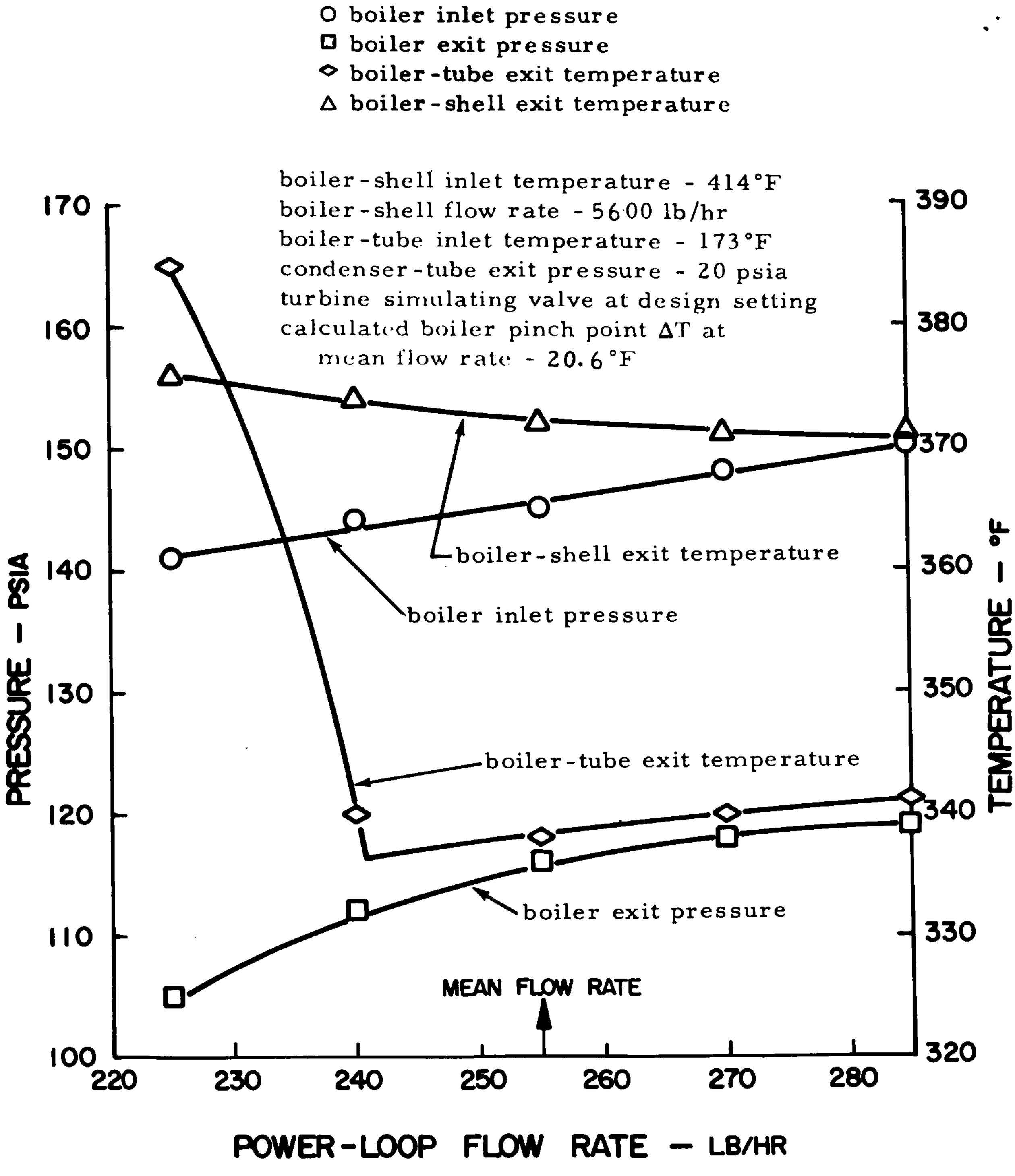

Figure 44 Boiler Dynamic Response Test No. 2. Steady-State Variation of Dependent Boiler Variables with Power-Loop Flow Rate

O boiler inlet pressure
□ boiler exit pressure
Δ boiler-shell exit temperature

power-loop flow sine wave amplitude ≈ ±20 lb/hr
inventory control - no accumulator

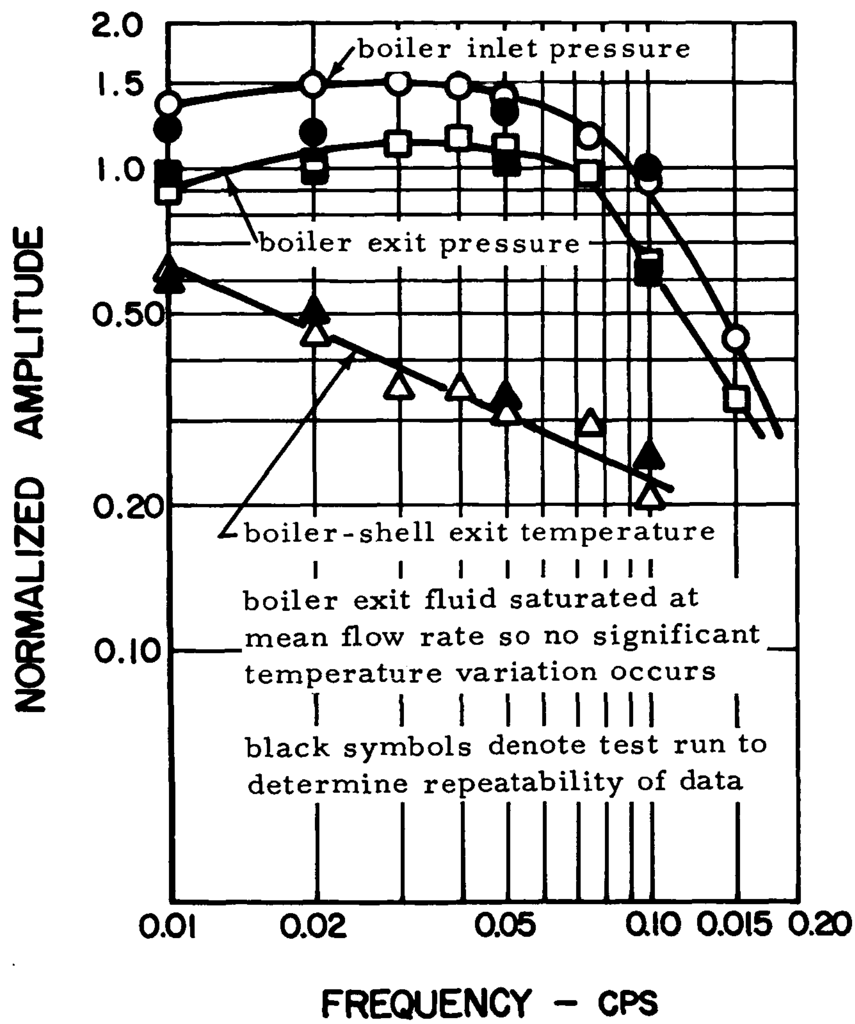

Figure 45 Boiler Dynamic Response Test No. 2. Frequency Response-Amplitude Normalized to Steady State

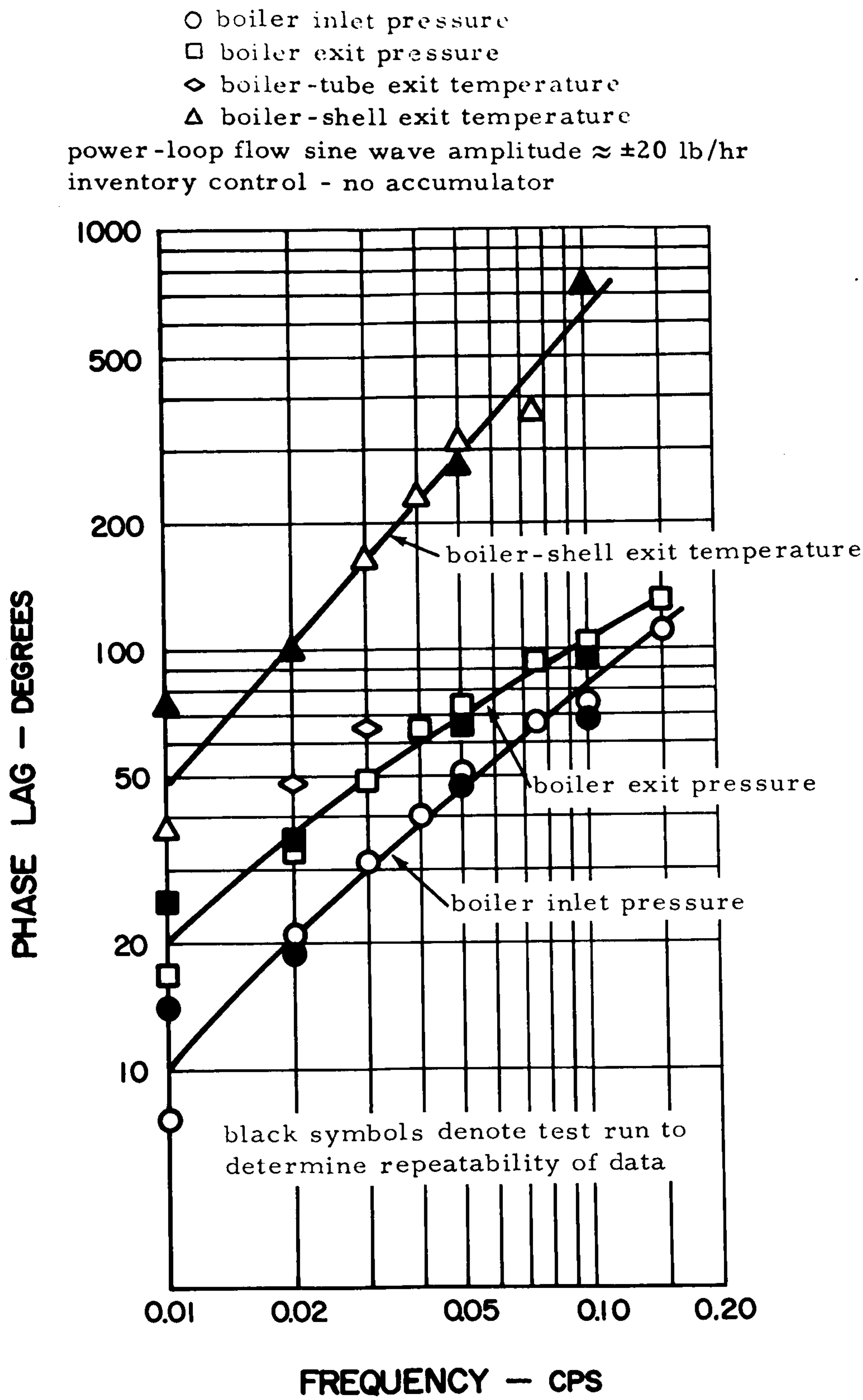

Figure 46 Boiler Dynamic Response Test No. 2. Frequency Response - Phase Shift

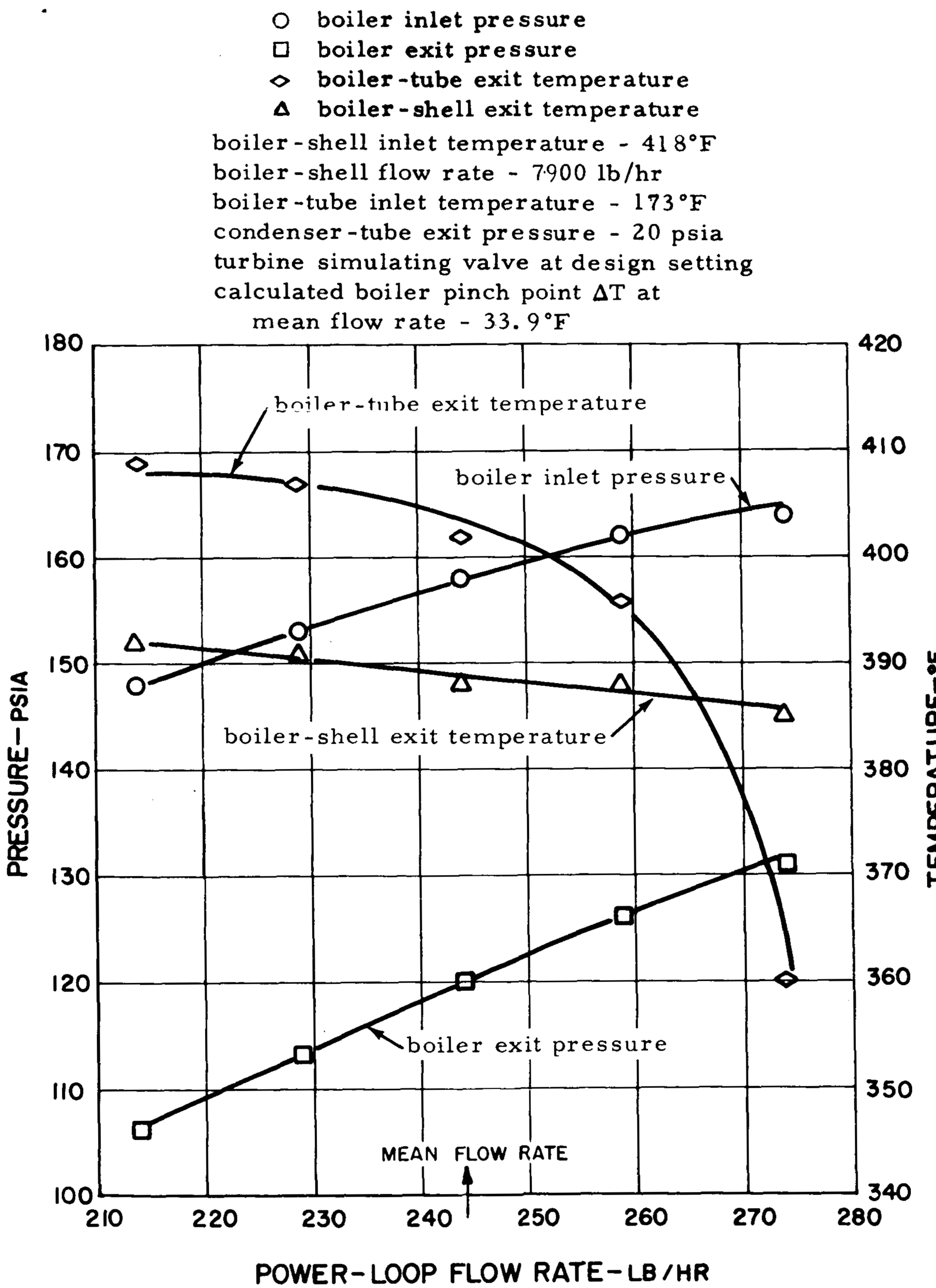

Figure 47 Boiler Dynamic Response Test No. 3. Steady-State Variation of Dependent Boiler Variables with Power-Loop Flow Rate

O boiler inlet pressure
□ boiler exit pressure
◇ boiler-tube exit temperature
△ boiler-shell exit temperature

power-loop flow sine wave amplitude ≈ ±20 lb/hr
inventory control - no accumulator

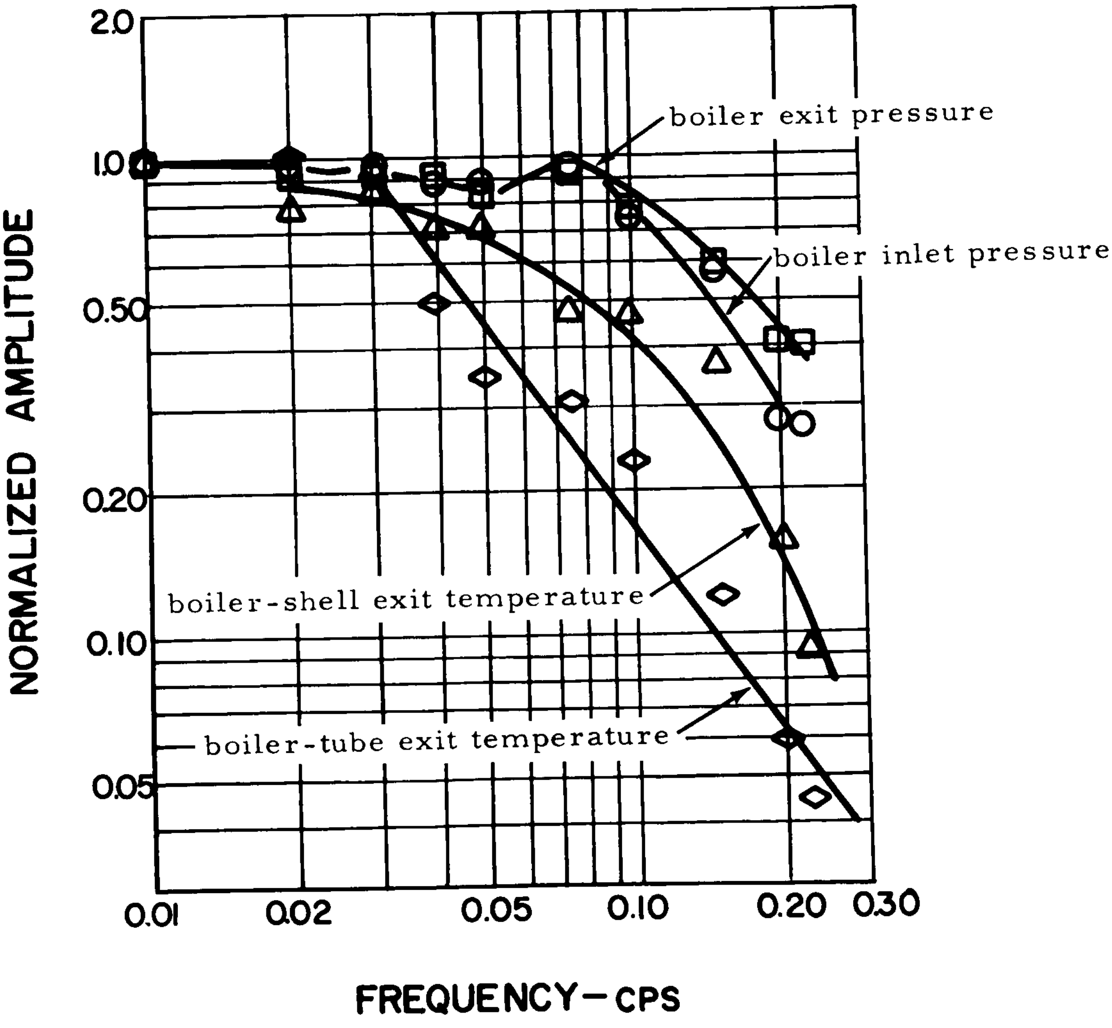

Figure 48 Boiler Dynamic Response Test No. 3. Frequency Response-Amplitude Normalized to Steady State

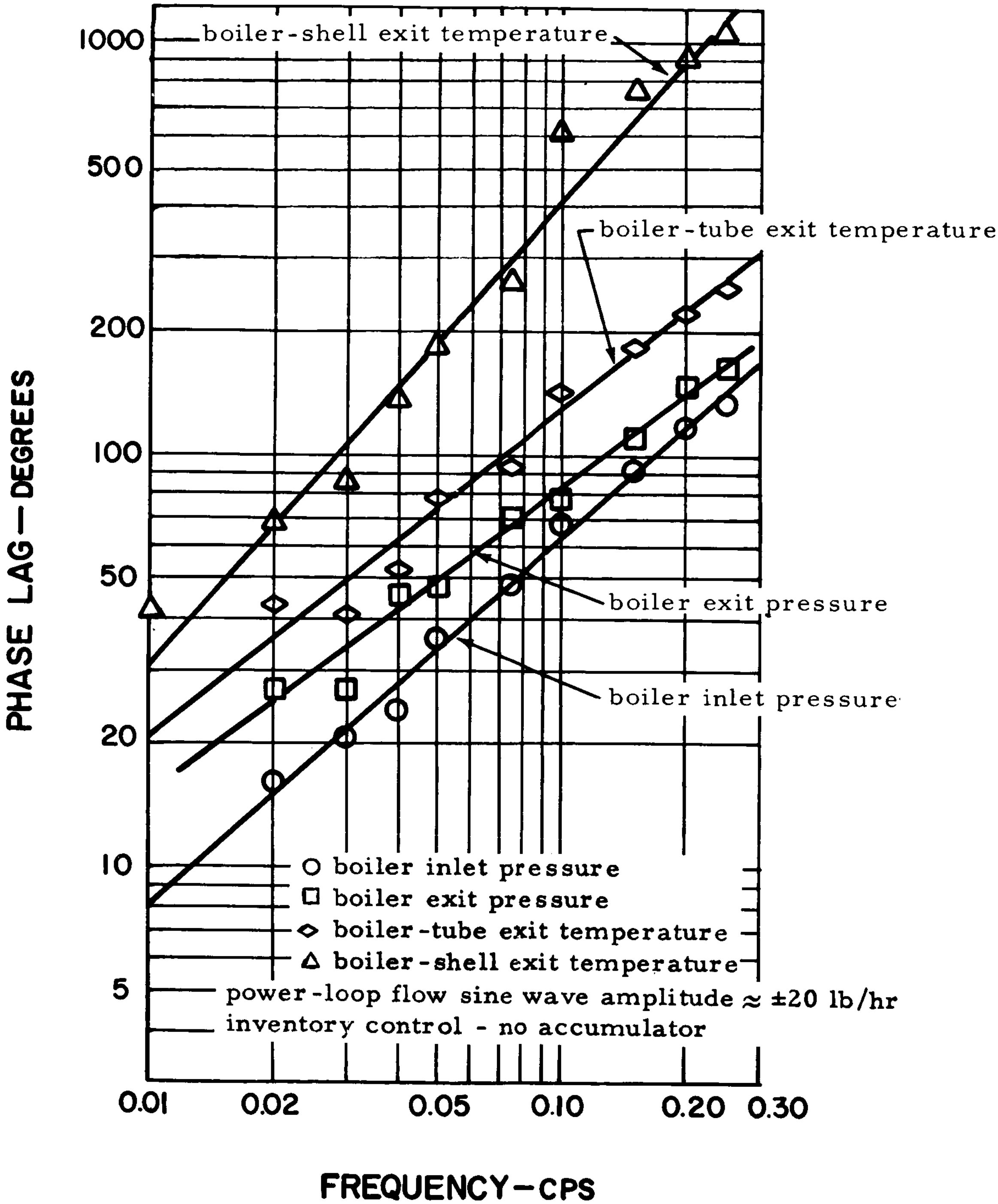

Figure 49 Boiler Dynamic Response Test No. 3. Frequency Response-Phase Shift

○ boiler inlet pressure
□ boiler exit pressure
◇ boiler-tube exit temperature
△ boiler-shell exit temperature

boiler-shell inlet temperature - 418°F
boiler-shell flow rate - 4600 lb/hr
boiler-tube inlet temperature - 173°F
condenser-tube exit pressure - 20 psia
turbine simulating valve at design setting
calculated boiler pinch point ΔT at
mean flow rate - 25.4°F

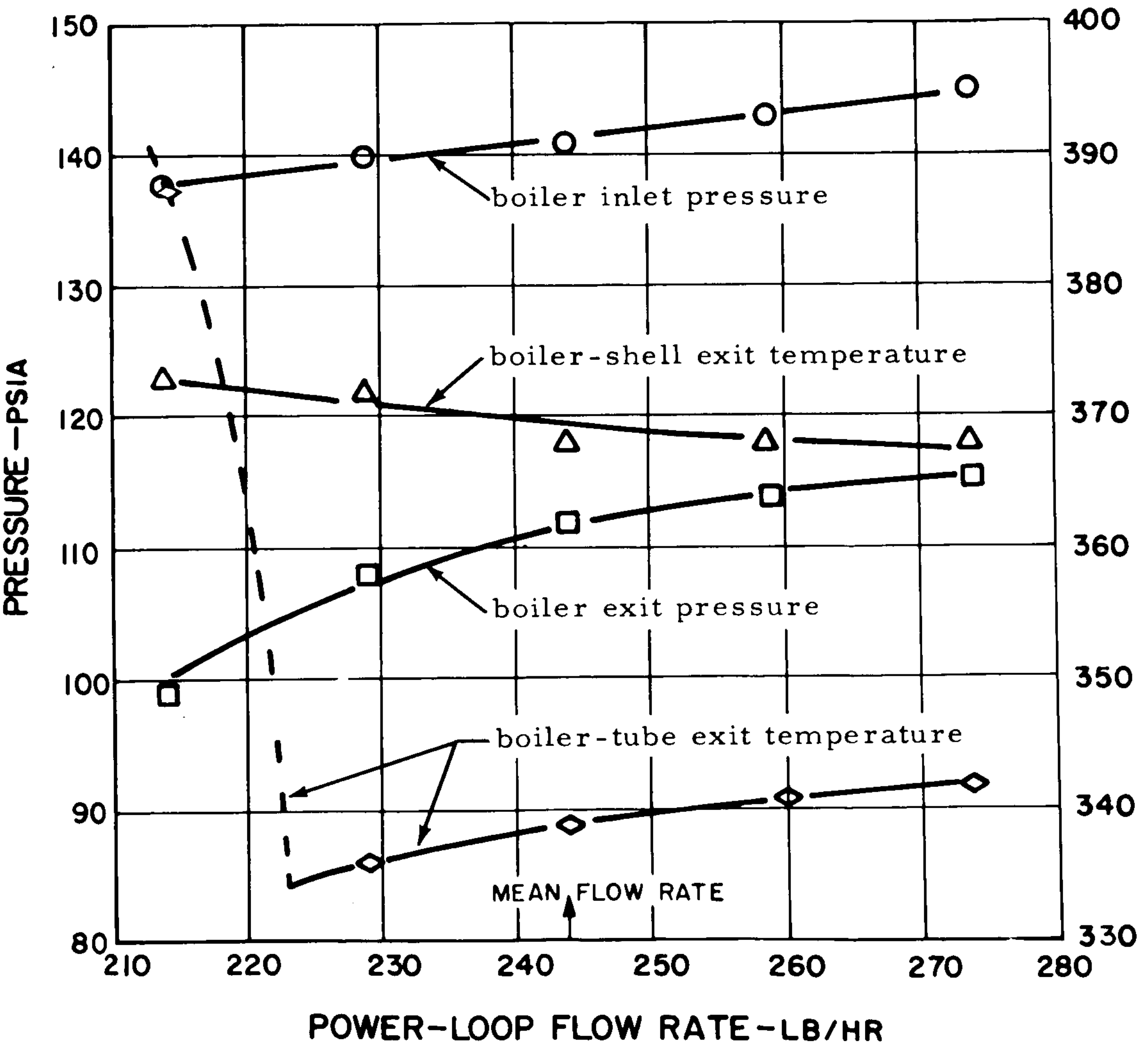

Figure 50 Boiler Dynamic Response Test No. 4. Steady-State Variation of Dependent Boiler Variables With Power-Loop Flow Rate

O boiler inlet pressure
□ boiler exit pressure
◇ boiler-tube exit temperature
△ boiler-shell exit temperature

power-loop flow sine wave amplitude ≈ ±20 lb/hr
inventory control - no accumulator

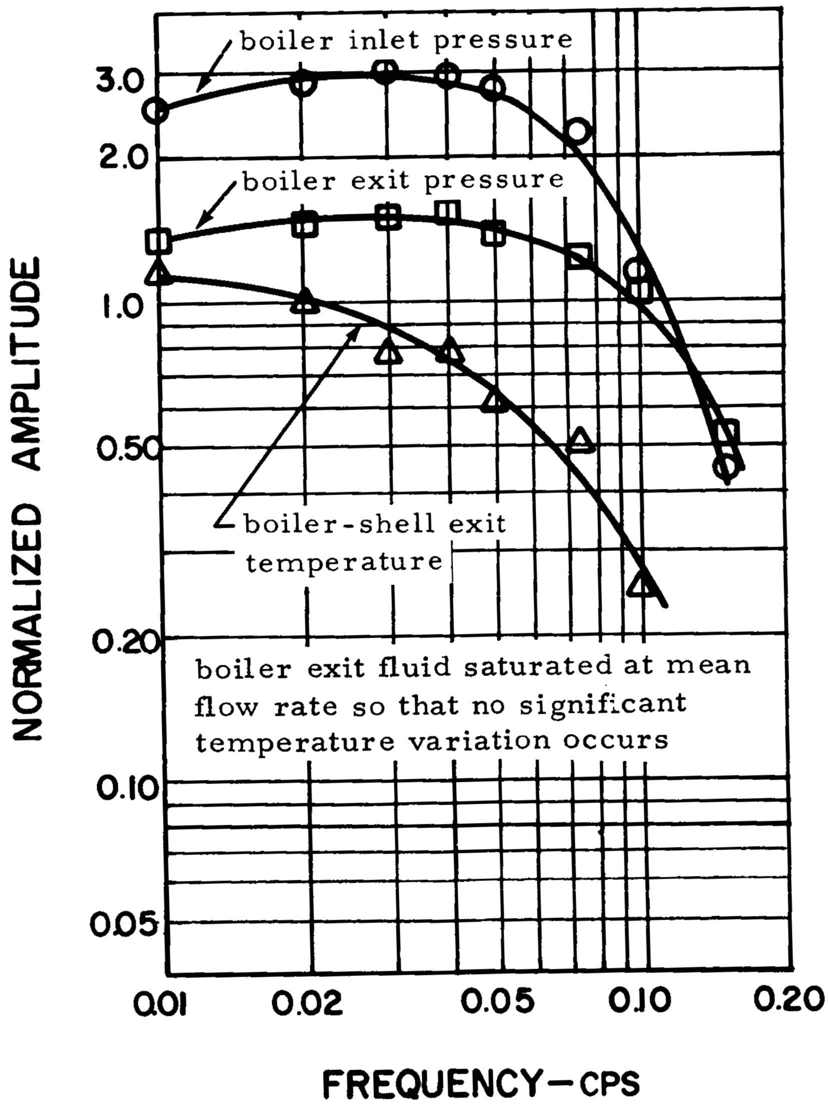

Figure 51 Boiler Dynamic Response Test No. 4. Frequency Response-Amplitude Normalized to Steady State

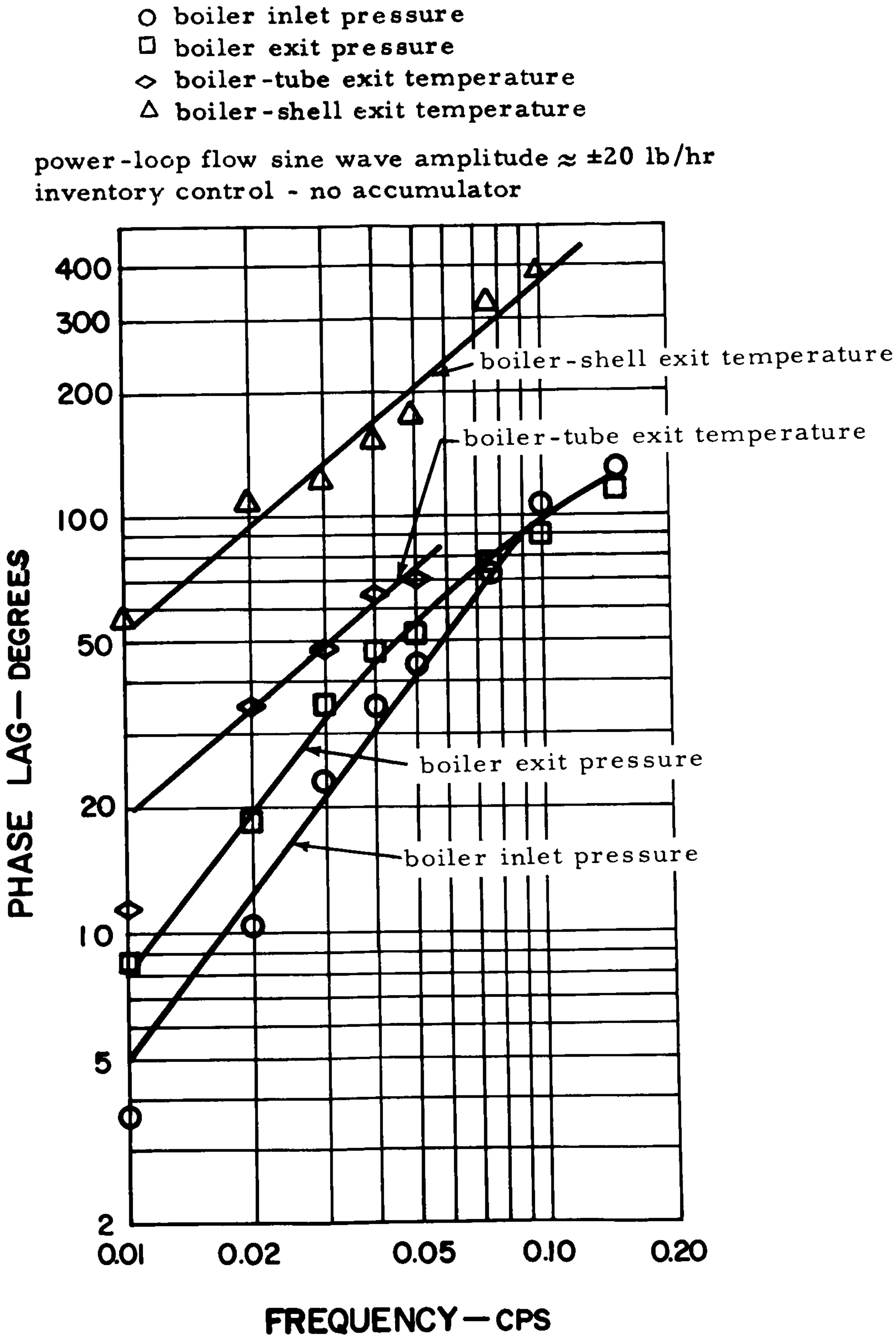

Figure 52 Boiler Dynamic Response Test No. 4. Frequency Response-Phase Shift

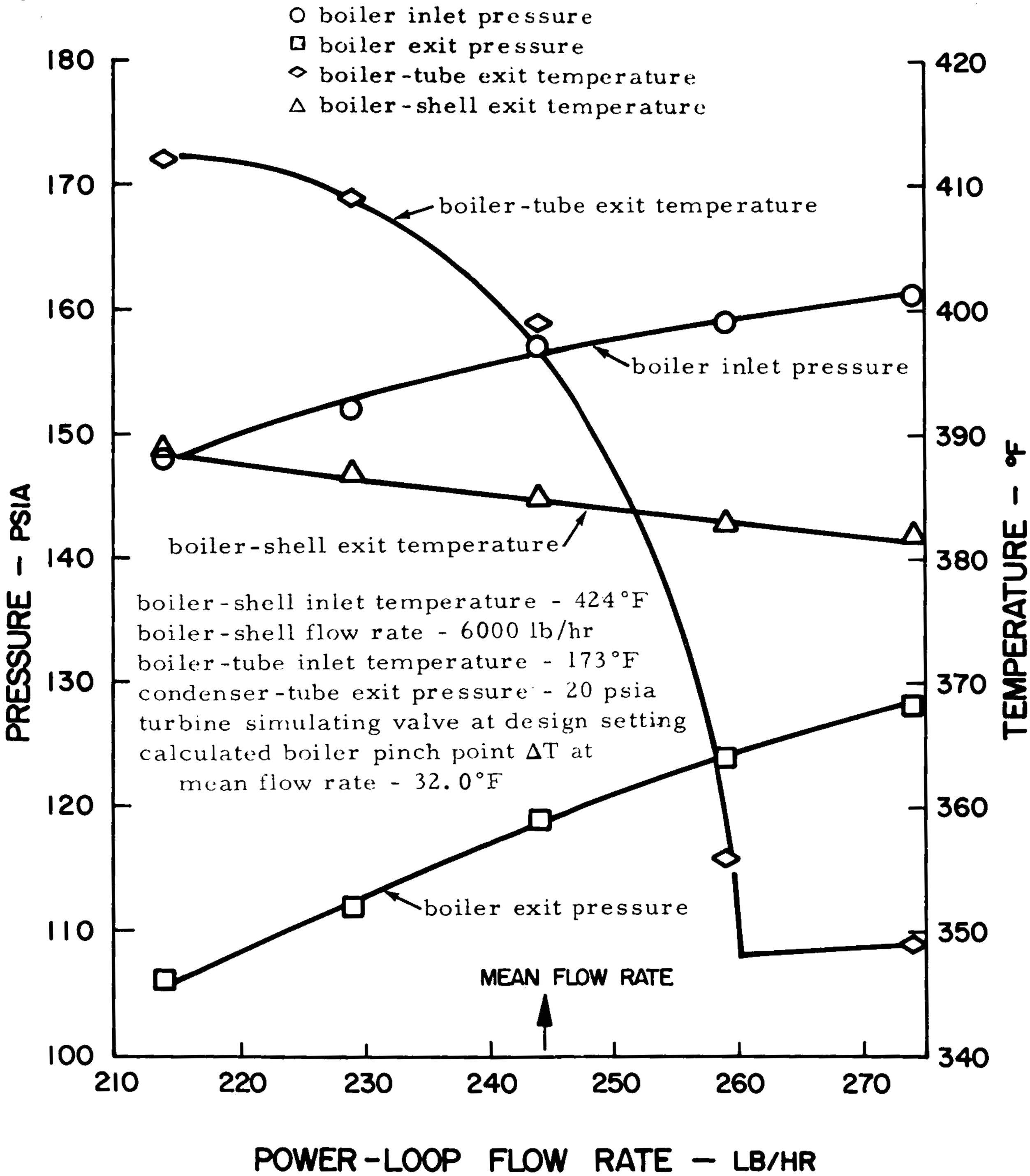

Figure 53 Boiler Dynamic Response Test No. 5. Steady-State Variation of Dependent Boiler Variables with Power-Loop Flow Rate

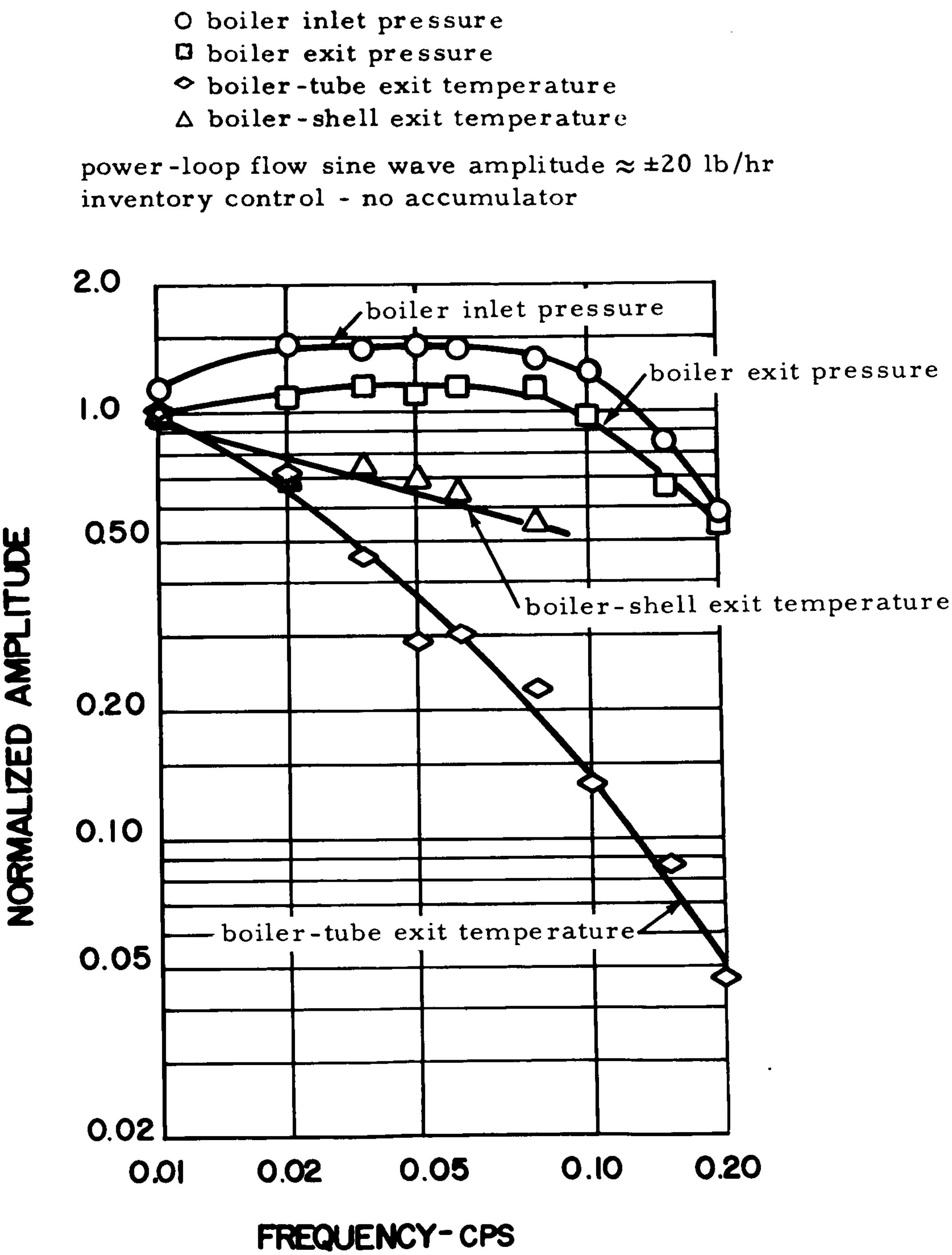

Figure 54 Boiler Dynamic Response Test No. 5. Frequency Response - Amplitude Normalized to Steady State

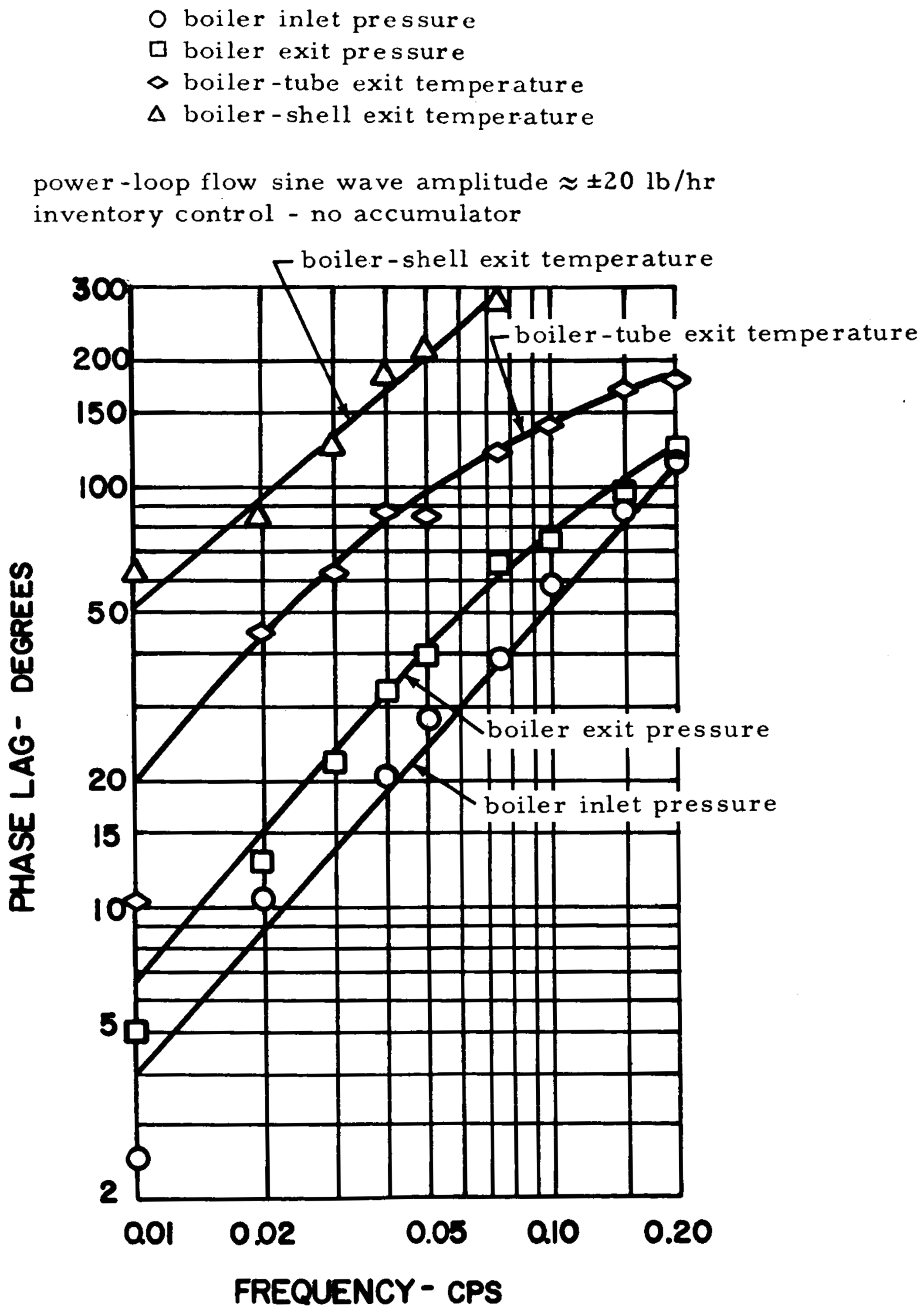

Figure 55 Boiler Dynamic Response Test No. 5. Frequency Response - Phase Shift

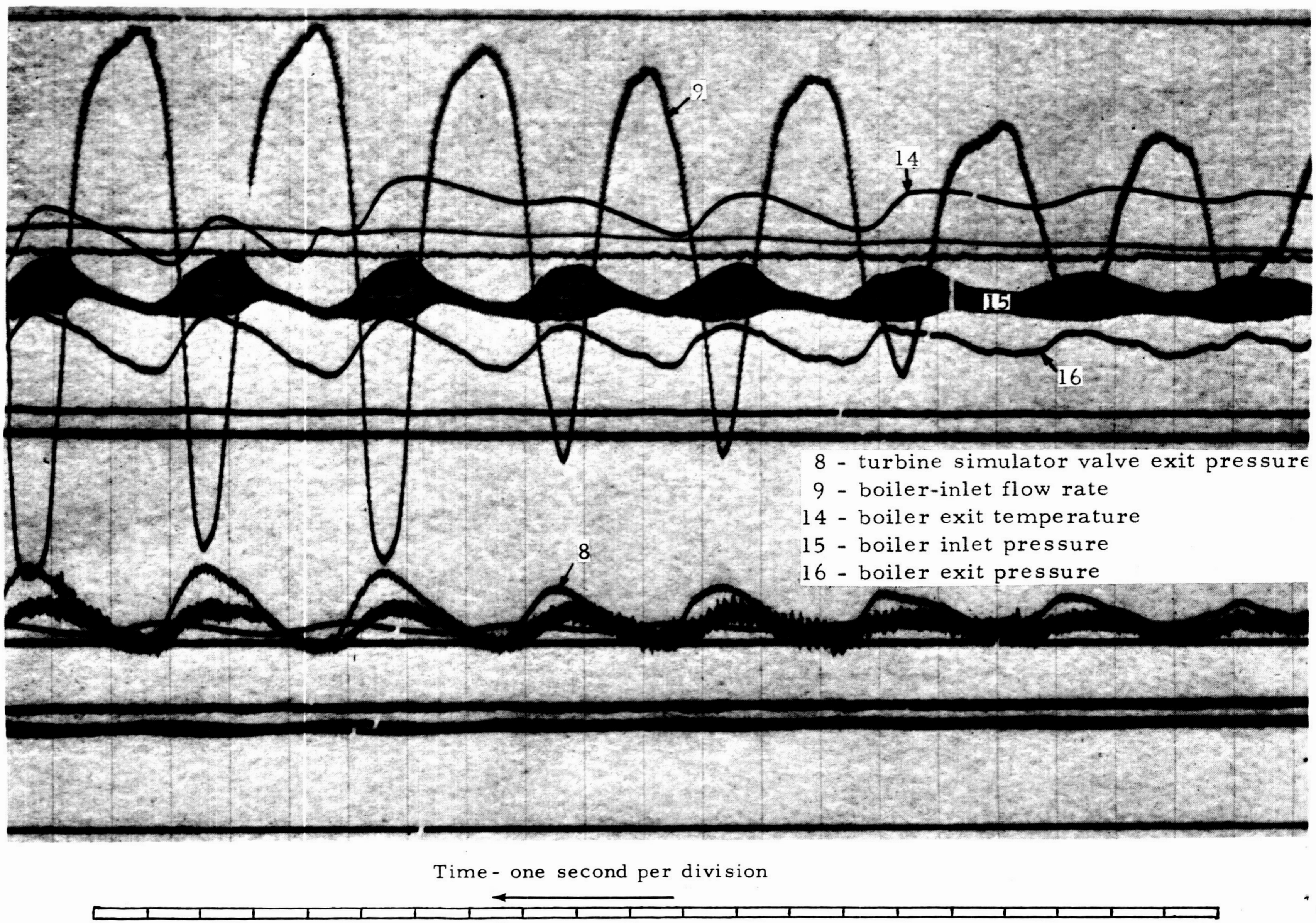

Figure 56 Oscillograph Recording of Divergent Instability

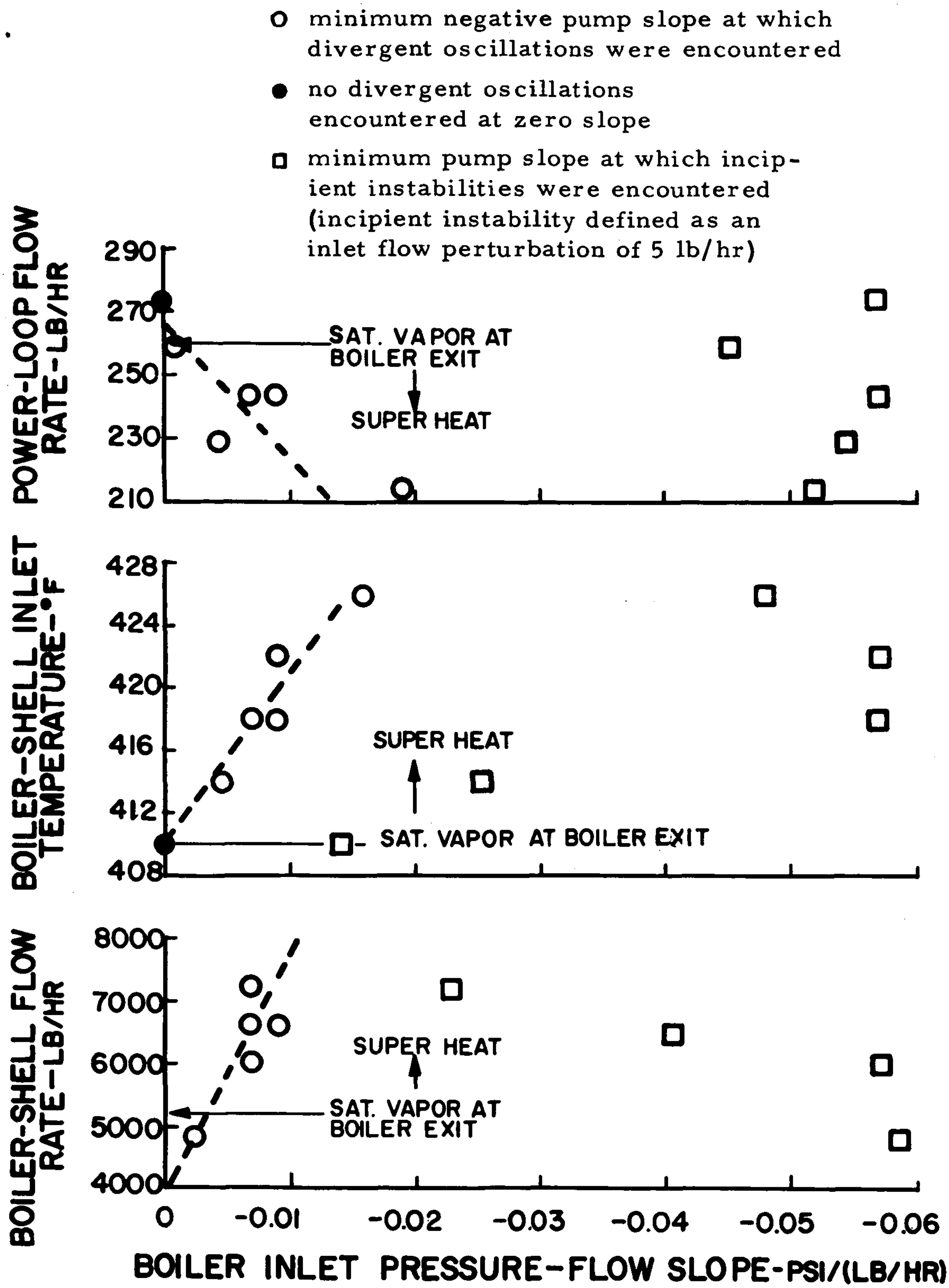

Figure 57 Power-Loop Stability Limits vs Pump Slope with Variable Boiler-Shell Flow, Boiler-Shell Inlet Temperature, and Power-Loop Flow

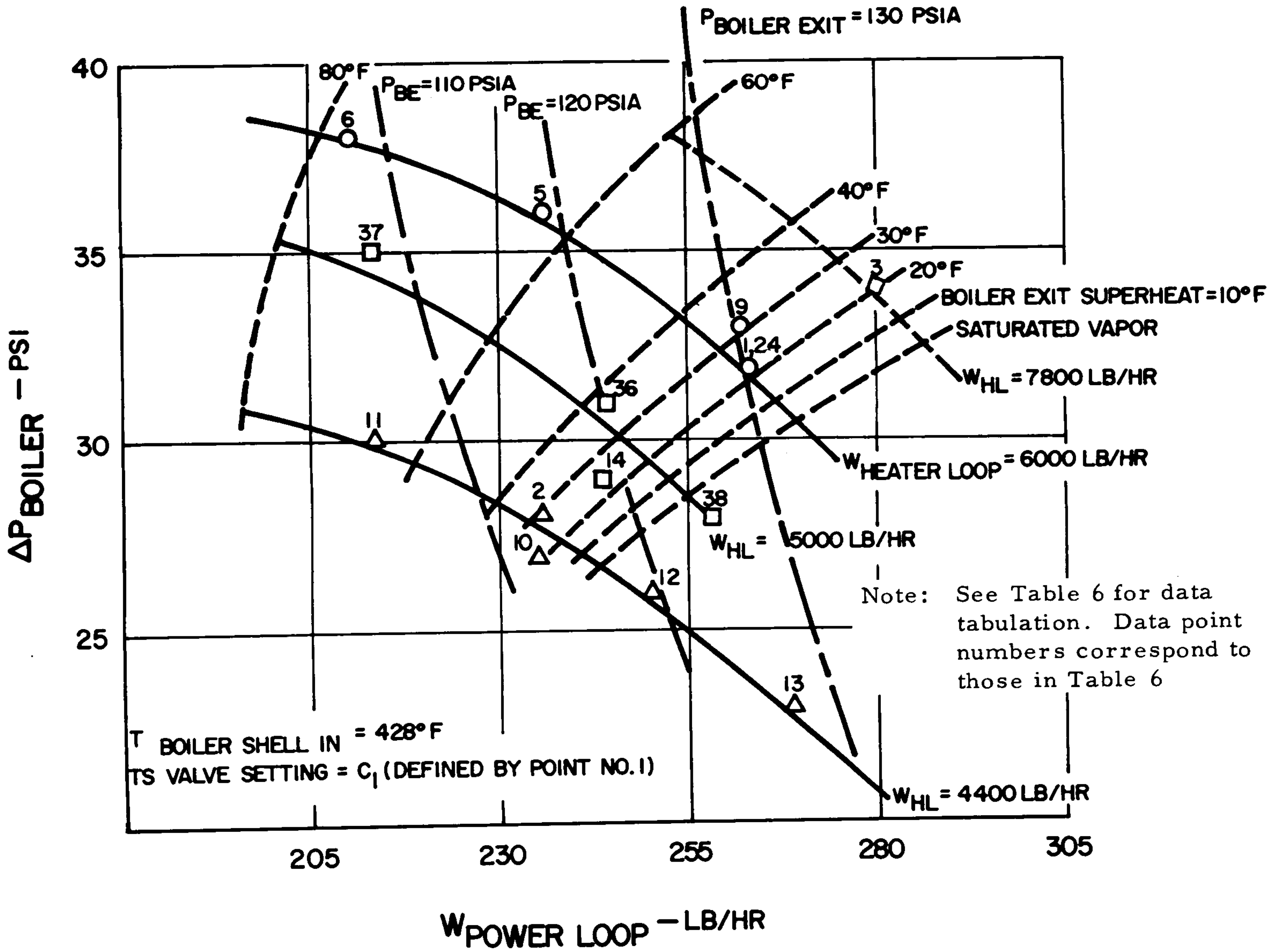

Figure 58 Exploratory Boiler Map. Boiler Pressure Drop vs Power-Loop Flow at Several Heater-Loop Flows

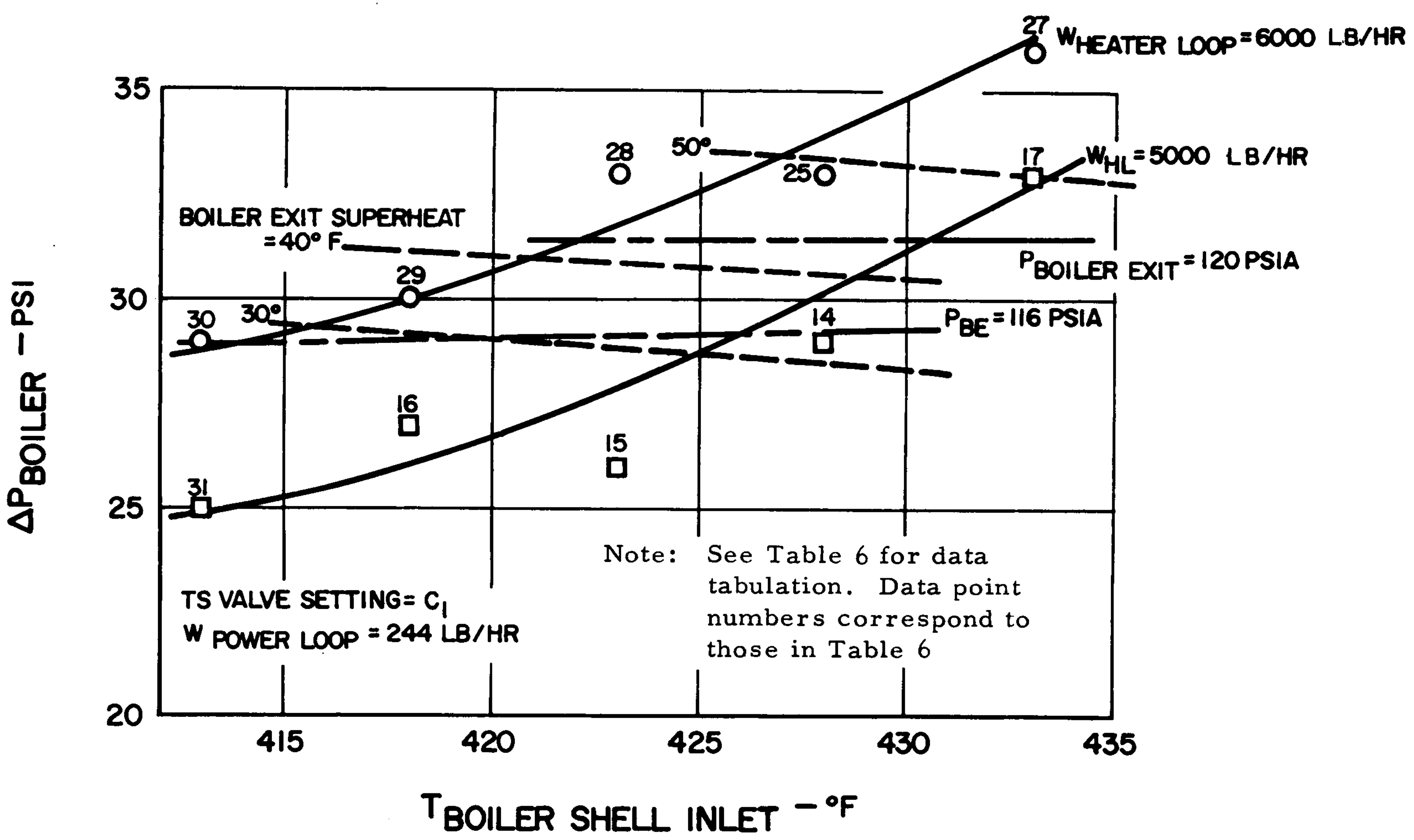

Figure 59 Exploratory Boiler Map. Boiler Pressure Drop vs Boiler Shell Inlet Temperature at Two Heater-Loop Flow Rates

Note: See Table 6 for data tabulation. Data point numbers correspond to those in Table 6

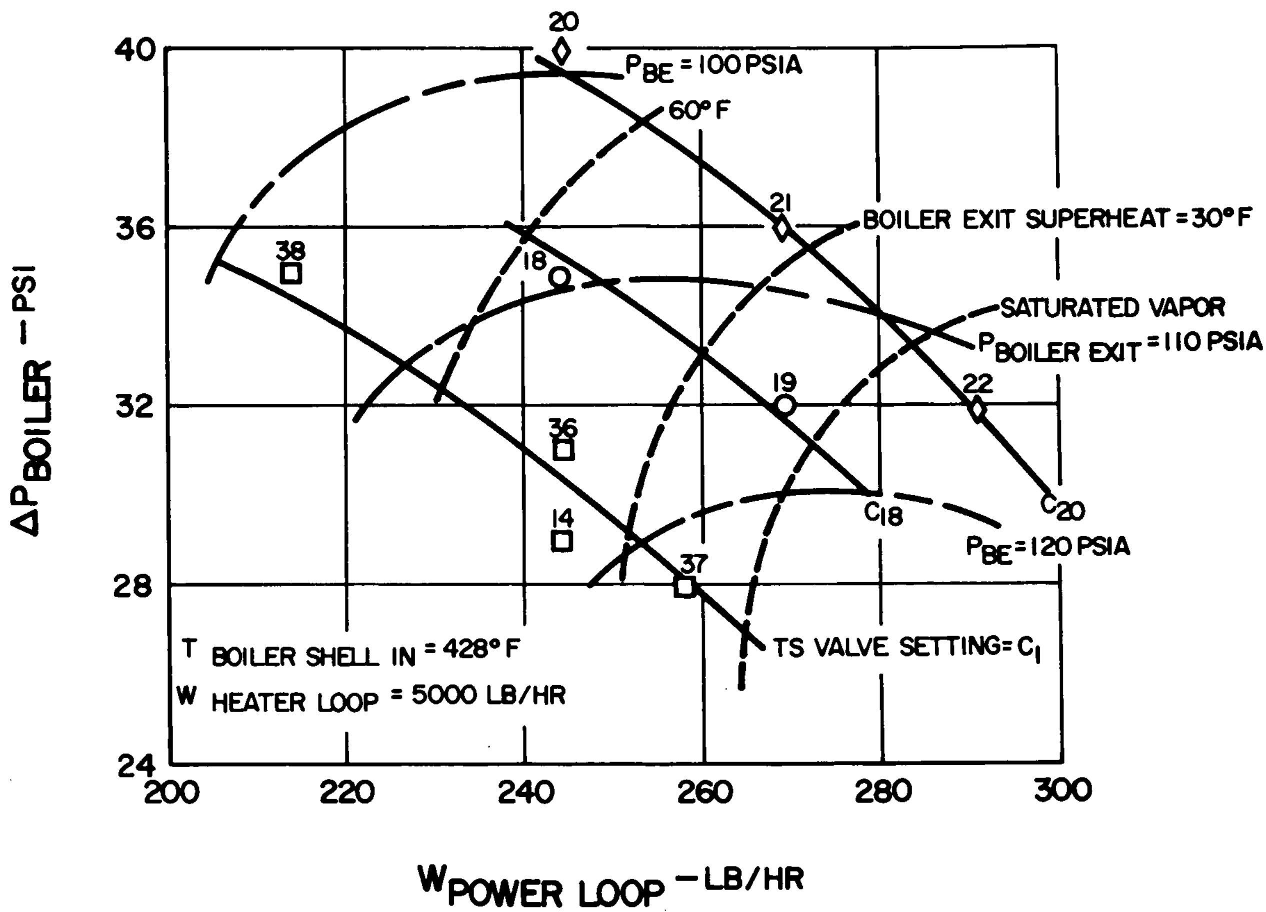

Figure 60 Exploratory Boiler Map. Boiler Pressure Drop vs Power-Loop Flow at Several Turbine Simulator Valve Settings

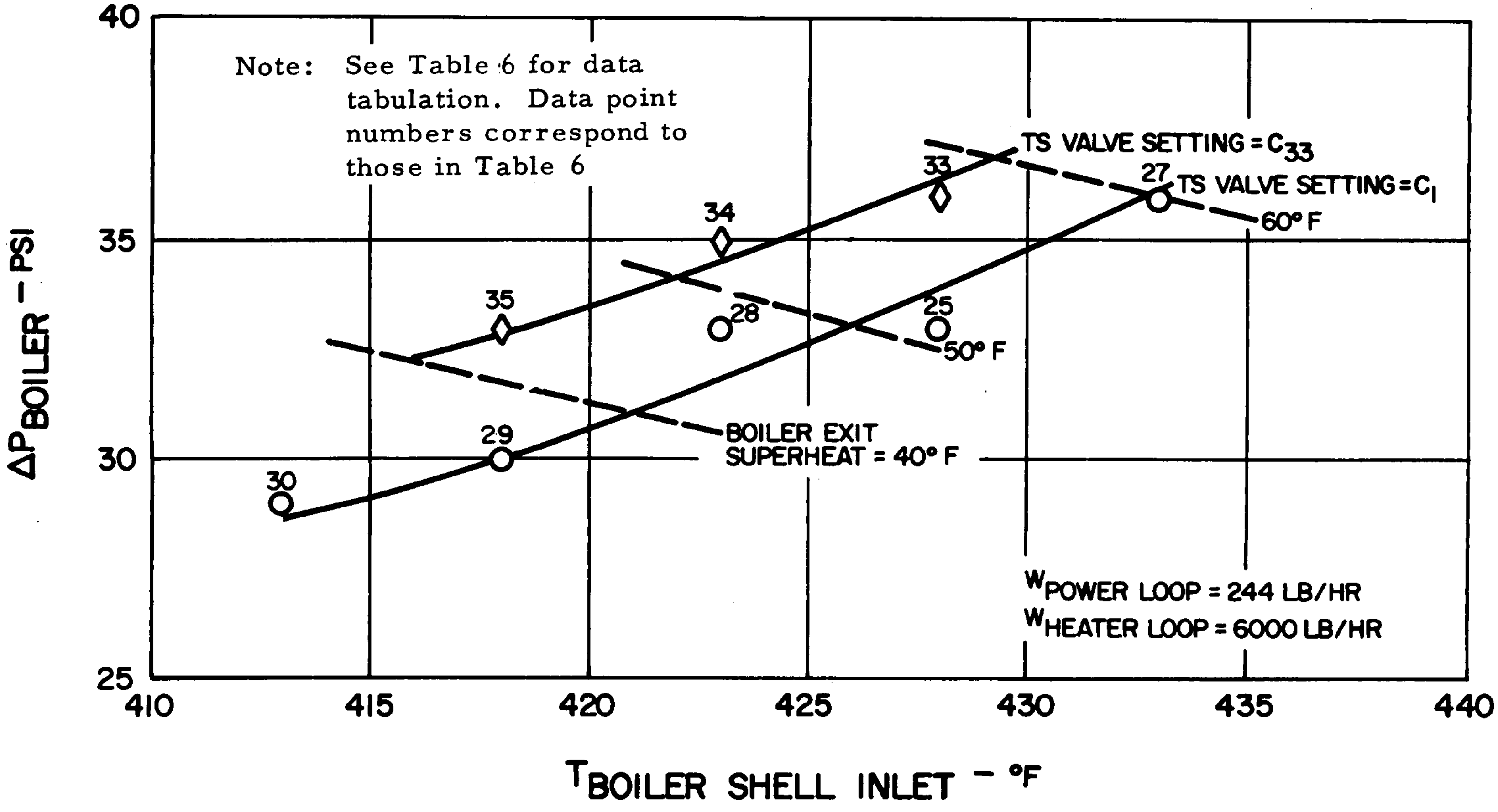

Figure 61 Exploratory Boiler Map. Boiler Pressure Drop vs Boiler Shell Inlet Temperature at Two Turbine Simulator Valve Settings

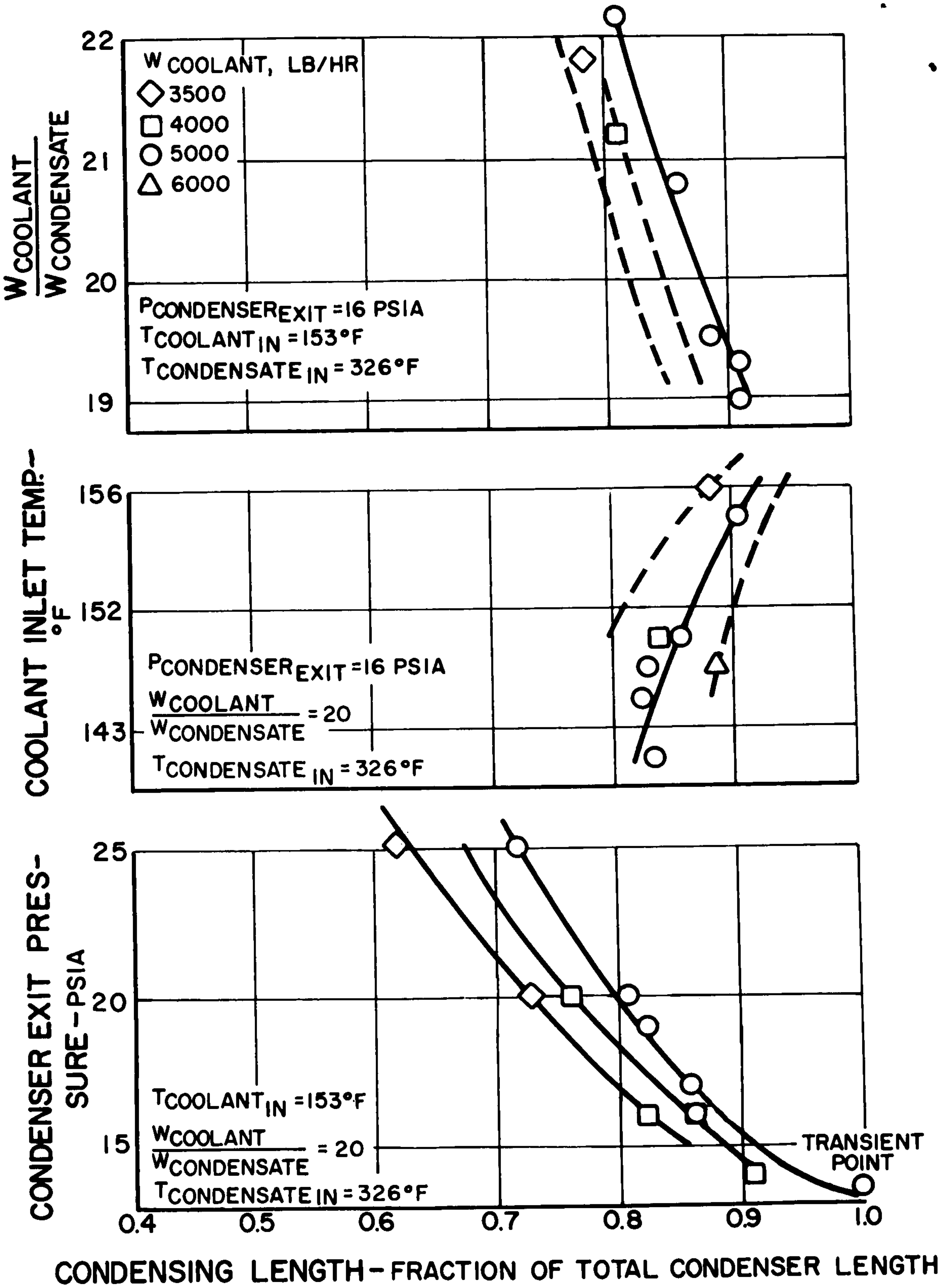

Figure 62 Exploratory Condenser Map

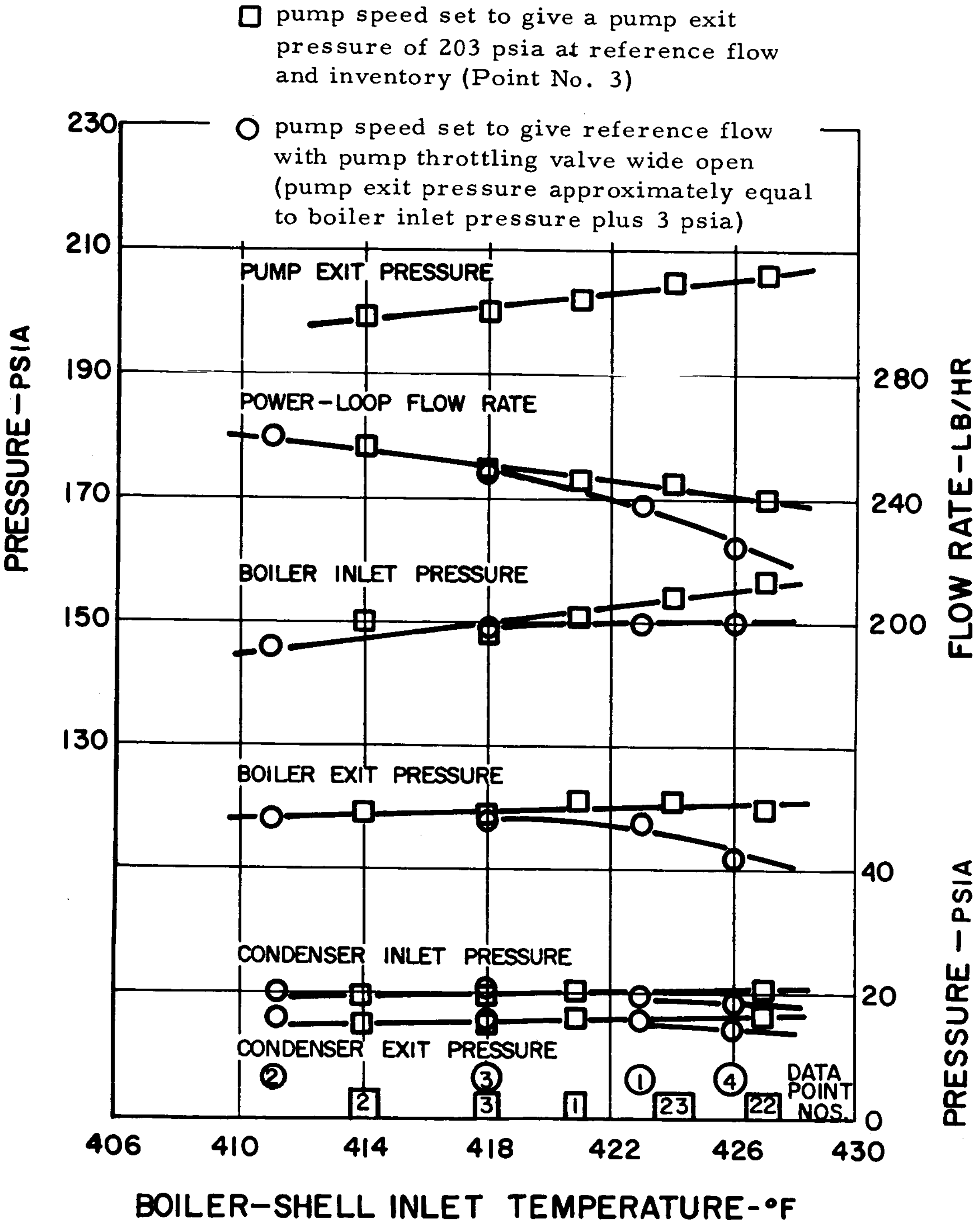

Figure 63 Variation of Power-Loop Pressures and Flow Rate with Boiler-Shell Inlet Temperature at Two Fixed Pump Throttling Valve Settings and Pump Speeds. Fixed Inventory Established at Point No. 3

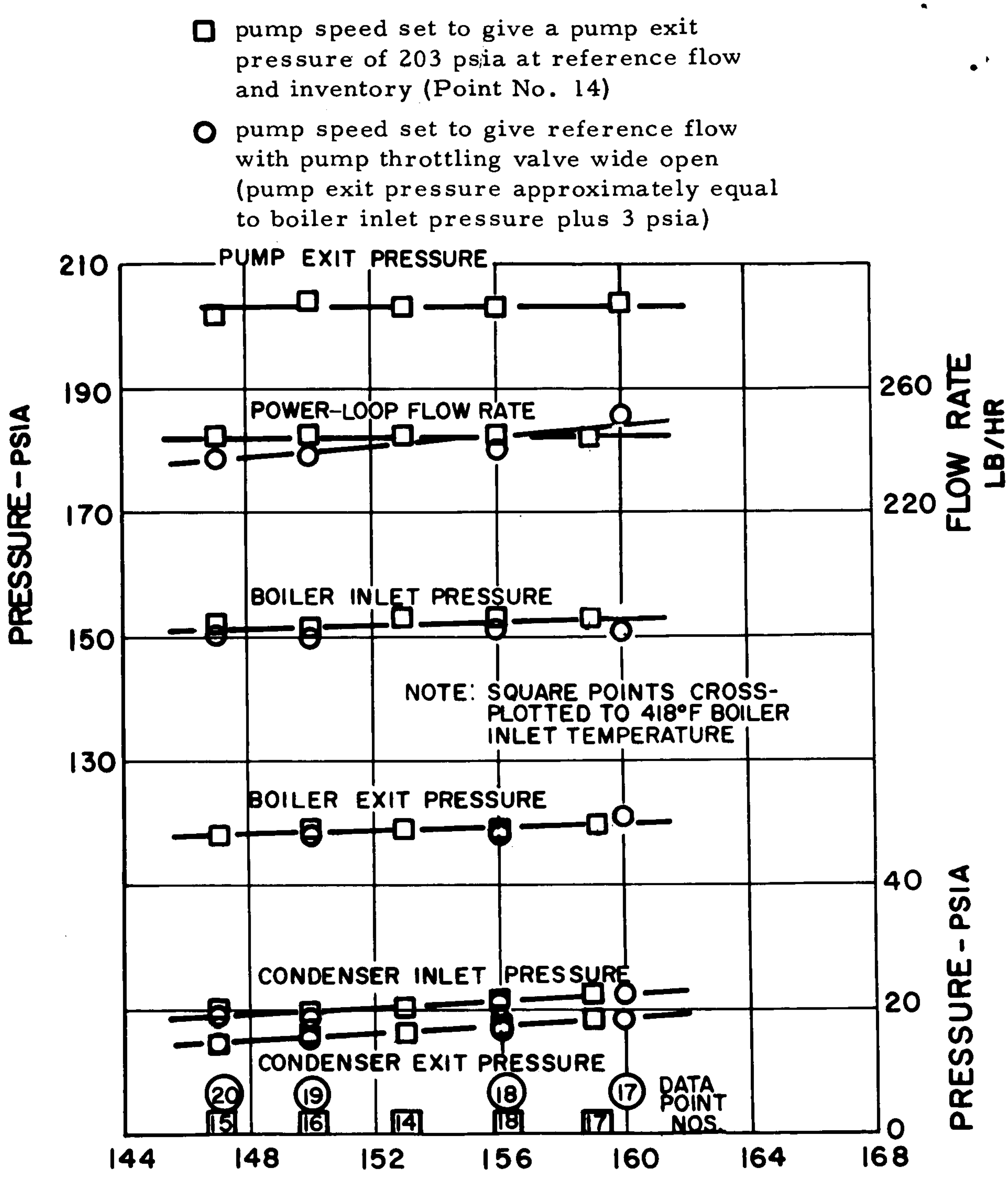

Figure 64 Variation of Power-Loop Pressures and Flow Rate with Condenser-Shell Inlet Temperature at Two Fixed Pump Throttling Valve Settings and Pump Speeds. Fixed Inventory Established at Point No. 14

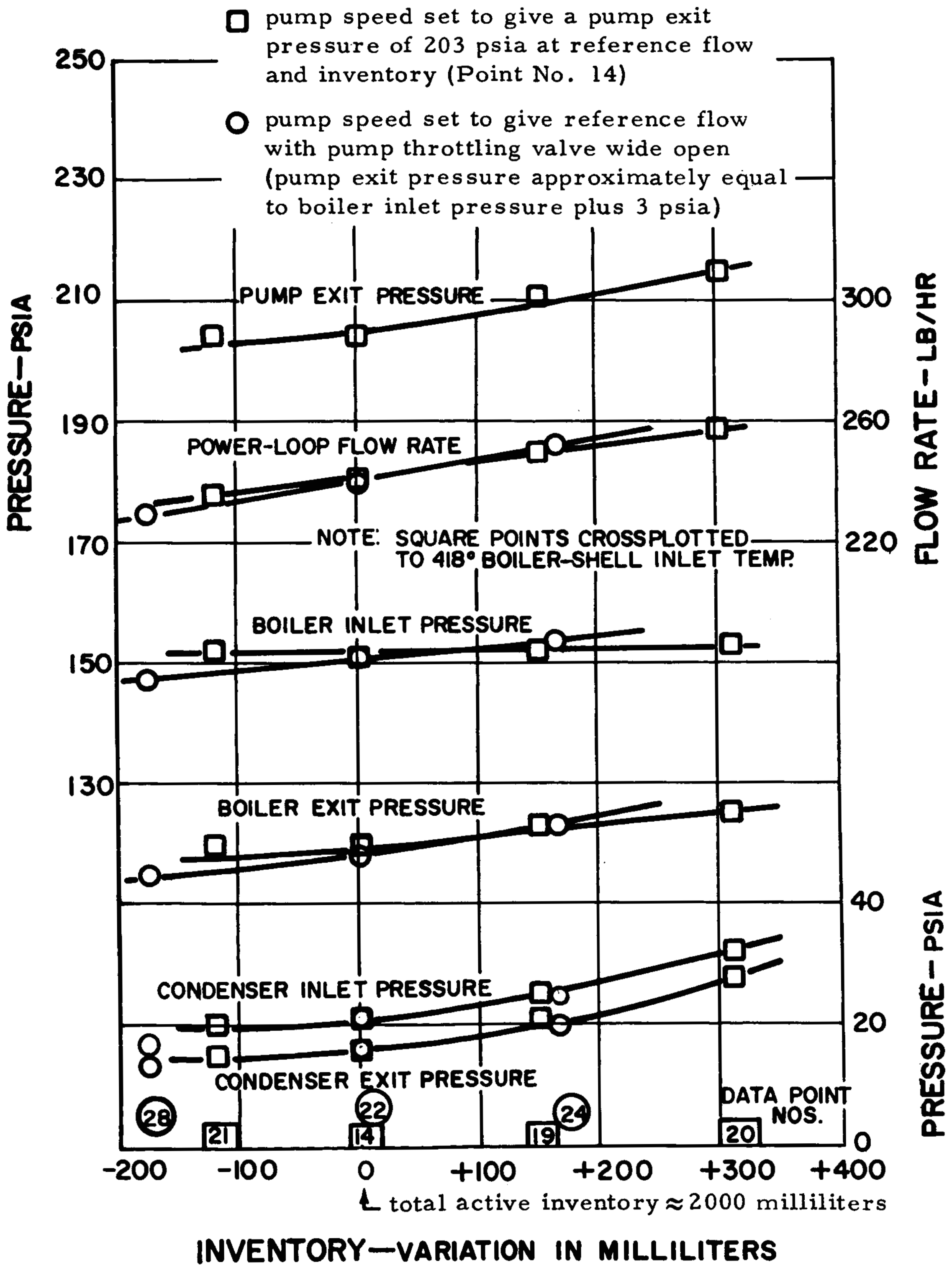

Figure 65 Variation of Power-Loop Pressures and Flow Rate with Power-Loop Inventory at Two Pump Throttling Valve Settings and Pump Speeds

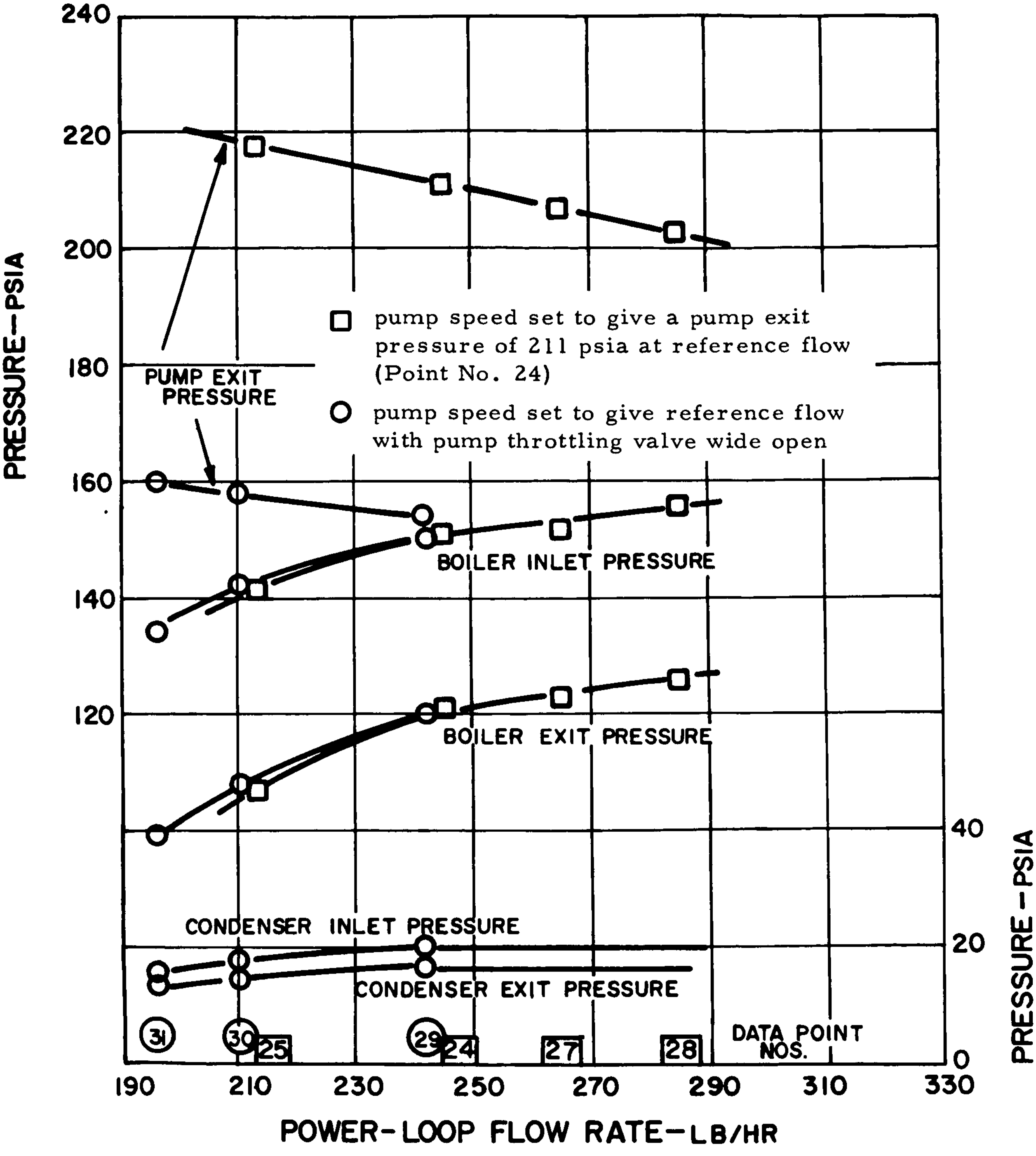

Figure 66 Variation of Power-Loop Pressures with Power-Loop Flow Rate at Two Pump Throttling Valve Settings and Pump Speeds. Fixed Inventory Established at Point No. 29 for Circular Points Only. Square Points Run with Accumulator

NASA-Langley, 1966 E-3565

"The aeronautical and space activities of the United States shall be conducted so as to contribute . . . to the expansion of human knowledge of phenomena in the atmosphere and space. The Administration shall provide for the widest practicable and appropriate dissemination of information concerning its activities and the results thereof."

—NATIONAL AERONAUTICS AND SPACE ACT OF 1958

NASA SCIENTIFIC AND TECHNICAL PUBLICATIONS

TECHNICAL REPORTS: Scientific and technical information considered important, complete, and a lasting contribution to existing knowledge.

TECHNICAL NOTES: Information less broad in scope but nevertheless of importance as a contribution to existing knowledge.

TECHNICAL MEMORANDUMS: Information receiving limited distribution because of preliminary data, security classification, or other reasons.

CONTRACTOR REPORTS: Technical information generated in connection with a NASA contract or grant and released under NASA auspices.

TECHNICAL TRANSLATIONS: Information published in a foreign language considered to merit NASA distribution in English.

SPECIAL PUBLICATIONS: Information derived from or of value to NASA activities. Publications include conference proceedings, monographs, data compilations, handbooks, sourcebooks, and special bibliographies.

TECHNOLOGY UTILIZATION PUBLICATIONS: Information on technology used by NASA that may be of particular interest in commercial and other nonaerospace applications. Publications include Tech Briefs; Technology Utilization Reports and Notes; and Technology Surveys.

Details on the availability of these publications may be obtained from:

SCIENTIFIC AND TECHNICAL INFORMATION DIVISION

NATIONAL AERONAUTICS AND SPACE ADMINISTRATION

Washington, D.C. 20546